**The Thesis Committee for Abdullah Ali L Alghamdi**
**Certifies that this is the approved version of the following thesis:**

# Experimental Evaluation of Nanoparticles Impact on Displacement Dynamics for Water-Wet and Oil-Wet Porous Media

**APPROVED BY**
**SUPERVISING COMMITTEE:**

**Supervisor:**

David A. DiCarlo

Steven L. Bryant

# Experimental Evaluation of Nanoparticles Impact on Displacement Dynamics for Water-Wet and Oil-Wet Porous Media

**by**

**Abdullah Ali L Alghamdi, B.S.E.**

**Thesis**

Presented to the Faculty of the Graduate School of

The University of Texas at Austin

in Partial Fulfillment

of the Requirements

for the Degree of

**Master of Science in Engineering**

**The University of Texas at Austin**

**August 2015**

# Dedication

To God, my family, my friends, and my sponsors at Saudi Aramco

# Acknowledgements

This research work reflects the great support and dedications that I have received throughout my graduate work studies at the University of Texas at Austin. It would not be enough for sure to express my sincere appreciation and gratitude to Dr. David DiCarlo as he was more than just research advisor. It was my complete privilege and honor working in his research team as he always has been there to guide, support and advise me throughout this project duration.

I would also thank Dr. Steven Bryant, Dr. Larry Lake and Dr. Kishore Mohanty for their useful feedback and great insights during my research work as well as my time as a student in their classes. Special thanks go to my follow research teammate Roy Wung for mentoring me to execute my experimental work and helping me with experimental setup. I would extend my appreciation list to include several members from the Petroleum and Geosystems Engineering Department and to Gary Miscoe and Glen Baum in particular for their support during the experimental setup preparation and for providing me with necessary equipment.

Great appreciations go to my follow graduate student Thamer Alsulaimani for being a great friend and for his continuous support and help during my academic and personal life aspects. My deepest gratitude and outmost thanks goes to my wife, my family and my friends for their love and support.

Finally, I would send my thanks to Saudi Aramco Management for awarding me the opportunity of pursing this graduate degree. Special thanks go to members from Southern Area Production Engineering Department and to EXPEC Advance Research Center.

# Abstract

## Experimental Evaluation of Nanoparticles Impact on Displacement Dynamics for Water-Wet and Oil-Wet Porous Media

Abdullah Ali L Alghamdi, M.S.E.

The University of Texas at Austin, 2015

Supervisor: David A. DiCarlo

The potential of utilizing nanoparticles for production enhancement during oil-water displacement can play a significant role to achieve efficient and sustainable production of resources as they have shown great promise in stabilizing emulsion inside porous media. Furthermore, the displacement of brine solution containing nanoparticles by another non-wetting phase such as n-octane under water-wet condition has been shown to produce the signs of nanoparticle-stabilized emulsion.

Because it is hypothesized that emulsion effects are caused by pore scale events that shear the fluids, this research aims to evaluate the impact of nanoparticles on different displacement scenarios (primary imbibition, primary drainage, secondary imbibition, and secondary drainage) and address the effect of wettability (oil-wet vs. water-wet), displacement types (different pore scale processes), and viscous stability (lower viscosity n-octane vs. higher viscosity tetradecane) on the generation of nanoparticle-stabilized emulsion in situ during immiscible displacement. Studying the

impact of these changes is of primary importance since they contribute to changing pore scale events, fluids positioning and distribution, and displacement stability.

Nanoparticle-stabilized emulsion has been associated with some indirect observable signs which include i) a rapid pressure drop increase exceeding the viscosity ratio between the brine and brine-nanoparticle dispersion, ii) a later breakthrough, , iii) a reduction in resident fluid residual saturation, and iv) a reduction of the invading phase endpoint relative permeability. Therefore, the impact of nanoparticles on the displacement was evaluated by measuring pressure drop data and effluent fluid histories. Those data were used to indicate the signs of nanoparticle-stabilized emulsion generation by interpreting pressure drop trends, water saturation histories, pressure drop ratio profile, residual fluid saturation, and endpoint relative permeability of the invading phase. Furthermore, the study attempts to examine the hypothesis that the displacement of a wetting hydrocarbon phase containing hydrophobic nanoparticles by another non-wetting aqueous phase will also generate nanoparticle-stabilized emulsion symptoms.

This research reveals that compared to the control case (no nanoparticles), nanoparticles have the greatest effect on drainage type displacement (hydrocarbon invasion) with pressure drop reaching up to 500 % or even greater compared to the initial pressure drop observed at the start of the displacement. It also shows that those particles have little effect on imbibition displacement (aqueous phase invasion). This was found to be true for both oil-wet and water-wet despite the fact that fluids are configured differently at the pore-scale level. As for a more viscous hydrocarbon phase (tetradecane), the observed effects are generally lessened. As for secondary drainage displacement, initial trapping and the distribution of the hydrocarbon phase has also reduced the severity of the emulsion generation process. Based on the previous findings, an attempt to test the hypothesis of displacing hydrophobic nanoparticle dispersion by an

aqueous brine solution under oil-wet condition was inconclusive due to the difficulty of maintaining stable hydrocarbon-nanoparticle dispersion.

The displacement profile for all imbibition cases showed no significant differences between nanoparticle case and control case. Yet, we observe that nanoparticles have caused a reduction in the residual hydrocarbon saturation. This reduction was slightly greater for water-wet core compared to oil-wet.

For these results I conclude that Haines jump and Roof snap-off may be one of the primary processes responsible to generate nanoparticle-stabilized emulsion during drainage displacement. However, observing emulsion symptoms during secondary drainage in oil-wet cores suggest either a) exact configuration is not important or b) possible alteration in the rock wettability by nanoparticles to produce the same configuration. The viscosity results suggest that nanoparticle effects have largely altered the conformance of the displacement. The presence of ethylene glycol and/or other coating chemicals used to maintain stability of nanoparticle dispersion may have caused the reduction of hydrocarbon phase residual saturation during all imbibition type displacement.

# Table of Contents

# List of Tables

# List of Figures

# Chapter 1: Introduction

## 1.1 MOTIVATION

As world population continues to expand, the demand for energy will also increase. According to Energy Information Administration (EIA), the global demand for energy will increase by almost 50% over the next 25 years. This has become a challenging issue for energy companies as almost 84% of the world's energy still depend on oil and gas production. Also, the days for what is called "easy to find and easy to produce oil" are almost over with companies facing a lot of subsurface complexities to extract hydrocarbon. That is why companies are spending millions of dollars to increase their operating efficiency to produce oil and reach much more intelligent and efficient production. As a result, it was necessary to utilize pore scale agents to perform some of the necessary actions to enable smarter production of these resources. Some of the oil reservoirs around the world have reached maturity with injected water, used to maintain reservoir pressure and displacing oil, breaking through faster than expected.

Optimizing production operation consists of enhancing both well Injectivity for the case of water disposal wells and productivity for mature oil producers. Earlier breakthrough of water usually starts with uneven water injection into disposal wells as water travels only to a high permeability zones and micro fractures. The communication network between fractures and subsurface layers also leads to pre-mature water breakthrough at the producing wells through the same type of high permeability sections. Therefore, an optimal injection process is conducted in a manner where injected water is evenly distributed to enhance sweep and contact with more rock surfaces. This would lead to optimize the pressure maintenance process in the subsurface as well as enhance sweeping action of resources. Similarly, water shut off operation conducted in oil

producing wells may prolong well life and reduce the production of produced water. This processes would also lead to evenly distributed pressure drawdown around the well and improve hydrocarbon recovery.

With advancement in chemistry and fluid treatment tools such coiled tubing, the oil industry has started several initiatives to use chemical methods to stimulate well Injectivity and productivity. The new tools have enabled selective zonal treatment which makes it possible nowadays to adopt chemical methods to matrix acidize wells or shut off undesired water zones. Recent studies have shown that nanoparticles can be used to improve fluid circulation during drilling by plugging high permeability layers. Other research have shown that co-injection of an aqueous phase containing nanoparticle with another immiscible phase at high shear rate can lead also into generating emulsion phase with high apparent viscosity. Those studies have shown that energy is required to generate such viscous phase of nanoparticle-stabilized emulsion as droplets of one fluid need to be dispersed in the other and nanoparticles need to be brought to the droplet interfaces.

This research focuses on evaluating the hypothesis that nanoparticle-stabilized emulsion can also be generated using pore scale events during “two immiscible fluid displacement” in porous media, i.e. during the displacement of one fluid by a second fluid which is immiscible with the first. During two immiscible fluid displacement, emulsion generation symptoms are linked directly with rapid increase in pressure drop, which exceeds the viscosity ratio between the brine and brine-nanoparticle dispersion, later front breakthrough, and reduction in resident fluid residual saturation. In fact, ongoing research has also tested to the potential of nanoparticles to increase carbon dioxide $CO_2$ trapping during $CO_2$ sequestration using the same pore scale events. The governing mechanisms, which are evaluated under both oil-wet and water-wet conditions as well as different

viscous instability conditions, utilize pore scale events of Haines jump and snap-off mechanisms during the displacement of wetting phase by non-wetting phase. The main challenge was to ensure the stability of those nanoparticles in their carrying solvent and that the dispersion is stable to be placed inside porous media. The findings and observations for several core flooding tests will be discussed in details to show those factors that may or may not contribute primarily to creating nanoparticle-stabilized emulsion during displacement. The nanoparticles chosen for these experiments are appropriate because of their performance in batch tests with two immiscible fluids. In particular, sonication for samples of the two immiscible fluids used in each experiment containing brine solution and the hydrocarbon fluids (with nanoparticle presence in either brine solution or oil phase) showed nanoparticle-stabilized emulsion forming once the sonication process is complete.

The potential benefits of this research is to develop a good understanding about the impact of several factors such as reservoir wettability, displacement viscous stability, and nanoparticle wettability on in situ emulsion generation processes during fluid displacements. This would lead into a better design of possible treatment options whereby nanoparticles can be used to selectively treat wells by shutting off undesired "thief" zones and help in establishing uniform and even distribution of either fluid injection in case of an injection well or fluid production in case of producing well.

## 1.2 THESIS OUTLINE

This thesis consists of six chapters that will shed light on the background of this study as well as the experimental evaluation results to test the hypothesis presented in this project. The first chapter introduces the research and highlights its motivation and

potential impact. Chapter two mainly discusses the literature reviews and up-to-date research findings related to this project. It presents the potential advantages for utilizing nanoparticles as agents to serve different purposes in both upstream and downstream oil production fronts. The third chapter focuses on the main hypothesis to be tested and addresses the main physical concepts related to it. It will also show how the claim will be evaluated and present the data which will be collected as part of the study evaluation. Both chapter four and five will discuss the experimental design, procedure, and results gathered from core flood experiments. While chapter four is focused on materials and methods used for evaluation, chapter five essentially discusses the experimental findings and observations and examines the effect of nanoparticles on displacement patterns for different wettability conditions and fluid properties. The final chapter of this report will summarize the results for this research as well as highlight possible future work necessary to expand based on its outcomes.

# Chapter 2: Literature Review

## 2.1 NANOPARTICLES APPLICATION IN THE OIL INDUSTRY

Nanoparticles are defined as a collection of atoms that are bonded together with a structural radius that is less than 100 nm. They are distinct compared to other forms of technology due to the substantial capabilities they provide in terms of their nanoscale proportions. Nanotechnology has taken so many forms in the oil industry that include nanosensors, nanofluid, and nanoparticles. These applications have recently gained a growing interest over the past years due to the potential they provide in terms of their ability to modify magnetic, optical, and electric properties.

### 2.1.1 Nanoparticles for Subsurface Reservoir Characterization

Reservoir characterization is considered one of the significant components for reaching optimum field development strategies. This importance is due to the fact that better subsurface characterization distinguishes essential features of reservoir heterogeneities that contribute to fluid flow in the pay zones. In addition, it has been shown that reservoir complexities impact the performance of water flood, production stimulation as well as future EOR process (Permadi et al., 2004; Belgrave et al., 1993). Nanoparticles can be utilized to complement existing conventional techniques used for reservoir evaluation, including geological mapping, core studies, wireline logging and other formation testing. In addition, stable dispersion of surface-treated superparamagnetic nanoparticles was shown to flow through micron-size throats across the reservoir (Yu et al., 2010). These capabilities can be combined with existing electromagnetic (EM) induction tomography to enable imaging of the flood front advancement (Rahmani et al., 2013). In this process, magnetic permeability can be

changed by magnetic nanoparticles and contrast agents can be traced to track the flood front inside the reservoir. As a result, properties affecting the flow paths can be inferred and quantified through tracing these particles (Rahmani et al., 2013). Models have been put in place to utilize magnetic particles impact and contrasting agents' response to generate a 3D image of the subsurface flood front in the reservoir of interest (Al-Shehri et al., 2013; Rahmani et al., 2015)

### 2.1.2 Enhanced Oil Recovery Applications

Enhanced Oil Recovery (EOR) as defined by Lake (1989) is the recovery of oil by injecting fluid that is not native to the reservoir and excludes water flooding and pressure maintenance process. EOR is achieved generally via lowering mobility ratio and/or increasing capillary number. This is typically reached by lowering the mobility of invading fluid, change wettability from oil-wet to intermediate wet or water-wet and reducing interfacial tension.

In relation to EOR, nanoparticles have been studied thoroughly to investigate their effect on the wettability alteration process. Onyekonwu and Ogolo (2010) discussed three different polysilicon nanoparticles (PSNP) which alter the rock wettability in different manners. Their results revealed that silane treated PSNP had an improvement of over 50 % after primary and secondary recovery on a water-wet rock. Ju and Fan (2008) addressed the challenges relating to the application of nanopowder in oil fields to enhance water injection by the effect of changing wettability through adsorption on porous walls of sandstone. Their result illustrated that wettability of surface sandstone can be changed from oil-wet to water-wet by adsorption of untreated lipophobic and hydrophilic polysilicon nanoparticles.

$CO_2$ flooding is considered one of the most widely used technique for enhanced oil recovery as it becomes more economical and environmentally viable (Enick and Klara (1990); Enick and Olsen (2011)). However, the efficiency for this process is low due to the poor sweep efficiency caused by viscous and gravity fingering. Those fingering effects are generated because of the density and viscosity contrast between water and invading $CO_2$. This has led the industry to add some surfactant and nanoparticle agents to the $CO_2$ mixture to increase its viscosity for better conformance control. When compared to surfactants, the adsorption energy of nanoparticles was found to be 3-4 orders of magnitude higher than that of surfactants (Espinosa et al., 2010; Hariz, 2012). This is generally due to the size of the particles and also due to the interfacial tension between $CO_2$ and water. It was also hypothesized that Roof snap-off will provide the necessary adsorption energy to bring the nanoparticles from the bulk phase into the interface between water and $CO_2$. In fact this hypothesis was placed under examination by (DiCarlo et al, 2011), (Aminzadeh, 2013) and (Chung, 2013).

### 2.1.3 Drilling Fluid Applications

The application of utilizing nanoparticles as an additive to drilling fluid has gained interest over the years. The ability for those nano-agents to alter the rheological properties of the drilling fluid has enabled them to yield much more intelligent fluid that maintains well control as well as reduces circulation losses into the formation. Drilling fluids are mainly used to cool down and lubricate the drill bit, remove cuttings, prevent formation damage, suspend cuttings and also cake off the permeable formations and, hence, retard fluid migration into the formation. In a recent work by Zakaria (2012), new class of nanoparticles have been developed and tested to evaluate their impact on fluid

circulation losses. When tested under a low pressure/low temperature API standard test, it was shown that more than a 70% reduction in fluid loss was achieved in the presence of nanoparticles compared to a 9% reduction in the presence of typical loss circulation materials (LCMs). In addition, the filter cake developed by the nanoparticles drilling fluid was found to be thinner compared to the control case that utilizes available LCMs. This observation of thin filter cake implies reducing the differential pressure required for drill pipe sticking as well as reducing formation damage (Zakaria et al., 2012). The advantage for utilizing nanoparticles to create novel drilling fluid has been extended to cover unconventional shale gas drilling applications.

During shale gas drilling, chemical shale inhibitors are used in both oil based mud as well as water based mud to keep the wellbore stable. They are required to reduce the severity of clay/shale interaction and decrease the chance for water invasion into the matrix and micro fractures. However, with the increase in strict environmental regulations to utilize environmentally friendly options, Sharma and others (2012) have shown that nanosilica particles may substitute existing inhibitors and become potential non-reactive additives to the drilling fluid. Their study findings show that utilizing nanosilica in water based mud could physically plug pores and micro-cracks and hence, prevent water invasion into shale formation.

### 2.1.4 Production and Process Enhancement

Reduction in power consumptions and enhancing the efficiency of production operations is one of the main goals that companies in the oil industry are trying to accomplish. This is mainly needed to reduce the dollar price needed to produce and process hydrocarbon which would make the operation smarter and more profitable. A

great example would be the ability to locally and selectively heat up deep sea pipelines and others found in a high pressure-low temperature environment to prevent hydrate formations during oil and gas production. In addition, heat can reduce the viscosity of heavy oil and or melt paraffin buildup in well pumping equipment. Currently, this task is achieved through direct electrical heating which is associated with a large amount of power consumption that can reach up to 1500 A and 52 kV (Roth, 2011; Urdahl et al., 2003). In addition, other electromagnetic and mechanical barriers such as bare cable vulnerability to damage and uneven heat distribution (Das, 2008) are also common and lead to subsequent well and flowline intervention operations. However, the great success of nanoparticles can also be extended to cover this area of upstream and downstream operations. In fact, magnetic induction heating utilizing superparamagnetic nanoparticles provides a potential solution to issues related to heating both flowline and reservoir selectively and efficiently. Similar to the process of "hyperthermia" used in biomedicine which uses microwave radiations to make water molecules oscillate back and forth to generate heat (hyperthermia source), magnetic induction heating occurs because of high frequency magnetic waves inducing the magnetic moment of superparamagnetic nanoparticles to oscillate (Rosensweig, 2002). Davidson and others (2012) have conducted several experiments to evaluate the extent to which suitable nanoparticles can heat a certain material containing magnetic particles or any material brought into contact with the particles. Their experiments were conducted, under a high frequency of alternating magnetic field, to evaluate the optimal case for achieving localized high heat transfer conditions utilizing super paramagnetic nanoparticles (Davidson et al., 2012).

The use of magnetic nanoparticles has also been extended to cover oil processing applications, especially when treatment space is limited like in offshore production platforms. Oil production at a mature stage is associated with large amounts of water

production. Stable oil droplet found in produced water imposes a serious challenge for oil companies to meet environmental regulations. These protocols dictate those companies to separate all impurities from the water prior to disposing it offshore. Therefore, research has been ongoing to address this challenge and considerable potential is seen in utilizing magnetic nanoparticles. In fact, Ko and others (2014) have conducted a proof of concept study to test magnetic separation of oil droplets from produced water. In their study, batch-scale experiments were performed and confirmed that 5 wt. % of decane-in-water emulsions droplets, which have negative surface charges, were successfully separated from water utilizing cationic surface-coated magnetic nanoparticles. The separation efficiency they found in their experiments was in the range of 85 to 99.99% depending on experimental conditions (Ko et al., 2014).

All in all, nanoparticle utilization represents significant potential to the energy industry as they enable more intelligent operations that may lead to increasing efficiency, lowering cost, and increasing recovery in many of upstream and downstream fronts as presented earlier. Yet, in most recent research, the focus has been centered on evaluating nanoparticle transport in porous media, which may open the door for their usage as technological tools to improve hydrocarbon recovery. In other words, nanoparticles can be tailored to increase oil recovery and enhance $CO_2$ storage by improving the mobility ratio inside the reservoir for better conformance control and also enhance $CO_2$ trapping via emulsification.

## 2.2 NANOPARTICLE-STABILIZED EMULSION

### 2.2.1 Nanoparticles as an Emulsifying Agents

Emulsions as defined by Tadros (2013) are a group of disperse mixtures that contain two immiscible liquids where the droplets of dispersed phase is surrounded by the other phase. To achieve emulsification, an emulsification agent, known as an emulsifier, is needed. Because of that, emulsion may be classified according to the type of dispersed fluid, continuous phase, and the nature of the emulsifier. Emulsions, sometimes referred to as "foam", are thermodynamically unstable and will eventually collapse into two main immiscible phases (Aminzadeh, 2013). These emulsions are in most cases stabilized by surfactants or particles which provided the energy needed in order for them to maintain their structure. However, the energy required to bring the stabilizing agents to the interface depends on the size, wetting nature (wettability) of the stabilizing agents, and the interfacial tension between fluids as shown in the water and $CO_2$ case (Binks, 2002). However and unlike surfactants, utilizing nanoparticles as a stabilizing agent for emulsification would generate higher adsorption energy due to particles size and high interfacial tension seen in the presence of nanoparticles (Espinosa et al., 2010; Hariz, 2012).

For oilfield applications, the advantages for using colloidal particles as a foaming agent have been addressed by many researchers including Bragg (1999) and Brag and Varadaraj (2003). These advantages include their lower cost as well as their ability to generate good quality foam with high apparent viscosity by altering parameters like concentration, salinity and pH. Also, the wettability of nanoparticles can determine the texture and the structure of the generated foam. In other words, hydrophilic coated nanoparticles, particles that are mainly attracted to the water phase, would try to bend the oil-water interface toward oil and thus stabilize oil-in-water foam. Similarly, hydrophobic

coated nanoparticles, which are attracted to the oil phase, would bend the oil-water interface toward water to create water-in-oil emulsion (Binks, 2002; Binks and Horozov, 2006). This process can be quantified by the contact angle (Θ) of the particles at the interface measured through the aqueous solution. This is shown clearly in Figure 2.1 as reported by Dickson (2004)

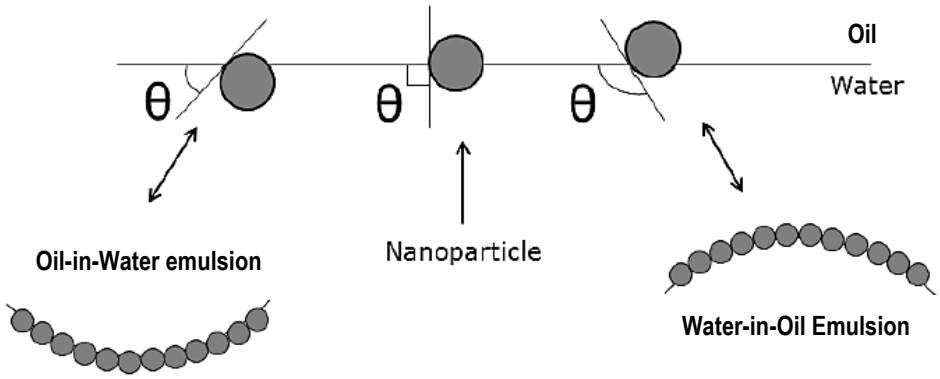


Figure 2.1: Contact angle on oil-water interface and its relationship to emulsion structure (Dickson et al, 2004)

One important aspect of utilizing colloidal particles as reservoir agents is to fulfill several actions that ensure their ability to be transported for long distances in porous media with almost no retention on rock surfaces. In addition, the dispersion of these particles should be stable and should withstand the harsh reservoir environment of high pressure, high temperature, and different salinity conditions and be able to perform their required commands based on their engineered purposes (Zhang et al., 2011). As a result, colloidal particles have to be designed according to these missions.

Several experimental studies have been conducted to test particle transport and adsorption in porous media. Chung (2013) discussed how "micro-size" particles have lower transport capabilities and higher retention, as well as reduction in pore volume and permeability due to their plugging. He noted that the use of nanoparticles instead of microparticles will enable them to travel long distances due to their small sizes. Caldelas and others (2011) have conducted several single-phase silica nanoparticle dispersion flow experiments in long columns filled with crushed sand and clay. The purpose of their work was to study nanoparticle retention for both surface-treated and untreated nanoparticles by varying several factors such as lithology, specific surface area of the medium, flow properties, salinity, and temperature. For the conditions studied for both coated and un-coated nanoparticles, retention in porous media is mainly dependent on the competition between adsorption, defined by van der Waals attraction between solid grain surface and nanoparticles, and desorption, which forms by Brownian motion and hydrodynamic drag. With other variables showing minor changes to the retention capacity, salinity was found to be the second factor to affect particles' solid grain attachment process. However, the type of nanoparticles' coating could impact retention capacity and offset the influence of other operating conditions such as salinity. In fact, series of sand-packed and core plug flow experiments revealed that with proper coating on both silica and magnetic nanoparticle' surfaces, the observed retention was below 10% of the amount injected into the porous media (Zhang et al., 2011). This observation was seen also in low permeability rock as well as larger concentrations of nanoparticle dispersions.

Nanoparticles coating is another major advantage of utilizing them as reservoir agents to promote for intelligent recovery processes. Besides insuring dispersion stability and transportability in porous media, the type of the particles and their surface treatment enables them to be tailored for different applications. The core material for the particles

can be made from benign silica or ferromagnetic substances which will response to an external magnetic field. Moreover, the external coating can be reactive, catalytic and or associative with the wetting nature of the particles which would enable them to be dispersed in several organic and non-organic solutions (Zhang et al., 2009). Surfactants' additives could be also employed through this surface treatment which is needed to maintain fluid interfaces, reduce surface tension, and/or perform other necessary actions based on surfactant type.

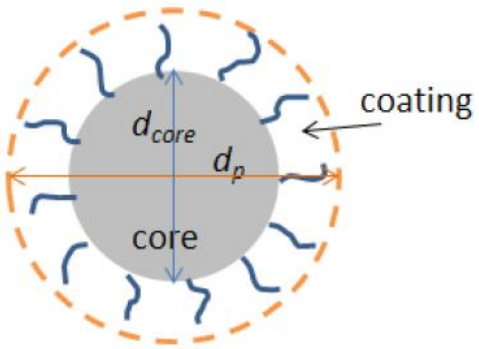


Figure 2.2: Schematic of a Surface-Treated nanoparticles (Zhang 2012)

### 2.2.2 Nanoparticles Emulsion in Porous Media

In general, foam can be formed via different mechanisms which will generate enough adsorption energy to bring the emulsifying agents to the interface between two immiscible fluids. In porous media, this has been observed to occur through two different processes 1) co-injection of fluids at high injection rate that is greater than the critical shear rate and 2) displacement of brine containing nanoparticle dispersion with octane or $CO_2$.

In the first process, both immiscible fluid with either one containing stabilizing agents or nanoparticles dispersion are injected spontaneously at high flow velocity. That velocity will result in the system having high kinetic energy which after a certain critical shear rate will cause the fluids to mix and the nanoparticles to adsorb at the interface. Espinosa (2011) and Roberts (2011) showed that co-injection of two fluids must exceed a certain critical shear rate for emulsion to form and be stable. In supercritical $CO_2$ and brine displacement, Espinosa (2011) measured the critical shear rate to generate CO2 foam stabilized by PEG-treated nanoparticles at 75 C and 1350 psi to be 2750 s-1. A similar work was performed by Roberts (2011), using decane at standard room conditions and estimated the critical shear rate to be about 8000 $s^{-1}$. However, this high shear will create a challenge from operational perspective, as achieving such shear rate is generally difficult. Also and as shown before, the critical rate depends on co-injection operating conditions such as pressure, temperature, and fluid system used to determine such rate. In addition, the implementation of using nanoparticles to generate foam should be based on processes associated with flow type, which is typically seen in porous media.

The main flow dynamics of major upstream operations in oil production involves one fluid displacing another fluid such as water injection as a part of improving oil recovery and maintaining field pressure. Immiscible fluid displacement is described as either drainage or imbibition depending on the rock's wettability. The wettability is defined as the tendency for one fluid to adhere to the solid surface (wetting phase) in presence of another immiscible fluid (non-wetting phase). Based on that, drainage is defined traditionally as the reduction of wetting phase saturation by non-wetting phase. Similarly, an increase in wetting phase saturation by displacing a non-wetting phase is known as imbibition. However, those definitions do not describe the case when porous media are intermediate or mixed wet. As a result and for the cases described in this thesis,

the reduction in dense phase (water) saturation is termed drainage while the increase in its saturation is called imbibition.

During water drainage process in water wet system, the interface of the least dense fluid (Octane or $CO_2$) invades pore throats of porous media due to the continuous increase in capillary pressure at the direction of the interface. The front will continue to invade until the interface reaches instability where it generates a critical curvature. Forcing the least dense fluid to drain the water out beyond this point will disrupt the system equilibrium stability of the interface causing the front to jump to the next available pore in a process known as Haines Jump (Haines, 1927; Melrose, 1965). During this process, a temporary reduction in the local capillary pressure is observed throughout the less dense fluid, and in particular is observed at the inlet of the pore body. If the magnitude of the reduction is large enough, the invading fluid will break (snap-off) inside the pore body (Roof, 1970). Roof snap-off will generally occur in smoothly constrained pore throats with small aspect ratio between pore throat and pore body (Kovscek et al., 2007). The snap-off condition is given by Peters (2012) below:

$$P_{snap} = \sigma\left(\frac{1}{r_n} - \frac{1}{r_t}\right) > \frac{2\sigma}{r_f}$$

In the equation above, $\sigma$ is the interfacial tension, $r_n$ is the throat inlet or neck radius, $r_t$ is the grain radius, and $r_f$ is the front curvature radius. A more rigorous condition due to Melrose (1965) recognizes that snap-off occurs when wetting phase volumes held at corners of the pore throat come into contact as curvature decreases. Application of this criterion to realistic pore geometry yields correct *a priori* predictions of drainage and imbibition phenomena, as reported by Gladkikh (2005).

As more droplets form inside the pore body, they coalesce and rejoin the upstream volume of invading fluid, and the invading fluid fills up the pore body. However, if nanoparticles are present and dispersed in water occupying the pores as both resident and wetting fluid, then it is hypothesized that Roof snap-off following Haines jump will provide the necessary adsorption energy to bring the particles to the interface and armor these droplets, hence , preventing them from merging together and filling up the pore body. As a result, $CO_2$ or Octane in water emulsion is created.

The adsorption energy (E) required to bring the nanoparticles to the $CO_2$ and water interface or Octane (Oil) and water interface is given by Binks and Horozov (2006) below:

$$E = \pi r^2 \sigma (1 - |\cos(\theta)|)^2,$$

where $r$ is the nanoparticle's radius, $\sigma$ is the interfacial tension between fluids, and $\theta$ is the contact angle as defined on Figure 2.1. The ratio between particles' attachment energy and the thermal energy indicate foam stability. As can be seen, the larger the ratio the easier for the particles to adsorb to the interface. Figure 2.3 illustrates the difficulty associated with stabilizing nanoparticles (oil-in-water) emulsion as the particle size increases from nano-scale to micro-scale. However, nanoparticle-stabilized foam tends to be more sensitive to thermal fluctuation. Despite that, 5-nm particles, for example, have a calculated adsorption energy of 43 kT which suggests that they are still unaffected by thermal variation.

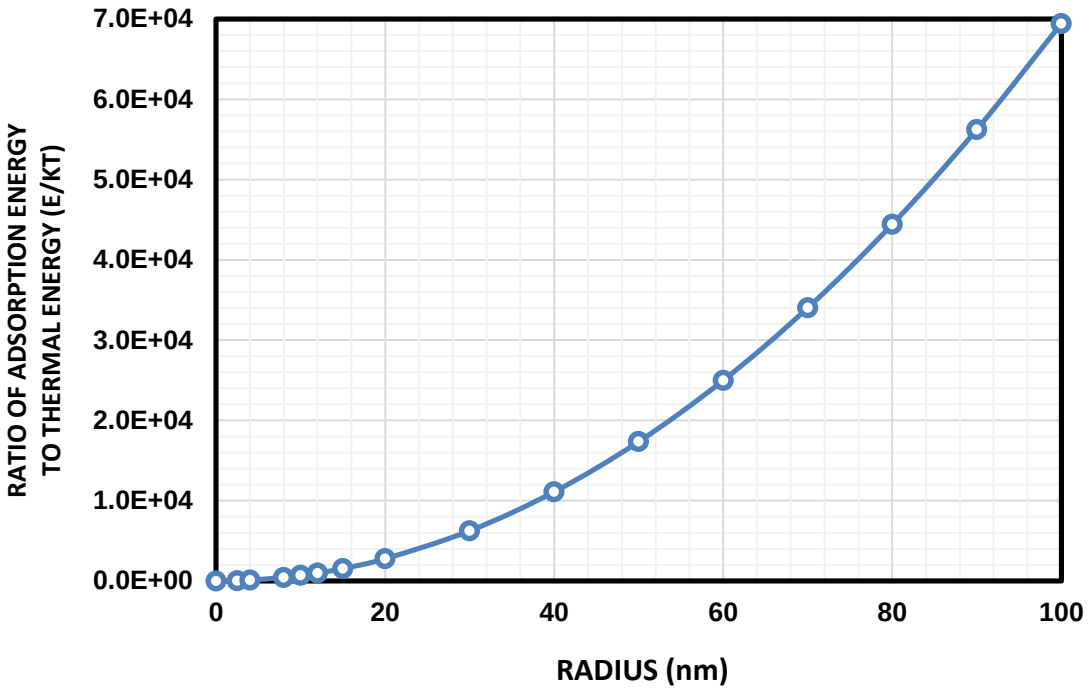


Figure 2.3: Attachment energy (E) of a spherical particular (Θ = 55 Degrees) at the planar n-octane-water interface as a function of particle radius.

### 2.2.3 Nanoparticles Impact on Displacement Dynamics

During fluid displacement, nanoparticle-stabilized emulsion indications have been observed in the displacement of brine containing nanoparticle dispersion by both $CO_2$ and Octane (Aminzadeh, 2013; Chung, 2013; DiCarlo et al., 2011). In all of the previous work, foam behavior was seen as a significant increase in pressure drop with a delayed breakthrough of either $CO_2$ or Octane. The increase in pressure drop was an indication of reduction in mobility due to the increase in the apparent viscosity of invading fluid which offsets the viscous fingering effect.

The findings of these experiments support the proposed hypothesis that Roof snap-off and Haines jump mechanisms are responsible for providing the necessary work

for pore scale emulsion generation. The test for this hypothesis was performed by running several water drainage experiments in water wet Boise sandstone cores. In some experiments, the core was initially saturated with 2 wt. % sodium bromide (NaBr) brine solution before it was invaded by Octane to mimic drainage in water wet conditions. The viscosity contrast between both fluids resulted in Octane fingers growing along with the displacement front due to Octane's higher mobility compared to brine. Other experiments replaced the sodium bromide solution with 1 wt. % sodium chloride (NaCl) and attempted the same displacement scenario. In both cases, the experiments were repeated after replacing the brine solution inside the core with (5 to 10 wt. %) nanoparticle dispersion in brine solution.

The displacement dynamics were scanned real-time using a modified medical CT scanner to track fluid phases at different cross sections starting from the core inlet. The experimental setup for the core flood is shown in Figure 2.4.

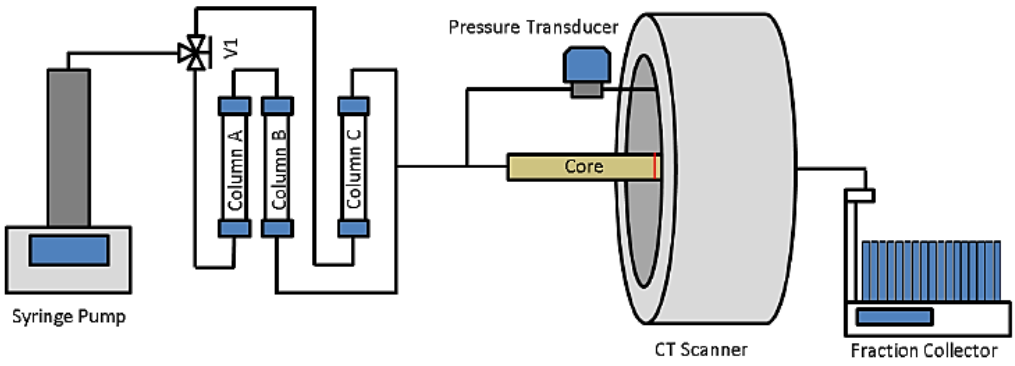


Figure 2.4: Schematic of the coreflood experiment for displacement of water and octane with CT scanner (Chung, 2013)

Placing nanoparticles in brine resulted in stabilizing the displacement pattern and decreased mean front velocity via emulsification. It is hypothesized that nanoparticles' armored droplets would disrupt the flow path by either plugging the pores or increasing the apparent viscosity due to emulsion generation. For both cases, this would translate into a larger increase in pressure drop and a latter breakthrough of Octane for the nanoparticle run compared to the case without nanoparticles (control) as shown in Figure 2.5.

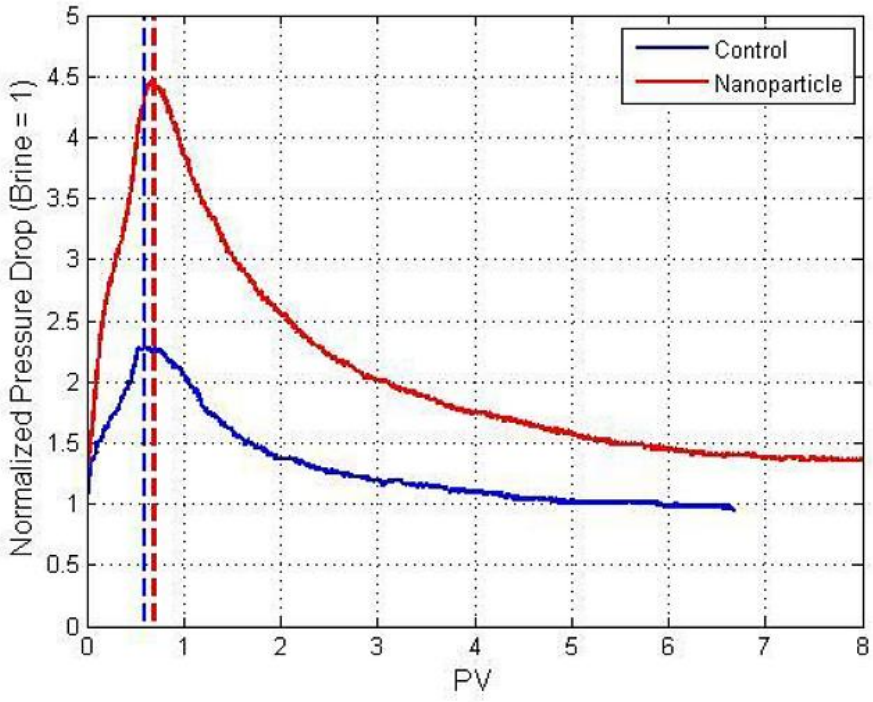


Figure 2.5: Pressured drop measurement vs. pore volume injected shown for drainage with nanoparticles (Red) and without nanoparticles (Blue). (Aminzadeh, 2013).

The observed reduction in mobility and front stabilization was captured using CT scanner. Figure 2.6 shows the scanner images for both the control and nanoparticle case

starting from the left (upstream of the core) to right (DiCarlo et al., 2011). The images were taken after injecting 0.1 pore volume (PV) into a Boise sandstone core fully saturated with 2 wt. % NaCl in one case and with nanoparticle dispersion in 2 wt. % NaCl in the other case. In those images, a 100% brine saturation is shown in red while full octane saturation is shown in blue. At the same image slice between the control and nanoparticle case, it can be noted that the scans from the nanoparticle case show less lateral variation of octane saturation compared to the control case. Also, it is important to highlight how octane was breaking through at the 5' position in slice number 9 for the control experiment. However, looking at the same position in the nanoparticle case indicate that octane has not yet arrived to this location.

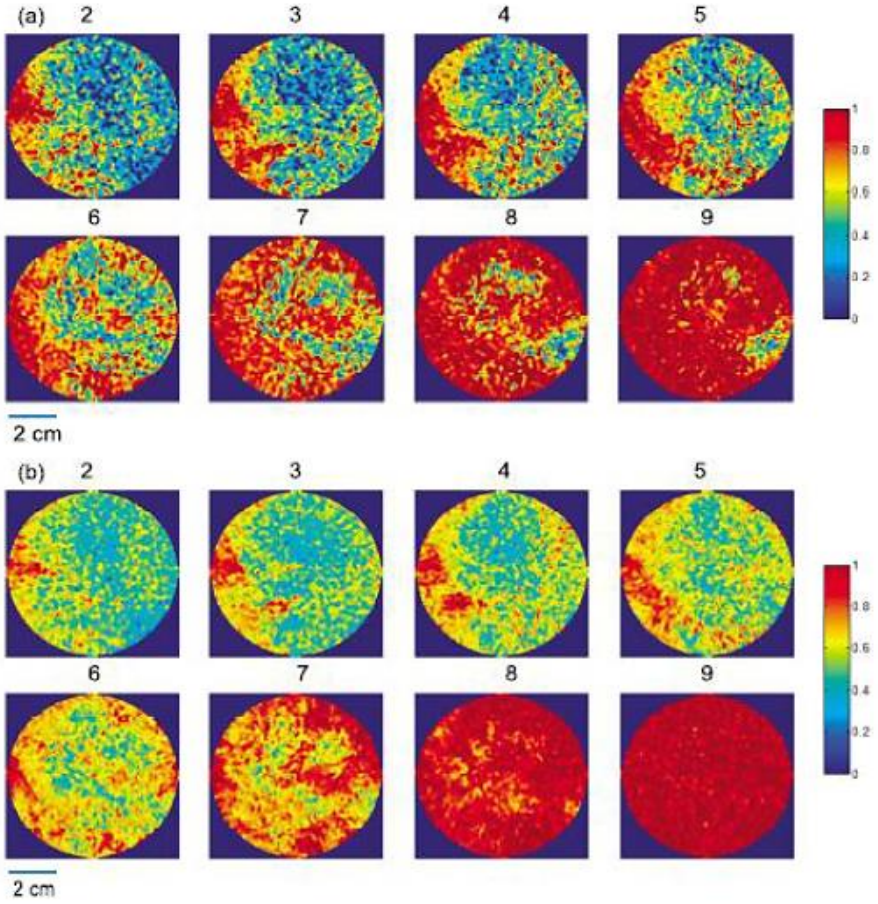


Figure 2.6: CT scans for n-octane injection into Boise sandstone core initially filled with a) 2 wt.% brine and b) 2 wt.% brine with 10 wt.% nanoparticles, each after injection of 0.1 PV (DiCarlo et al., 2011).

The ability to generate foam with nanoparticles, utilizing pore scale events such as Haines jump and Roof snap-off, has made it possible to employ those emulsifying agents for improving the efficiency of $CO_2$ trapping and flooding for enhanced oil recovery. It is really of primary importance to expand on this innovative approach for using nanoparticles for other upstream and downstream applications. Therefore, it is essential to further test the hypothesis that Haines jump and Roof snap-off, which occur

during water drainage in water wet rock, is the sole mechanism to create the needed conditions for emulsion to form.

The existing idea suggests that these pore scale events occur during the displacement of wetting fluid by non-wetting fluid in a core fully saturated with the wetting fluid. In addition, the hypothesis does not address fluid properties as a factor in the foam generation process in porous media. As a result, this thesis will further investigate this claim by conducting core flood experiments in both water-wet and oil-wet systems to capture the effect of rock's wettability on nanoparticle displacement performance. If the current hypothesis still hold strong, evidence of nanoparticle-stabilized emulsion may be observed during the imbibition displacement of hydrocarbon-nanoparticle dispersion by the aqueous brine solution in oil-wet system. In this research work, emulsion generation indications during the experimental displacement will be monitored through pressure drop measurement, fluid mobility ratio predictions, and residual saturation calculations. If emulsion signs are not observed during water-wet imbibition and oil-wet imbibition; then, other factors besides pore scale jump and snap-off mechanisms would contribute to the conditions needed for generating emulsion in porous media. These factors could be dependent on fluid properties such as density and viscosity as well as nanoparticles' wetting nature (hydrophilic vs. hydrophobic).

# Chapter 3: Research Hypothesis and Objective

## 3.1 INTRODUCTION

This chapter mainly discusses the objective of this research study and the hypothesis to be tested. Based on the findings and observations of previous work by DiCarlo (2011), Aminzadeh (2013), and Chung (2013), it is hypothesized that pore scale events of both Haines jump and Roof snap-off, which occur during the displacement of wetting phase by non-wetting phase, are responsible of providing the necessary work to bring nanoparticles to the interface of the two immiscible fluids once they are present in the system. Those events will cause nanoparticles to armor disconnected snapped-off droplets to not merge with each other and form nanoparticle-stabilized emulsion.

Because sings for nanoparticle-stabilized emulsion have been observed during the displacement of the aqueous phase containing nanoparticles by non-wetting hydrocarbon phase in water-wet setting. Our main hypothesis is to test the displacement of a wetting hydrocarbon phase containing hydrophobic nanoparticles by another non-wetting aqueous phase such as brine solution and check if nanoparticle-stabilized emulsion symptoms are present in addition to determining those factors impacting the process for nanoparticle-stabilized emulsion generation. Along the way, we attempt to observe any interesting behavior that the particles will have on the displacement.

This hypothesis will be examined by conducting several core flood experiments under both water-wet and oil-wet condition utilizing different viscosity fluids in order to address the effect of viscous stability, rock wettability, and nanoparticle wettability on emulsion generation process. As the emulsion phase is not observed in the effluent samples during these flow experiments, other, indirect signs of emulsion generation are used to decide on the likelihood of emulsion creation inside porous media. Some of these signs were observed during the previous work by DiCarlo (2011), Aminzadeh (2013),

and Chung (2013). They are based on the recorded pressure drop data as a function of time for both control (no nanoparticle in any fluid) and test (nanoparticles present in one fluid phase) runs. The pressure drop data will be used to calculate the pressure drop ratios (mobility reduction factor). Also, the tests include measuring effluent fluid mass histories to calculate the residual fluid saturation inside the core. This information along with fluid viscosity data can be used to also estimate the displacement end point relative permeability of the invading phase. During each experimental evaluation, symptoms like excessive pressure drop build up, where "excessive" means it exceeds the viscosity ratio between brine and nanoparticle-brine dispersion of 1.18, is indication of multiphase flow and the generation of more viscous phase inside the core. The sharp increase in pressure drop is also attributed to relative permeability effect as changes in either phase saturation will affect the pressure drop build up behavior. The presence of nanoparticles is hypothesized to armor the disconnected droplets of the non-wetting phase during the invasion process. As more of the non-wetting phase is trapped in a form of nanoparticle-stabilized emulsion, this caused the relative permeability of the non-wetting phase to be reduced as flow fraction for the non-wetting phase is now more restricted.

Also, reported findings based on CT scan imaging by Aminzadeh (2013) and Chung (2013) confirmed trapping more of the invading non-wetting fluid during drainage type displacement in water-wet porous media. In consequence, reduction in resident fluid residual saturation is expected. They have shown that as well as reduction in the end point relative permeability. For experiments involving nanoparticle runs, the nanoparticle dispersion is placed in either brine solution or the hydrocarbon phase depending on the experimental protocol intended to be tested. For experiments involving hydrophilic nanoparticles, the particles are placed in brine at all time and were either displaced by hydrocarbon phase during drainage experiments or injected with brine solution during

imbibition tests. As the last experiment for this study is designed to test the main hypothesis of this research, hydrophobic particles is placed in the hydrocarbon phase to be displaced by brine solution.

In all of these tests, the stability of the displacement as well as the effect of rock's wettability are to be addressed to see their impact on the displacement dynamics since they tend to control the physics of how fluids flow inside the rock. As a result, it is important first to review displacement mechanisms involving the displacement of two immiscible flow from wettability and displacement stability perspective.

## 3.2 REVIEW OF DISPLACEMENT MECHANISMS IN POROUS MEDIA

As the hypothesis for this project is based on pore scale displacement events, it is important first to understand the processes that govern the displacement profile for two immiscible fluids. Immiscible displacement, as described before, is classified as either imbibition or drainage. The type of the displacement in this thesis is based on the increase or decrease of the dense phase saturation, which is water or brine solution in this case. As a result, the injection of brine solution or nanoparticle dispersion in brine into the core is called imbibition. Similarly, a reduction in the saturation of brine solution or nanoparticle-brine dispersion by another immiscible fluid is categorized as drainage.

The displacement stability for both drainage and imbibition is determined by evaluating two important numbers, namely, the mobility ratio and capillary number. The mobility ratio (M) is defined as the ratio between the injected (2) and displaced (1) phases and is given by:

$$M = \frac{\lambda_2}{\lambda_1} = \frac{k_{r2}\mu_1}{k_{r1}\mu_2}$$

where $\lambda$ is the phase mobility, $k_{ri}$ is the relative permeability for phase $i$, and $\mu_i$ is the viscosity of phase $i$. $i$ is denoted by (2) for the injected phase and (1) for displaced phase. End point relative permeability, at the end of the displacement when resident fluid saturations reach residual state, is used to estimate the endpoint mobility ratio. For one dimensional horizontal displacement (no gravitational force), this ratio provides an idea about the displacement stability from viscous fingering perspective. If the value of M > 1, the displacement is generally classified as unstable while if M < 1, the displacement is then stable with less or no viscous fingering.

The second stability indicator for one dimensional flow is capillary number $N_{ca}$. This number is defined as the ratio between viscous forces and capillary forces as described below:

$$N_{ca} = \frac{v_2 \mu_2}{\sigma cos\theta}$$

Where $v_2$ and $\mu_2$ are the velocity and the viscosity of the injected phase and $\sigma$ is the interfacial tension between both phases. $\theta$ represents the contact angle between fluids. Capillary number is usually used to generate capillary desaturation curves as shown in Figure 3.1. This plot shows how residual fluid saturation decreases as the capillary number increases for both wetting phase and non-wetting phase.

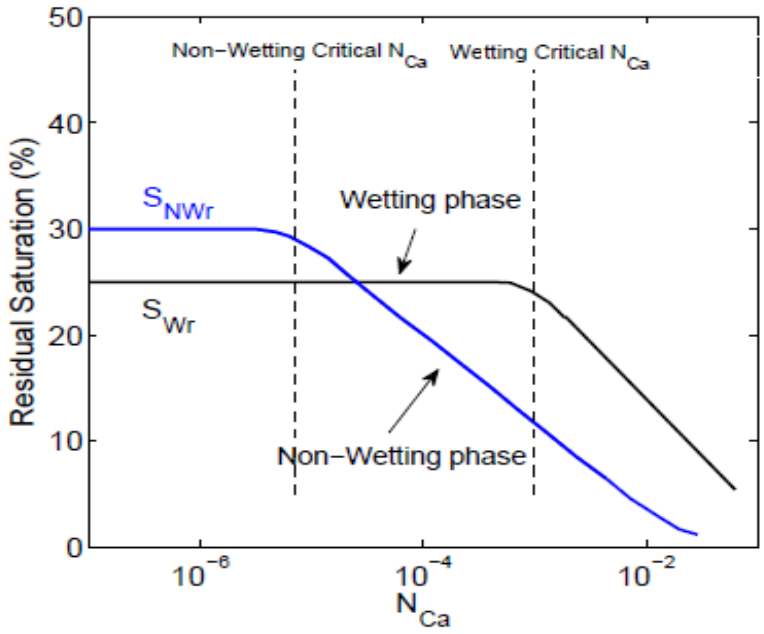


Figure 3.1: Capillary desaturation curve in a well sorted fairly homogeneous porous medium shown for both wetting phase (black) and non-wetting phase (blue), (Lake 1989).

Similar to the mobility ratio, capillary number controls the stability of the displacement from capillary fingering point of view. Capillary fingering has been observed usually at extreme low viscous forces conditions when capillary forces dominate. This effect will be magnified with increasing rock's heterogeneity. Typically, a capillary number greater than $10^{-5}$ suggest that viscous forces dominate and capillary fingering is small or negligible. However, if this number is reduced below $10^{-5}$, then capillary forces dominate the displacement. (Aminzadeh, 2013)

The values of the mobility ratio and capillary number control the stability of the displacement. Regardless of whether the displacement is drainage or imbibition, those numbers are affected by rock wettability, fluid viscosities, and interfacial tension. In

addition to these factors, the distribution of fluids inside porous media determines how one fluid displaces another under different conditions.

During drainage flow, water is being displaced out by another immiscible phase, which is an oil-like hydrocarbon phase. The pore scale displacement mechanisms are dependent on the wettability of the rock. If the rock is water-wet, a local increase in non-wetting hydrocarbon saturation happens through Haines jump. During this jump, the pressure becomes high enough for the hydrocarbon fluid to pass through throats and jumps to the next available pore entries as long as that pressure exceeds the capillary pressure required to access those pores. As described by Aminzadeh (2013), this pore scale event is known as converging-diverging pore-throat displacement. Roof (1970) showed that during this jump, an invading oil trying to displace water in water-wet rock will experience a local reduction in capillary pressure as the interface between both fluids attempts to jump to the next pore throat. This will create local instability for the non-wetting phase (oil) at the pore entry causing it to snap-off and form a droplet inside the pore body. As more droplets form inside the pore body, they merge together into single phase and fills up the entire pore body to displace the water in this case Figure 3.2 describes this process in stages.

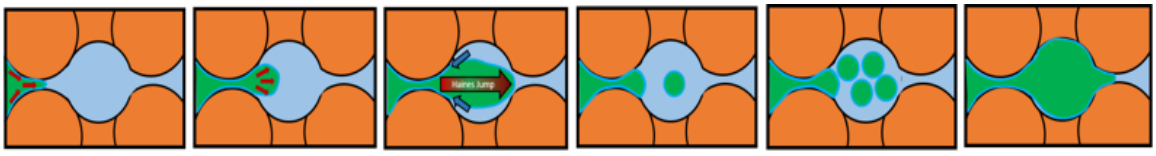


Figure 3.2: Schematic of Haines jump and Roof Snap-off process during wetting phase (light blue) displacement by non-wetting phase (green) in a single-constricted channel consisting of narrow pore throats leading to large pore bodies filled with wetting phase without nanoparticles.

Both Haines jump and Roof snap-off are reported to be occurring during the displacement of wetting phase by non-wetting phase. In fact, those processes are most likely to occur in smoothly constricted pores that has the ratio of pore throat to pore body to be small as described by Kovscek (2007). This suggests that similar to the water displacement by non-wetting (oil) fluid in water-wet rock, those types of mechanisms are likely to occur as well whenever oil-like fluid is displaced by water in oil-wet conditions.

As for non-wetting phase displacement by wetting phase such as water invading a water-wet core that is saturated with oil, this displacement as per the definition stated before is known as imbibition since water saturation is increasing in this case. If the rock is water-wet, the horizontal one dimensional imbibition is generally stable and the front travels in a piston like manner, assuming that water viscosity is larger than oil viscosity otherwise it is unstable from viscosity ratio perspective. If the rock is oil-wet, the displacement is still viscously stable based on the assumption that water viscosity is larger than oil viscosity. However, in this case, it would be much more difficult to displace the oil in the same way that was described when the rock is water-wet. This is because of the wettability effect as the capillary forces are larger in this case and additional viscous drag is needed to recover oil from oil-wet surfaces. Therefore, unlike water imbibition into water-wet rock, there is a chance for fingering effect to form. The severity of the finger perturbation is dependent on rock's heterogeneity as well as oil viscosity.

In general, imbibition is associated with two main pore scale events. One is called piston like displacement and the other one is known as snap-off. For piston like displacement, both pore throats and bodies fills up as water front advances. This type of displacement is typical for water-wet system with oil having a lower viscosity compared to invading water. On the other hand, imbibition snap-off is different than that of Roof

snap-off discussed before. In this case, snap-off filling can happen anywhere in porous media and is a function of pore size distribution, throat geometry and capillary pressure. The process can occur through the layer flow (film flow along wetted grain surfaces) ahead of the main wetting (water) front. As wetting fluid in the corners of pores start to expand as a result of decrease in capillary pressure, snap-off will occur as soon as these corners become connected to each other. Another possibility is when variation in throat sizes and geometry can lead into having the wetting phase front advances faster in some parts of the pore network which eventually block the displaced oil coming from slower displacement throats and pinch it out and leave it behind.

Understanding these pore scale events in both drainage and imbibition in both oil-wet and water-wet is of primary importance to examine the hypothesis of this project. Moreover, determining whether the displacement is stable or not could play a significant part in either magnifying or offsetting these pore scale events.

## 3.3 RESEARCH HYPOTHESIS

This study continues to evaluate the existing hypothesis that Roof snap-off which occurs during Haines jump is the key mechanism to generate nanoparticle-stabilized emulsion during immiscible displacements. As those processes are observed during the displacement of wetting phase by non-wetting phase, then, it is likely to find these pore scale events occurring during water displacement by oil in water-wet core (Drainage in water-wet) as well as water injection into an oil saturated core that is oil-wet (Imbibition in oil-wet). Following work by DiCarlo (2011), Aminzadeh (2013), and Chung (2013) indicated several features in the displacement performance during drainage in water-wet system, where octane or $CO_2$ displaced brine-nanoparticle solution. These features

include sharp increase in pressure drop response, residual calculation increase for octane or $CO_2$, and most importantly more stabilized octane or $CO_2$ invasion with reduced fingering effect observed by CT scanner. As explained before, once the droplets of non-wetting phase such as octane or $CO_2$ form inside the pore body, it is hypothesized that Haines jump and Roof snap-off which cause these droplets to form will provide the necessary adsorption energy for the nanoparticles of the right surface coating to armor the droplets preventing them from merging together as illustrated in Figure 3.3. This process requires nanoparticles to be in the displaced phase in order for them to stabilize a displacing-phase-in-displaced phase emulsion. In other words, for water-wet porous media, oil-in-water emulsion is generated during the displacement of the aqueous dispersion of nanoparticles by non-wetting hydrocarbon phase. Similarly, for oil-wet rock, water-in-oil emulsion is stabilized during the invasion of the aqueous phase into a core saturated with oleic dispersion of nanoparticles.

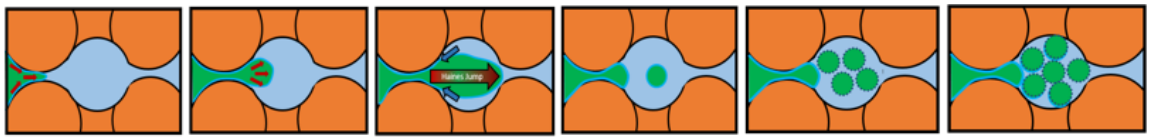


Figure 3.3: Schematic of Haines jump and Roof Snap-off process during wetting phase (light blue) displacement by non-wetting phase (green) in a single-constricted channel consisting of narrow pore throats leading to large pore bodies filled with wetting phase containing nanoparticles. Droplets of non-wetting are armored by nanoparticles (dark blue).

All in all, the objective of this research work is to examine the previously discussed claim by conducting series of core flooding experiments in permeable Boise sandstone under both water-wet and oil-wet conditions. These evaluation tests will be conducted in a sequence changing one variable at a time. The first variable to change is

the wettability of the rock. Next, the viscosity of the hydrocarbon phase is changed to alter the viscous stability of the displacement. In most of the experiments, nanoparticles are placed in the aqueous phase. However, in the last experiment, we attempt to flow brine to displace oleic dispersion of nanoparticles under oil-wet conditions. The aim is to confirm whether the hypothesis will still hold true for water imbibition into an oil-wet core saturated with oil phase containing nanoparticles. This is performed to build on the similar case of water drainage by oil in water-wet core. Nanoparticle-stabilized emulsion is expected to from whenever non-wetting phase is trying to displace wetting phase at the presence of nanoparticles. This is because of the fact that in such displacement scenario, non-wetting phase fluid will go through the mechanism of snapping off during Haines jump process.

As discussed before, we will carefully monitor the indirect indicators for nanoparticle-stabilized emulsion. On the other hand, if nanoparticle-stabilized emulsion features are not observed during water imbibition in an oil-wet core saturated with hydrocarbon phase containing nanoparticles, there might be some factors contributing to that process other than Roof snap-off and Haines jump mechanisms. In summary, this experimental evaluation study aims to conduct several core flooding operations by varying different conditions. The tested conditions include changing rock's wettability, displacement viscous stability and sequence by including a post flush, and finally nanoparticles wettability from hydrophilic to hydrophobic. The experiments were performed in sequence by varying one variable at a time in order to accurately evaluate the impact of rock wettability, displacement stability, fluids density and viscosity, and nanoparticles wettability on the emulsion generation process. At the end, the research provide a much more refined explanation for the factors that may or may not promote for nanoparticle-stabilized emulsion to from in porous media.

# Chapter 4: Materials and Methods

## 4.1 Overview

This chapter presents the experimental design and procedures followed in order to gather the data needed to meet the research objectives. Several core flooding were conducted on Boise sandstone cores using a brine solution and oil-substitute alkanes (n-Octane and n-Tetradecane) with different viscosity values to vary displacement viscous stability conditions. The experiments were repeated after flushing the core with a proper solvent (Isopropyl alcohol or Acetone) and replacing the brine solution with surface-treated nanoparticles dispersed in brine. The experimental runs were conducted under low-pressure and room temperature conditions. In some of these experiments, the wettability of porous media was adjusted from being water-wet to oil-wet in order to examine the wettability effect on the displacement dynamics. While in this study, drainage is defined as a decrease in water (brine) saturation as it is being displaced by anther fluid, imbibition is the displacement type that involves brine solution injection into the core. During the displacement, pressure drop trends and residual fluid calculations were measured and recorded to assess the potential for foam generation as well as indicate any effect on flow dynamics.

## 4.2 Experimental Design and Setup

This section lists all the materials and equipment used to complete all of the experiments. In addition, experimental procedures are described in details along with the set-up schematics used during each stage of the experiments.

### 2.2.3 Materials

Table 4.1 lists the materials used in preparing the core and chemical solutions needed for flooding experiments. All experiments were conducted in a foot-long (30.48 cm) Boise sandstone cores with one inch diameter (2.54 cm). Because all experiments were conducted at low-pressure lab conditions (generally less than 75 psi), there was no need to deploy core holder. Instead, sandstone cores were epoxied either inside polycarbonate tubing (PC) or polyetherimide tubing (ULTEM) depending on fluid chemical resistance and compatibility. The epoxy core preparation steps are detailed in Appendix A1. A bench was used to serve as the setup main structure necessary to support the system which include the epoxied core, flow tubes, valves, and other glass accumulators during the displacement. A schematic showing the bench dimensions is shown in Figure 4.1.

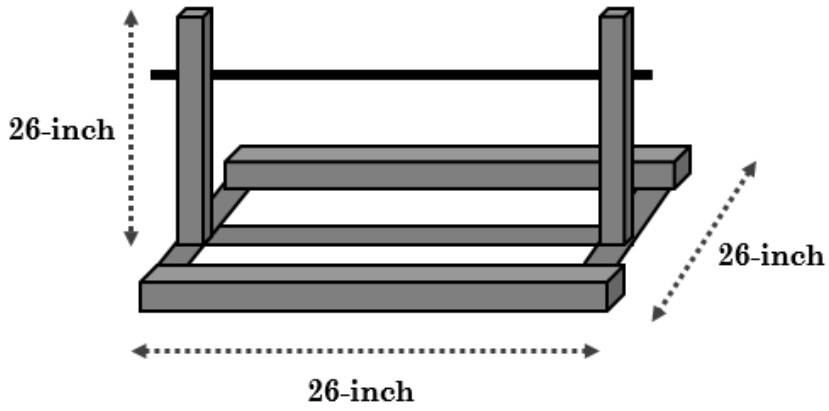


Figure 4.1: Schematic of the experimental bench used for displacement tests with dimensions.

| List of Material Used For Experiments | |
|---|---|
| Core Epoxy Preparation | • Polycarbonate (PC) Tubes<br>• Polyetherimide (ULTEM) Tubes<br>• End Caps<br>• 5-mintue epoxy (Devon)<br>• Epoxy Resin (Miller-Stephenson EPON Resin 828)<br>• Hardener (Miller-Stephenson Versamid 125)<br>• Rubber Stopper and Wax Papers |
| Setup and Equipment | • PFA Tubing and Fittings<br>• 2-Way and 3-Way Valves (Swagelok)<br>• Glass Columns Accumulators (Kontes Chromaflex)<br>• Syringe Pump (Teledyne ISCO model 1000D)<br>• Vacuum Pump (Emerson model C63CXGZP-4780)<br>• Peristaltic pump (Masterflex L/S model 07522-20)<br>• Peristaltic pump Viton Tubing (Model 96412-16)<br>• Pressure Drop Transducer (Rosemount)<br>• Fractional Collector (Teledyne ISCO Retriever 500)<br>• Thermo-Scientific Barnstead E-Pure System<br>• PC with LabVIEW connected to Pressure Gauge |
| List of Fluids and Chemicals | • Deionized Water ($H_2O$)<br>• 5 nm Surface-Treated Nanoparticles as a dispersion of 20 wt.% in Water (Nissan EOR-5XS)<br>• 10 nm silica particles dispersed in toluene as 40 wt. % in Toluene (Nissan TOL-ST)<br>• Sodium Chloride (NaCl) – 99% Pure (FisherScientifc)<br>• n-Octane ($C_8H_{18}$) – 97% Pure (ACROS)<br>• n-Tetradecane ($C_{14}H_{30}$) – 99% Pure (ACROS)<br>• Hexane ($C_6H_{14}$) – 97% Pure (FisherScientifc)<br>• 2-Propanol (IPA) ($C_3H_8O$) – 97% Pure (FisherScientifc)<br>• Toluene ($C_7H_8$) – 97% Pure (FisherScientifc)<br>• Dichlorodiphenylsilane ($C_{12}H_{10}Cl_2Si$) – 99% Pure (ACROS)<br>• Chlorotrimethylsilane ($C_3H_9ClSi$) – 97% Pure (ACROS) |

Table 4.1: List of equipment, materials, and chemicals used to achieve research objective.

### 4.2.2 Core Preparation

***Core Epoxy Preparation***

Several cores were cut from a Boise sandstone block unit with each core having different porosity and permeability. The core dimensions were set to be one-foot long and one-inch diameter in order to assess one-dimensional flow displacement behavior with and without nanoparticles being present in the system. As a cheap and fast substitute to using a standard core holder, a total of ten cores were epoxied inside different tubes with different end caps. Tubes with end caps made of polycarbonate (PC) materials were used mainly for experiments conducted under water-wet conditions. On the other hand, cores intended for oil-wet core flood evaluation had to go through a wettability alteration process to change their wettability from water-wet to oil-wet. Such process involves using some corrosive chemicals such as hexane, acetone, and organosilane solutions that are not compatible with PC. Therefore, a much more resistant ULTEM tubes and end caps were used for core preparation prior to oil-wet experiments. Core epoxy steps are detailed in Appendix A1.

***Vacuum-Saturation***

Prior to starting the core flood experiments, the wettability of the core will either be left as is (water-wet) or adjusted (oil-wet). In addition, it has to be saturated with the right initial fluid as per the experimental protocol. Sometimes cores are cut while they are partially saturated. In such case, the core has to be heated and dried inside an oven for at least 20 hours at a temperature range of 85 to 100 degrees C. This need to be completed first prior to proceeding with any further preparation steps. Once that is ensured, the core is then vacuumed with a vacuum pump which applies a pressure of -27 in Hg (-0.4 psi) to

remove any trapped air. The setup used for core vacuuming and saturating is illustrated in Figure 4.2. As shown, the pump is connected to a flask full of desiccants to prevent fluid moisture to travel to the pump. In this process, the core is mounted on a stand vertically with the top being connected to the vacuum pump. The bottom of the core is then connected to a glass accumulator placed vertically higher than the core to utilize gravity to force fluid into the core during the saturation process. The glass column is then filled with the initial fluid residing the core.

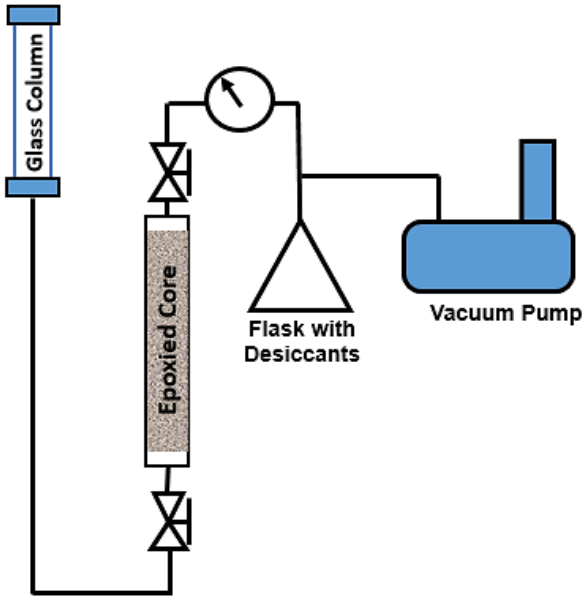


Figure 4.2: Schematic of the vacuum and saturation set-up

Once the vacuum-saturation system is set, the following steps describe the method used to vacuum and saturate the core implemented in this study as follow:

1. Starting with all valves at the top and bottom being closed, open the valve at the top of the core and switch on the vacuum pump. Ensure that the valves at the bottom is closed throughout this stage.
2. Keep vacuuming the core for at least 10 hrs. The vacuum pressure can be read from the pressure gauge connected to the pump and should maintain constant value (- 27 in-Hg).
3. Once vacuum is complete, take off the core from the stand and measure the dry weight of the core prior to saturating it with intended initial fluid. Record the dry weight.
4. Mount the core back again to the stand and ensure all valves are closed.
5. With top valve closed and connected to the vacuum pump, open the valve at the bottom and let fluid inside the glass accumulator imbibe inside the core. Allow some time for this process to take place and wait until the fluid inside the glass column is not changing.
6. Vacuum may be applied to ensure that the core is completely saturated. After that, the core weight is measured and recorded. The pore volume of the core is then calculated as per the equation below:

$$Pore\ Volume\ (PV) = \frac{W_{wet} - W_{dry}}{\rho_i}$$

This vacuum and saturating approach was even optimized beyond the procedure listed above to ensure that no trapped air is held inside the core. This was completed by considering degassing the initial fluid residing the glass accumulator. Also, after

vacuuming, $CO_2$ gas is then allowed to flow through the core. After that, the core is vacuumed again before pumping $CO_2$ back again to the core. This processes is needed so that $CO_2$ displaces any trapped air and it has more solubility in water compared to air. Once the $CO_2$ and vacuuming sequence is conducted for at least two times. The core is then vacuumed again and dry weight can then be measured. During this time, the degassed initial fluid is allowed to imbibe by cracking the bottom valve to be slightly open to control imbibition rate to not exceed 1 ml/min. This is done while the core is still being vacuumed and that the top valve is still open. Once breakthrough of the initial fluid is observed, the bottom valve is then fully opened and the vacuum pump is switched off and the core is given sometime for natural flow due to gravitation forces to push any trapped air out. Once continuous phase of fluid is observed flowing at the outlet of the core, the core top and bottom valves are then closed and core wet weight is then measured.

***Wettability Modification***

For experiments designed for water-wet cores, no wettability alteration is needed as the silica surfaces of the Boise sandstone are initially water-wet. As a result, the core can then be dried first at an oven before proceeding to the vacuum-saturation stage as discussed in the previous section. On the other hand, studying the effect of nanoparticles on the displacement behavior for oil-wet cores requires a wettability alteration process to be conducted first. In this experiment, the sandstone grains are to be treated chemically so that rock surfaces become water-repellent. In this project, a wettability change protocol described by Mohanty was implemented to alter the wettability of the core to make it hydrophobic. By now, the core has already been heated as well as vacuumed and

saturated with initial fluid. For all wettability modification experiments, the initial fluid was set to be hexane as it will be used as part of alteration process. The change in wettability from water-wet to oil-wet was achieved by performing the following steps:

1. Setup the wettability modification apparatus as shown in Figure 4.3. The experiment is to be conducted inside the fume hood for health and safety reasons.
2. Prepare 7 wt. % Dichlorodiphenylsilane (DCDPS) in Hexane and 7 wt. % Chlorotrimethylsilane (CTMS) in Hexane.
3. Start by taking the pump intake suction tube to Hexane container and start pumping at 5 ml/min to saturate the core with 2 pore volumes (PV) of Hexane.
4. Shutdown the pump and take the intake suction tube to the second container containing the solution of 7 wt. % DCDPS in Hexane and start up the pump to pump nearly 5 PV of the solution keeping the same flowrate of 5 ml/min.
5. Shutdown the pump again and place the intake suction tube back into the Hexane container and pump nearly 5 PV Hexane.
6. Then displace it with nearly 5 PV of 7 wt. % CTMS in Hexane.
7. After that, pump nearly 5 PV again of Hexane into the core.
8. Finally, displace the Hexane with 5 PV of n-Octane or n-Tetradecane depending on the experimental protocol for the core displacement which will be conducted next.

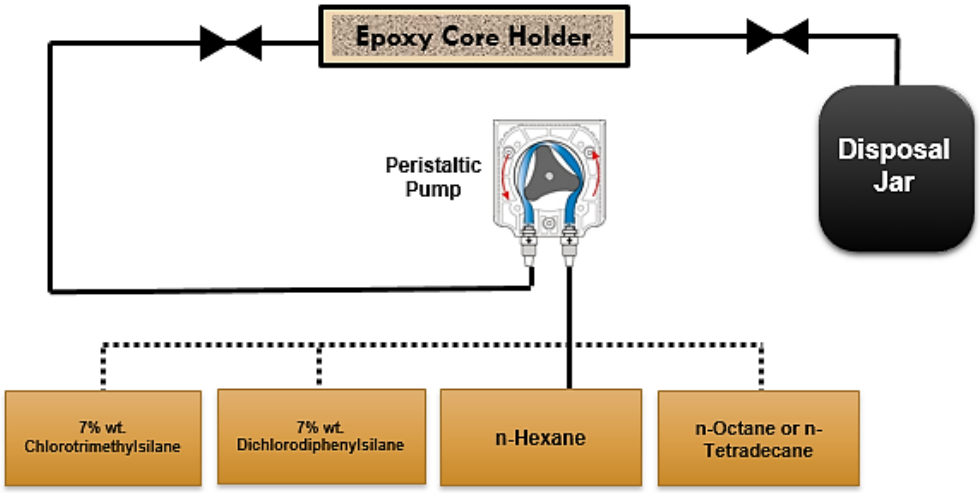


Figure 4.3: Schematic of the wettability modification experimental setup. Dashed lines represent upcoming displacement steps as discussed in details in the procedure

In this procedure, the core had to be heated first at an elevated temperature that is greater than 80 degrees C for at least 20 hours before it was vacuumed and saturated with hexane. This step is significant in order to eliminate any water that is physically adsorbed to the grain surfaces. Once all adsorbed water is removed, the silica surfaces are going to be left with hydroxyl groups (≡Si—O—H). It is important to highlight that all organosilane solutions used in this modification process are very sensitive to water and water moisture. As a result, it is recommended to handle this stage of core preparation with the core having minimum exposure to the air. The fundamental mechanism for wettability alteration was based on the chemical reaction of DCDPS with hydroxyl group. The product of this reaction will establish a strong attachment bond between the oxygen on the silica surfaces and silicon-phenyl group of the DCDPS. As the silicon atom is still attached to the two phenyl (benzene) groups, those groups will create an external layer which makes the rock surface now hydrophobic. Figure 4.4 shows how the reaction takes

place during the wettability modification process. According to Unger (1979), DCDPS is believed to react monofunctionally with hydroxyl group. This means that one out of the two chlorine atoms will react with the hydrogen atom of the hydroxyl group, thus, leaving some surfaces still unreacted and hydrophilic. Therefore, CTMS was pumped after the DCDPS to react with the untreated sites and ensure that all water-wet (≡Si—O—H) surfaces were converted hydrophobic (≡Si—O—Si $(C_6H_5)_2$)

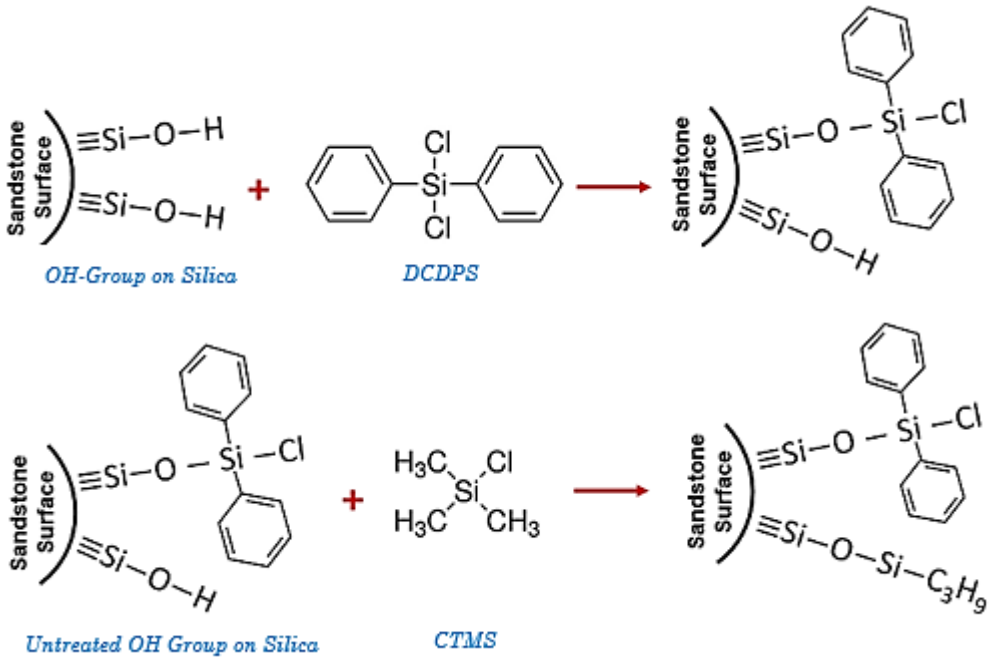


Figure 4.4: Diagram showing the wettability modification reaction to synthetically change the hydrophilic surfaces to hydrophobic surfaces by two steps chemical reactions involving DCDPS (upper reaction) and followed by CTMS injection in the second step. (Unger 1979).

## 4.3 FLUID DISPLACEMENT EXPERIMENTAL PROCEDURE

This section describes the procedures performed to conduct one dimensional flood into both water-wet and oil-wet sandstone cores. For water-wet, the core flooding operation was conducted right after the vacuum-saturation stage. As for oil-wet cores, fluid displacement was performed post the wettability alteration experiment. Each displacement experiment is divided into two main runs. The first run is called control which does not include the use of nanoparticles during the experiment. Also, during this experiment, single phase permeability is measured as will be described in details in the upcoming section. The main goal for the control run is to establish a baseline for the displacement behavior. The second run involves utilizing nanoparticles during the core flood operation and is termed nanoparticles run. In all of the flooding experiments presented in this research, the impact of nanoparticles on the displacement will be evaluated based on pressure drop response, mobility reduction factors, residual fluid saturation, and breakthrough time of the main displacement front. Therefore, all experiments were conducted while measuring and recording the following parameters to assess the previously mentioned impact indicators:

- Fluid density and viscosity.
- Pressure drop response recorded via a pressure transducer and recorded by LabVIEW in a computer.
- Fluid effluents are collected during the displacement using a fraction collector.

The experiments will be conducted in sequence by varying one condition at a time while maintaining other factors constant to reduce the number of variables. This is needed in order to narrow down those conditions that contribute to the generation of nanoparticle-stabilized emulsion. These testing conditions include changing the

wettability from water-wet to oil-wet, changing the viscosity of the resident fluid to create viscous instability, and finally changing the wettability of nanoparticles by switching from hydrophilic nanoparticles to hydrophobic ones.

### 4.3.1 Control Experiment and Permeability Measurement

Figure 4.5 shows the main experimental setup for core flooding. The dotted lines indicate flow path and direction. As stated before, this run serves as a base case to evaluate displacement performance with no presence of nanoparticles.

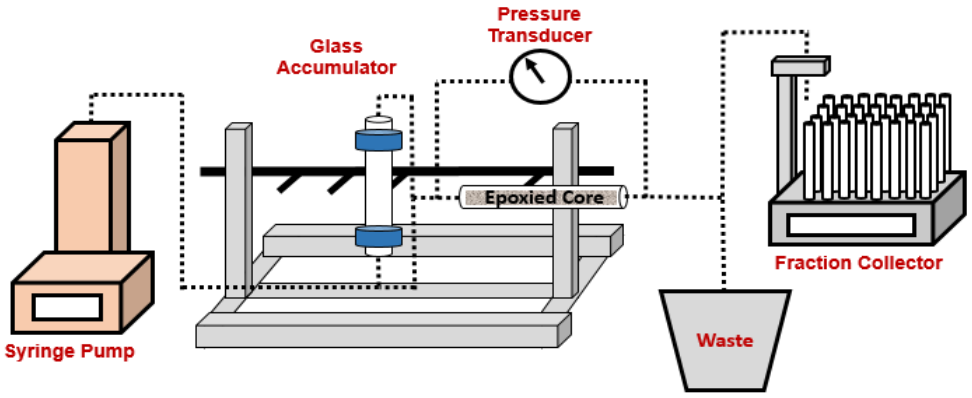


Figure 4.5: Schematic of the coreflood system designed here for control case and permeability measurement purposes

Measuring single phase permeability is necessary to examine its effect to the foam generation process. Permeability is a rock property and is defined as the ability for porous media to transmit fluids. Single phase permeability can be calculated from Darcy's law which is shown in one-dimensional form as:

$$q = \frac{kA}{\mu L}\Delta P$$

The method to estimate the permeability is to measure steady state pressure drop at different flow rates. Then calculate the ratio $\frac{A\Delta P}{\mu L}$ for each rate. A plot of q vs. $\frac{A\Delta P}{\mu L}$

should yield a straight line with a slope equals to the permeability of the rock. The following steps are followed to measure the permeability of the core as follow:

1. Start by setting up the experimental apparatus as shown in Figure 4.5.
2. Start preparing all chemical solution to be used during this experiment which include both initial fluid residing the core as well as the invading fluid depending on the protocol being fluid.
3. In all cases, 1 wt. % NaCl solution should always be loaded into syringe pump.
4. Fill the glass accumulator with the other immiscible oil-like fluid used in this experiments which can be n-octane, n-tetradecane or toluene.
5. Ensure that flow lines are gas free and also filled with right fluid as per the sequence of the displacement.
6. Permeability measurement should be conducted using the initial fluid which was used during vacuum saturation stage.
7. Figure 4.6 show the flow path in solid blue line. Figure 4.6 (a) assumes that brine is the initial fluid to reside the core. On the other hand, part (b) of the figure shows the case when the hydrocarbon phase (octane and tetradecane) considered to be the initial fluid to be displaced. All valves in the setup should be open and closed to mimic the flow direction described.
8. Start the syringe pump at 1 ml/min. Brine solution is injected directly into the core as shown in Figure 4.7 (a). In this case, the experiment is set to test the performance of drainage displacement. If imbibition is the intended protocol for the experiment, then the permeability measurement and flow path should follow Figure 4.7 (b).
9. Record the pressure drop across the core using a LabVIEW program.

10. Change flow rates and record steady state pressure drop that corresponds to each rate.
11. Values from different rates were averaged to obtain core permeability.

Once the permeability is determined, then the valves are switched so that brine solution is injected at the same rate of 1 ml/min either to the core to displace the residing alkane (imbibition) or to the mounted glass column to displace either octane or tetradecane into the core (drainage). During this, pressure drop was recorded real-time and effluent samples were collected using fractional collector. Figure 4.7 illustrate the flow direction for both drainage (a) and imbibition (b) experiments for the control run.

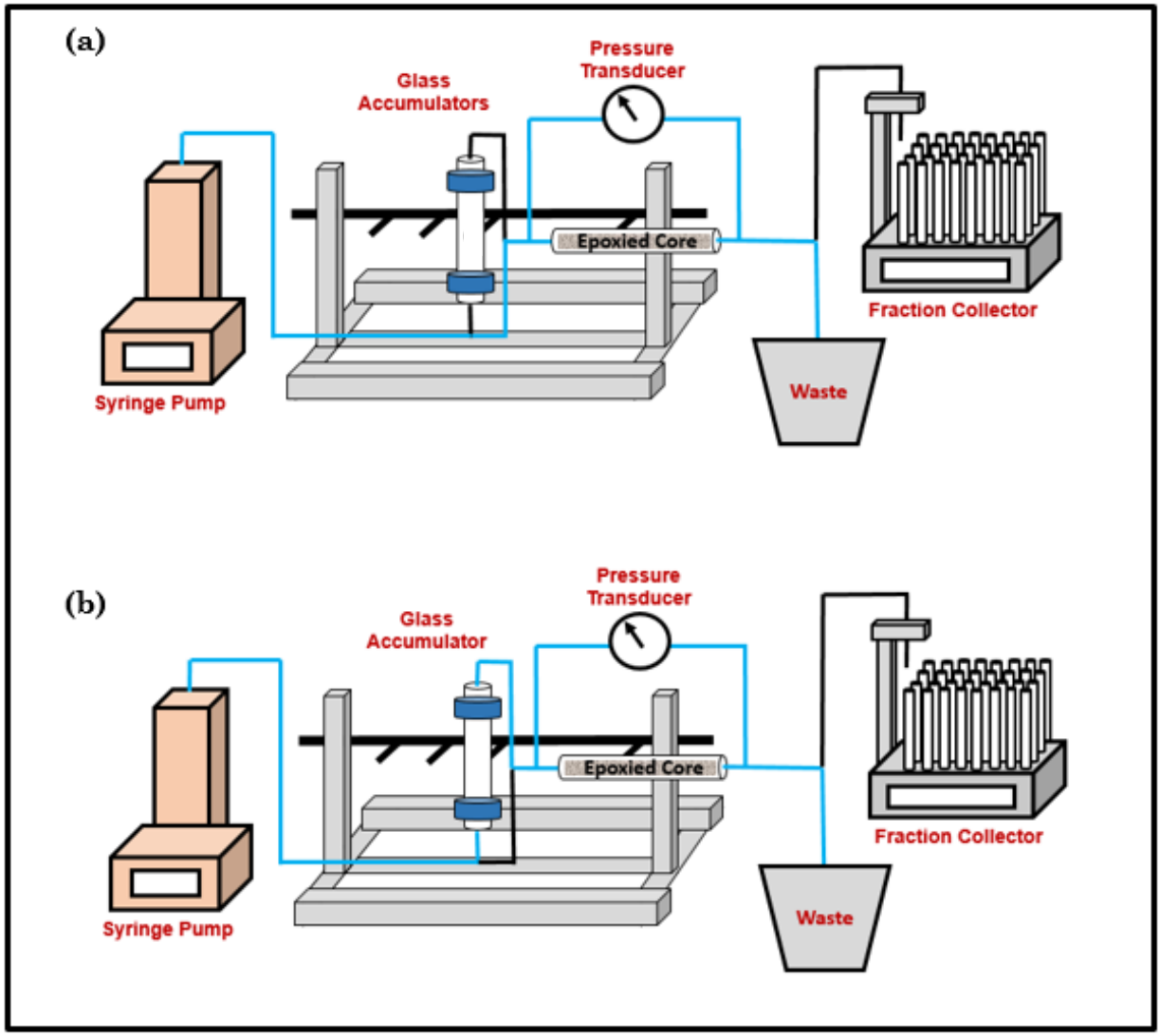


Figure 4.6: Schematic of the coreflood system showing flow path and direction to saturate the core and measure core permeability using initial fluid which can be either the aqueous phase (brine or nanoparticle-brine dispersion) as shown in (a) or the hydrocarbon phase as shown in (b).

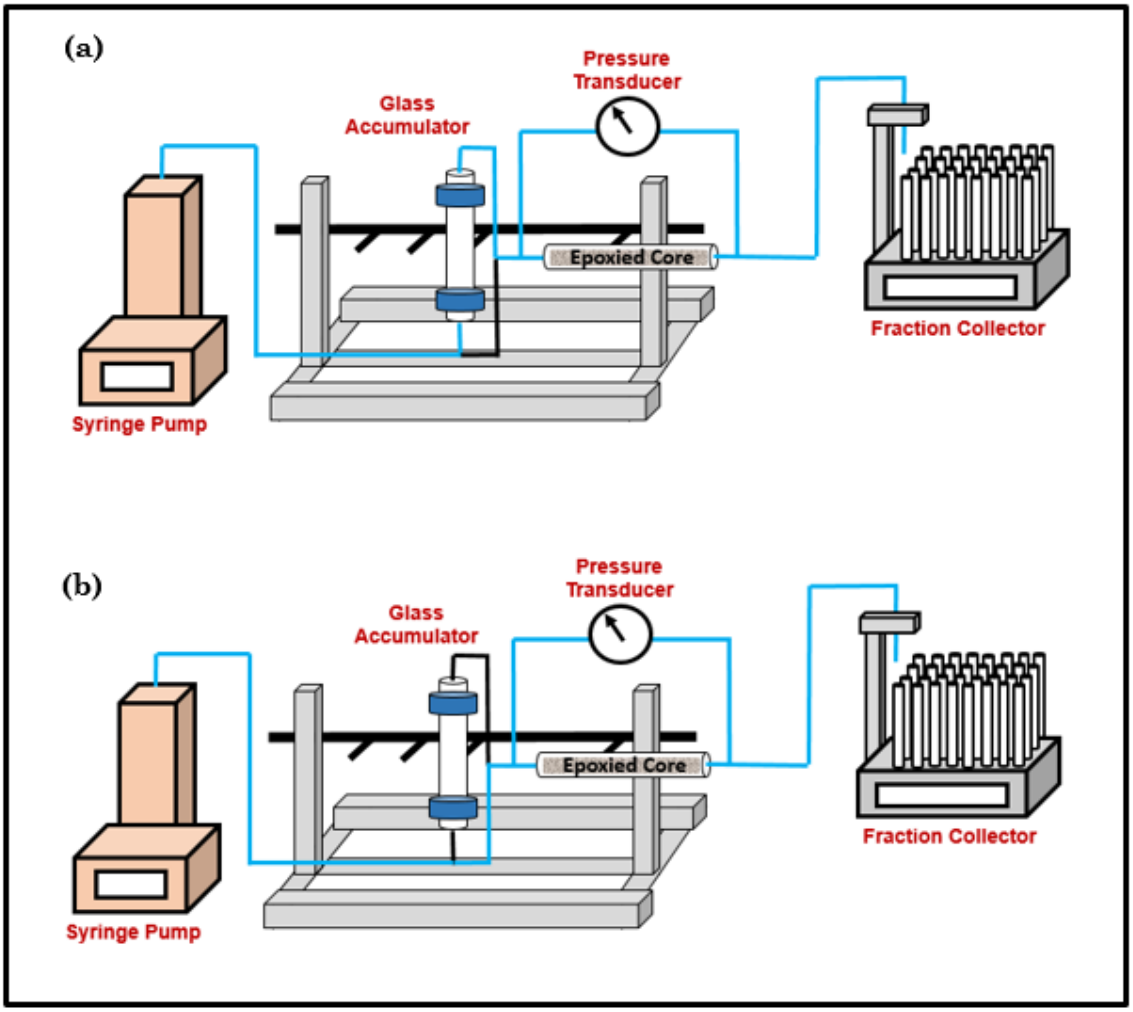


Figure 4.7: Schematic of the coreflood system showing flow path and direction for (a) drainage displacement case or (b) imbibition displacement case.

In some cases, a post-flush run followed the main displacement scenario. This was done to capture the effect of having residual fluid saturation on the displacement dynamics.

### 4.3.2 Nanoparticles Displacement Run

After completing the control experiment, the core has to be flushed with the proper solvent which needs to be miscible with both brine and either n-octane or n-tetradecane. In this study, Isopropyl alcohol (IPA) was used as the proper solvent to displace brine, octane, and tetradecane. IPA was pumped into the core for at least 10 PV from both sides of the core to ensure that the core is completely flushed and ready to be used again for nanoparticles displacement run. The process for flushing the core and conducting core flooding operation with nanoparticles being present in the system is summarized as follow:

1. Load the syringe pump with IPA.
2. Refer to Figure 4.6 (a) of the control experiment to identify IPA flow path.
3. Pump at least 3 PV of IPA into the core at 1 ml/min rate.
4. Once pressure drop reaches steady-state, increase the pumping rate to 2, 3, and 4 ml/min.
5. Single phase permeability can be calculated again to verify that the core permeability is the same as the value obtained prior to control experiment.
6. If the value is different, attempt to continue pumping IPA from both direction of the core for at least 8 PV at slow rates.
7. As the core resident fluid is completely displaced out, prepare the necessary fluid for this experimental run based on the intended protocol.

***Experiments with Hydrophilic NP in Aqueous Phase (EOR-5XS)***

Most of the experiments conducted in this study are mainly designed to have either brine solution or nanoparticles-brine dispersion invades a core that is initially saturated with either n-octane or n-tetradecane. In those experiments, nanoparticles brine

solution was prepared by having 5 wt. % nanoparticles (EOR-5XS) dispersed in 1 wt. % NaCl water solution. Since those nanoparticles are received initially dispersed in water by 20% by weight, it was necessary to dilute them. The final breakdown of the substances making up the total mixture for the experiments involving hydrophilic nanoparticles were 25% EOR-5XS dispersion, 1% NaCl, and 74% deionized water. In all of the flooding runs that uses those particles, they were dispersed in brine and injected to the core. The process for conducting imbibition displacement is given here as follow:

1. Modify the experimental setup presented before in the control experiment by mounting two additional glass accumulators. The new setup is illustrated in Figure 4.8 (a).
2. Fill in all accumulators with their corresponding fluid so that column A is filled with mineral oil, column B is filled with nanoparticles brine dispersion, and column C is filled with either n-octane or n-tetradecane.
3. Start first by saturating the core with either n-octane or n-tetradecane depending on the experimental protocol intended. This can be done as shown in Figure 4.8 (b). In this stage, syringe pump loaded initially with brine was set to pump brine at 1 ml/min to saturate the core.
4. Once the core is fully saturated, valves can be switched so that brine is now pumped at the same rate of 1 ml/min to displace mineral oil which in return start to displace nanoparticles solution into the core. Figure 4.8 (c) represents the displacement path for nanoparticles injection into the core (imbibition).
5. A post flush of either n-octane or n-tetradecane is then pumped at the same rate back into the core which is now at residual saturation. Flow path for this stage mimics the displacement presented in Figure 4.8 (b).

As for drainage displacement where the aqueous phase is initially residing the core and to be displaced by hydrocarbon phase, the process is also given as discussed in the imbibition displacement except that the core is first saturated with aqueous phase (brine or brine-nanoparticle solution) in a process illustrated by Figure 4.8 (c). Then, the hydrocarbon phase (octane or tetradecane) can be pumped to start the drainage displacement as per Figure 4.8 (b).

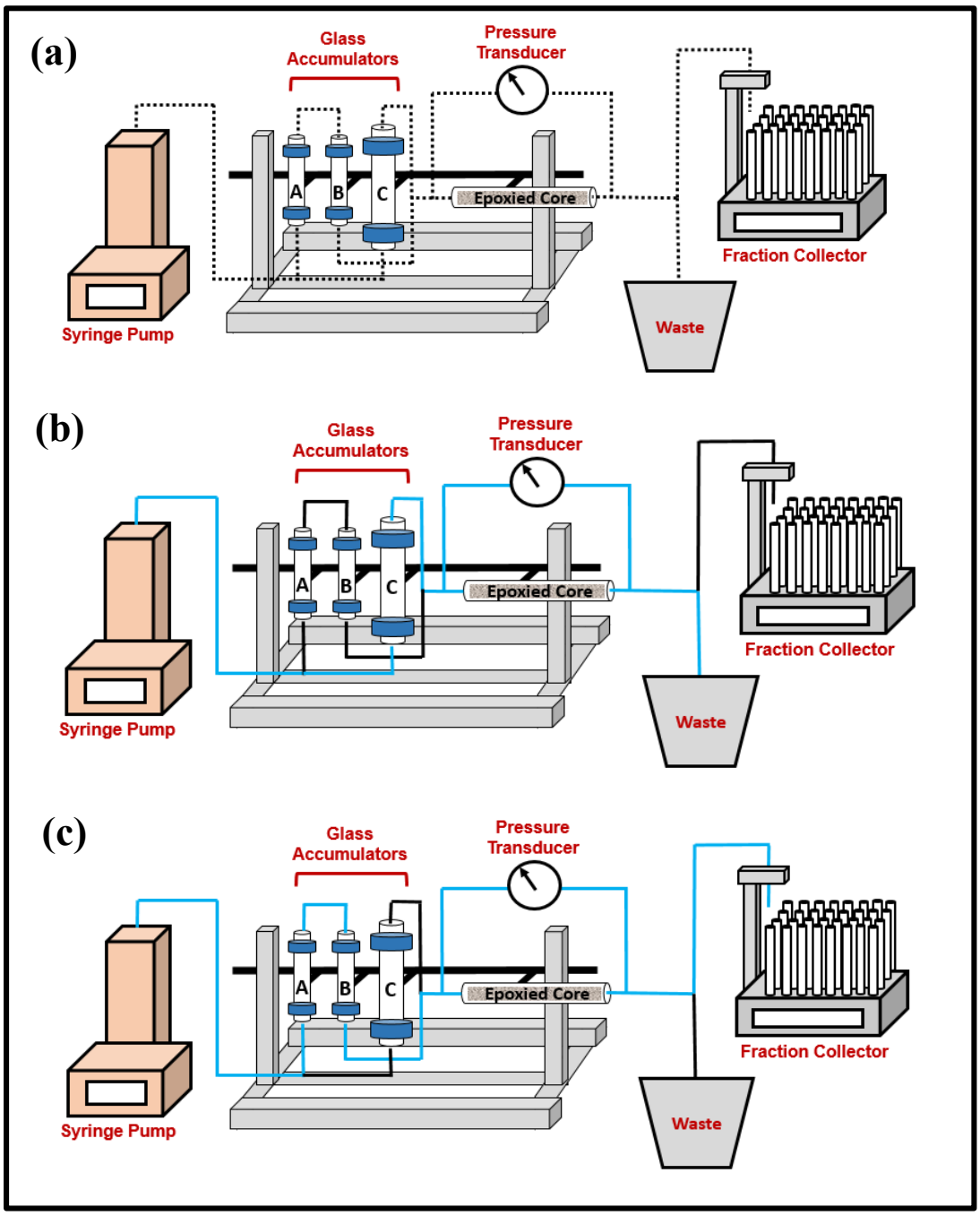


Figure 4.8: (a) The general layout of the coreflood setup for nanoparticle run showing (b) the flow path of injecting hydrocarbon phase to saturate the core or conducted drainage flow and (c) imbibition displacement or flow path to saturate the core with aqueous phase.

***Experiments with Hydrophobic NP in Hydrocarbon phase (TOL-ST)***

For experimental protocols that involve utilizing hydrophobic nanoparticles, nanoparticles have to be dispersed in hydrocarbon phase. TOL-ST nanoparticles dispersion, received initially form Nissan Chemicals as 40 wt. % dispersion in toluene, were used as hydrophobic nanoparticles. Similar to n-octane and n-tetradecane emulsions generated with hydrophilic EOR-5XS particles, sonication test between TOL-ST nanoparticles and water shows the formation of water-in-oil emulsions as shown in Figure 4.9.

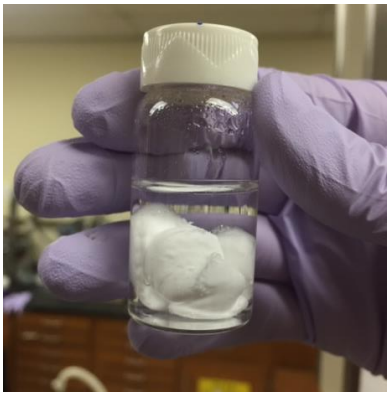

Figure 4.9: A picture of water-in-oil emulsion generated by sonication involving brine as the aqueous phase and toluene as the hydrocarbon phase.

In this experiment, the control run consists of 1% wt. NaCl brine solution invading a core which is initially saturated with hydrocarbon phase before following up that with a post flush of oil invading the core back again. As for the nanoparticles run, the core has to be saturated with 5 wt. % TOL-ST particles in oil phase to assess their performance on the displacement. The plan was initially to utilize the n-tetradecane as a proper substitute for viscous oil phase (viscosity is 2.34 cp). However, the attempt to create a stable dispersion of nanoparticles in tetradecane was not successful as the final

solution showed that particles were separated. It was found that those hydrophobic particles must be contained in organic solvent with acceptable minimum polarity index such toluene or isopropyl alcohol (IPA). Using n-tetradecane as hydrocarbon phase has caused the polarity of the mixture to be reduced from 2.4 to 0. Therefore, it was necessary to maintain the mixture polarity at a certain level so that nanoparticles are kept dispersed in solution and are not separated out. In addition to polarity, it was also necessary to maintain higher viscosity of hydrocarbon phase in order to maintain viscous instability. This was challenging as the toluene viscosity is low (0.59 cp) while IPA is miscible with water. After several attempts and tests, it was decided to use toluene as a main hydrocarbon phase. By applying this, the new hydrocarbon solution has enough polarity to keep silica particles in suspension and stably dispersed despite still having lower viscosity of 0.59 cp. The experimental procedure for nanoparticles displacement is summarized as follow:

1. Modify the experimental setup as illustrated in Figure 4.10.
2. Fill in all accumulators with their corresponding fluid so that column A is filled with 5 wt. % nanoparticles-toluene dispersion and column B is filled with toluene solution.
3. Start first by saturating the core with 5 wt. % nanoparticles-toluene dispersion. This can be done as shown in Figure 4.11 (a). In this stage, syringe pump loaded initially with brine was set to pump brine at 1 ml/min to displace the nanoparticle-toluene solution to saturate the core.
4. Once the core is fully saturated, valves can be switched so that brine is now pumped at the same rate of 1 ml/min to invade the core. Figure 4.11 (b) represents the displacement path for the stage of flooding operation.

5. A post flush of toluene is then pumped at the same rate into the core which is now at residual saturation. Flow path for this stage mimics the displacement presented in Figure 4.11 (c).

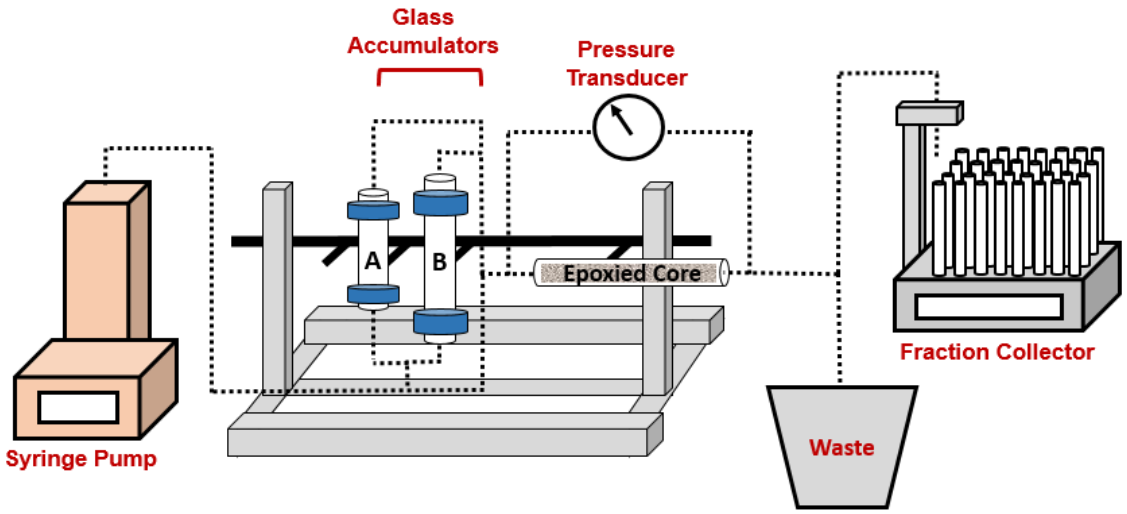


Figure 4.10: Schematic of the coreflood system designed for the nanoparticle case involving hydrophobic nanoparticles, TOL-ST.

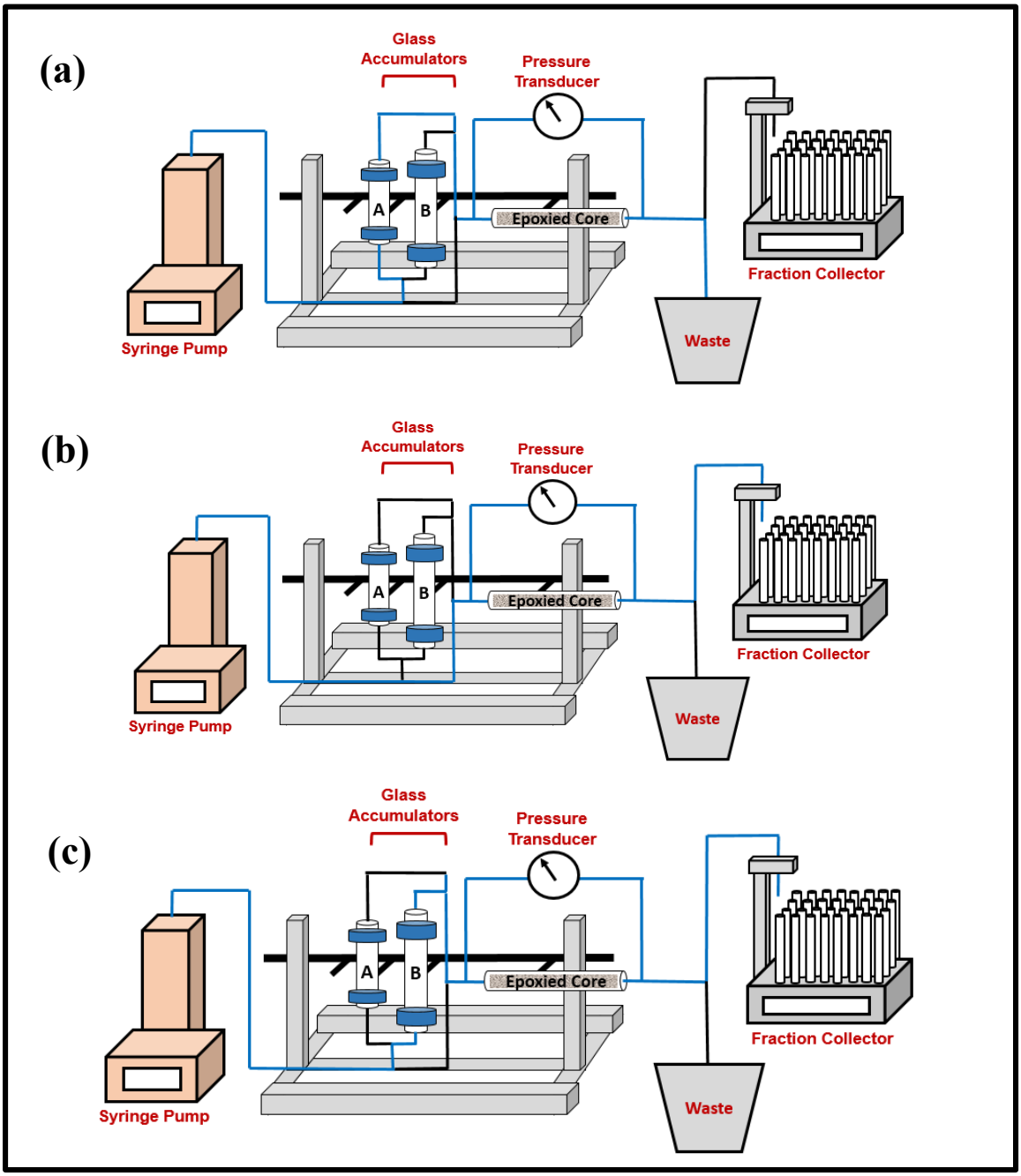


Figure 4.11: The schematic for coreflood system designed for hydrophobic nanoparticle run using (TOL-ST) showing (a) flow path to saturate the core with 5 wt. % nanoparticles in toluene, (b) flow path for primary imbibition displacement, and (c) flow path for secondary drainage via toluene injection.

### 4.3.3 Experimental Protocol Summary

This section summarizes core and fluid properties for each experiment conducted as part of this research evaluation. It also presents the protocols followed for each core displacement case. Table 4.2 shows all the Boise sandstone cores initial properties that include porosity (pore volume), permeability, and wettability. The experimental protocols are presented in Table 4.3 for each core. The protocols are designed to test nanoparticles displacement impact under different conditions such as wettability, viscosity ratio between injected and displaced fluid, and nanoparticles' wetting nature and location. The flow rate is wet to be 1 ml/min for all cases. The results will be discussed in the next chapter (chapter 5). Fluid properties are measured at standard room conditions and listed in Table 4.4.

| Core # | Core Description | Porosity / Pore Volume | Permeability (md) | Wettability |
|---|---|---|---|---|
| A | 30.48 cm long , 2.54 cm diameter | 21.5 % , 33 ml | 376 | Water-Wet |
| B | 30.48 cm long , 2.54 cm diameter | 19.5 % - 30 ml | 1265 | Water-Wet |
| C | 30.48 cm long , 2.54 cm diameter | 21.6 % - 34 ml | 2500 | Oil-Wet |
| D | 30.48 cm long , 2.54 cm diameter | 20.0 % - 30 ml | 3240 | Oil-Wet |
| E | 30.48 cm long , 2.54 cm diameter | 21.0% - 33 ml | 2646 | Oil-Wet |
| F | 30.48 cm long , 2.54 cm diameter | 21.0% - 32 ml | 2830 | Oil-Wet |
| G | 30.48 cm long , 2.54 cm diameter | 21.0% - 33 ml | 2638 | Water-Wet |
| H | 28.80 cm long , 2.54 cm diameter | 19.5% - 28 ml | 2500 | Oil-Wet |
| I | 30.48 cm long , 2.54 cm diameter | 22.0% - 34 ml | 2900 | Water-Wet |
| J | 28.80 cm long , 2.54 cm diameter | 14.3% - 21 ml | 1560 | Water-Wet |

Table 4.2: Description of Boise sandstone cores used in this project showing core physical properties such as porosity, permeability, and wettability.

Table 4.3: Experimental Protocols for displacement tests conducted on each core showing the condition being tested.

| Core | Core Resident Fluid | Injected Fluid | Run # | NP Type | Condition Tested |
|---|---|---|---|---|---|
| A | 1 wt.% NaCl brine | n-Octane | Control | - | - |
| | 5 wt.% NP in 1 wt.% NaCl brine | n-Octane | NP | EOR-5XS | - |
| B | 1 wt.% NaCl brine | n-Octane | Control | - | - |
| | 5 wt.% NP in 1 wt.% NaCl brine | n-Octane | NP | EOR-5XS | - |
| C | n-Octane | 1 wt.% NaCl brine | Control | - | |
| | n-Octane | 5 wt.% NP in 1 wt.% NaCl brine | NP | EOR-5XS | Wettability |
| D | n-Octane | 1 wt.% NaCl brine | Control | - | - |
| | n-Octane | 5 wt.% NP in 1 wt.% NaCl brine | NP | EOR-5XS | Wettability |
| E | n-Tetradecane | 1 wt.% NaCl brine | Control | - | |
| | n-Tetradecane | 5 wt.% NP in 1 wt.% NaCl brine | NP | EOR-5XS | Viscous Instability |

Table 4.3 (Continued)

| | | | | | |
|---|---|---|---|---|---|
| F | n-Tetradecane | 1 wt.% NaCl brine | Control | - | |
| | n-Tetradecane | 5 wt.% NP in 1 wt.% NaCl brine | NP | EOR-5XS | Viscous Instability |
| G | n-Octane | 1 wt.% NaCl brine | Control | - | |
| | n-Octane | 5 wt.% NP in 1 wt.% NaCl brine | NP | EOR-5XS | Wettability Change |
| H | Toluene | 1 wt.% NaCl brine | Control | - | |
| | 5 wt.% NP in Toluene | 1 wt.% NaCl brine | NP | TOL-ST | NP Wettability |
| I | n-Tetradecane | 1 wt.% NaCl brine | Control | - | |
| | n-Tetradecane | 5 wt.% NP in 1 wt.% NaCl brine | NP | EOR-5XS | Wettability Change |
| J | 1 wt.% NaCl brine | Tetradecane | Control | - | - |
| | 5 wt.% NP in 1 wt.% NaCl brine | Tetradecane | NP | EOR-5XS | Viscous Stability |

| Fluid Description | Viscosity (cp) | Density (g/cc) | Interfacial Tension with water (mN/m) |
|---|---|---|---|
| 1 wt.% NaCl brine | 1.01 | 1.02 | - |
| 5 wt.% NP 1 wt.% NaCl brine | 1.21 | 1.1 | - |
| n-Octane | 0.54 | 0.703 | 51 |
| n-Tetradecane | 2.34 | 0.765 | 45 |
| Toluene | 0.59 | 0.86 | 35 |
| Mineral Oil (Light) | 44 | 0.83 | 48 |
| 5 wt.% NP in Toluene | 0.75 | 0.889 | 35** |

Table 4.4: Fluid properties such as viscosity, density, and interfacial tension with respect to the aqueous phase are shown in the table for various fluids. ** Assume same as Toluene.

# Chapter 5: Results and Discussions

## 5.1 EXPERIMENTAL WORK SEQUENCE

This chapter will focus on presenting the outcome of this research by presenting all data and findings observed during all conducted experiments. As mentioned before, this research is set to examine the hypothesis that pore scale events occurring during the displacement of wetting phase by non-wetting phase will eventually contribute to forming pore scale droplets that nanoparticles, if present in the system, may armor and prevent from subsequent coalescence. In turn these armored droplets will affect the overall flow. Here, we do not attempt to observe actual armored droplets, but the effect of them on the flow. This is done by measuring the pressure drops and recovery curves during the displacements with and without nanoparticles. By observing similarities and differences between the control and nanoparticle case we make determinations on the effect of the nanoparticles and whether these effects are consistent with nanoparticle armoring. We demonstrate the effects by starting with first reviewing and then repeating experiments where octane displaces water in water-wet media.

## 5.2 LOWER-OIL VISCOSITY DISPLACEMENT

### 5.2.1 Displacement in Water-Wet Porous Media

This section focuses on all experimental tests conducted on water-wet porous media where the impact of nanoparticle presence in the system of the displacement is evaluated. The hydrocarbon phase that will be used for these tests is n-octane which has lower viscosity than that of either brine or nanoparticle-brine dispersion.

***Primary Drainage (Core-B)***

A core flooding experiment was conducted on Core-B to evaluate nanoparticles impact on primary drainage process in water-wet Boise sandstone core. Prior to n-octane injection into the core, the core was initially saturated with brine for the control case and nanoparticle-brine dispersion for the second case.

Figure 5.1 shows the pressure drop trend as a function of pore volume injected. The blue curve represents the pressure drop for the control experiment while the red curve shows the pressure drawdown behavior for the nanoparticles case. The dashed lines show the breakthrough time for both displacements. As shown in the plot, both displacement cases showed a similar pattern of pressure build up behavior where drawdown was increasing with more pore volume injected until a peak pressure drop value is reached followed by a general decline trend reaching a certain leveling off values by the displacement end.

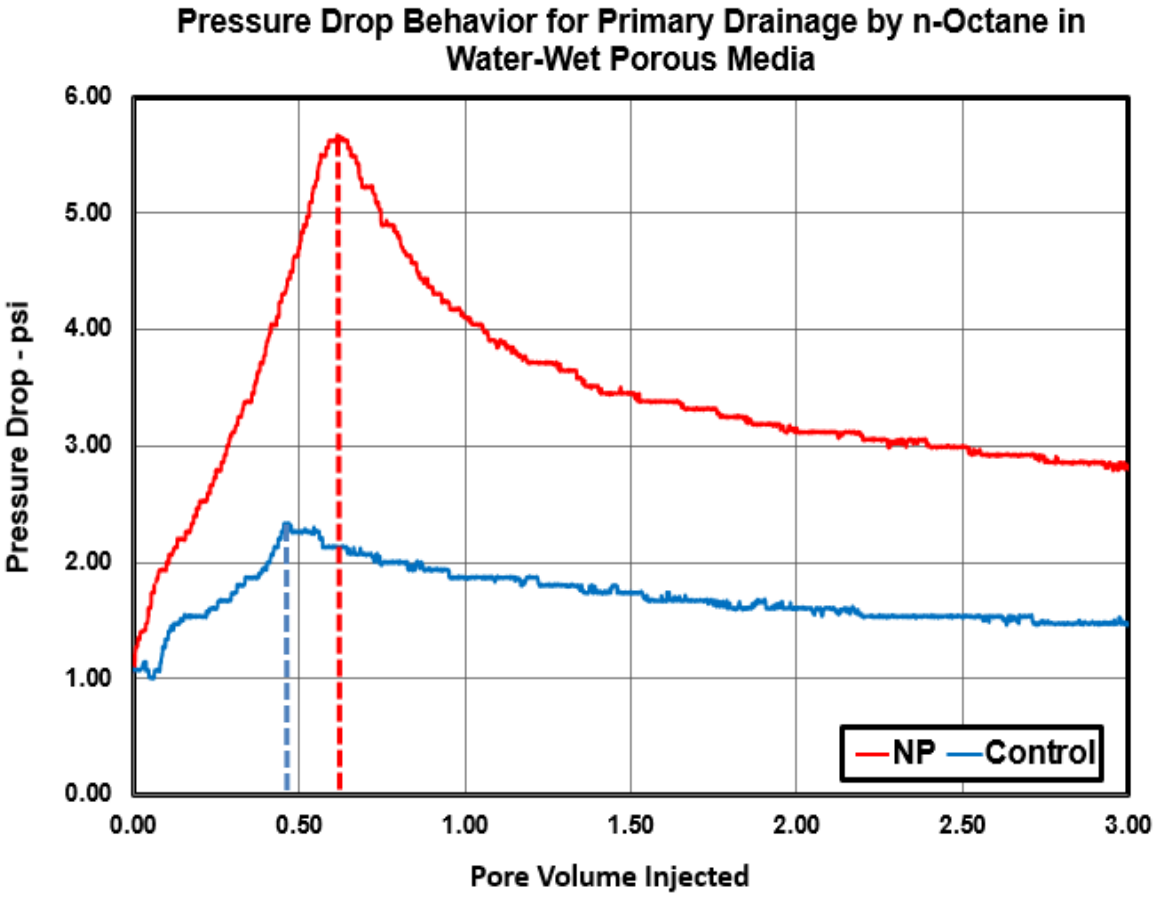


Figure 5.1: Measured pressure drop as a function of pore volume injected for control (blue) and nanoparticle case (red) for primary drainage into water-wet core-B using n-octane. The dashed lines indicate breakthrough time.

For the control experiment as shown in Figure 5.1 by the blue curve, the pressure drop was increasing and reached a maximum value of 2.25 psi at 0.46 PV. After that, the pressure drop started to gradually decline and reached an asymptote value of about 1.47 psi at 3.0 PV. In this case, the pressure drop peak value corresponds to the breakthrough of n-octane from the core outlet as observed in the fraction collector. As for the nanoparticle case as illustrated in Figure 5.1 by the red curve, the pressure drop showed a similar performance to that of control case with sharp increasing trend as pressure drop

reached a maximum value of 5.62 psi at 0.64 PV. After that, the pressure drop started to decline and reached an asymptote value of about 2.80 psi at 3.0 PV. In this case, the pressure drop peak value corresponds to the breakthrough of n-octane from the core outlet as observed in the fraction collector. It can be seen from Figure 5.1 that the nanoparticle case had a later breakthrough time that is 0.18 PV more compared to the control case (0.64 PV compared to 0.46 PV). In addition, nanoparticle experiment ended up with a higher pressure drop that was 1.33 psi larger than that of the control case (2.80 psi compared to 1.47 psi). We next present the water cut and core saturation profiles.

Figure 5.2 shows the water cut data which was collected during this displacement process. The blue curve shows the water cut values measured as a function of pore volume injected for the control experiment while the red curve shows the water cut for the nanoparticle case. For the control case, the water cut value maintained a value of 1 until the breakthrough time of 0.46 PV after which the water cut started to drop rapidly until it reached 0 as n-octane was only flowing at residual aqueous phase (brine) saturation. As for the nanoparticle case, the water cut value maintained a value of 1 until the breakthrough time of 0.64 PV after which the water cut started to drop rapidly until it reached 0 as n-octane was only flowing at residual aqueous phase (brine-nanoparticle solution) saturation. Comparing both control and nanoparticle experiments, we see that the water cut reduction for the nanoparticle run occurred at later pore volume injected time that was 0.18 PV more compared to the control. Also, the water cut profile for the nanoparticle case was observed to have frequent bumps showing a sudden and low value increase in water production after the time of breakthrough.

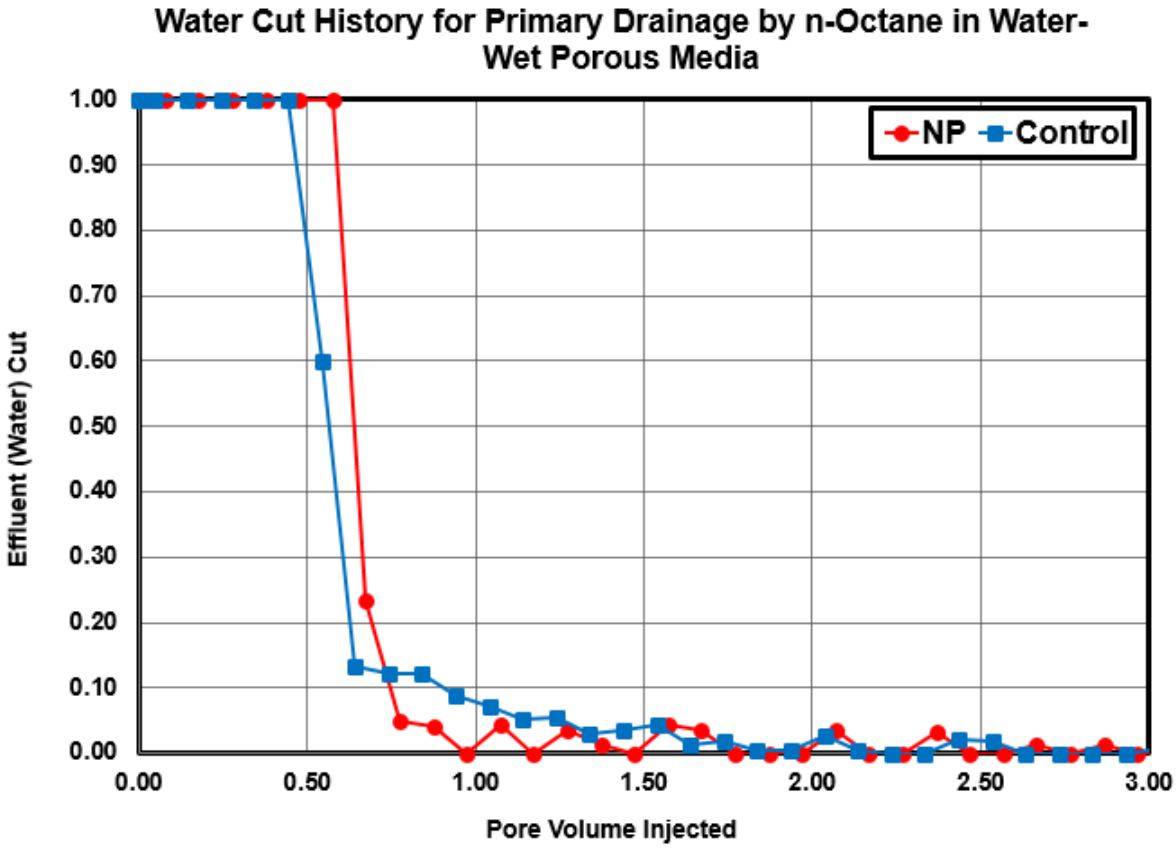


Figure 5.2: Raw effluent (water) cut data as a function of pore volume injected for primary drainage using n-octane in water-wet core-B for both control (blue) and nanoparticle case (red).

The residual saturation of brine or brine containing nanoparticles was calculated based on the water cut measured in the effluent samples collected during the displacement. The core water saturation profiles are shown in blue for the control case and in red for the nanoparticle case as clearly illustrated in Figure 5.3. The water saturation was calculated by comparing the total volume of water recovered and the pore volume of the core. The residual aqueous phase saturation for the control case was 35%. As for the nanoparticles run, the residual saturation was reduced to 24% indicating an average reduction of 11 saturation units.

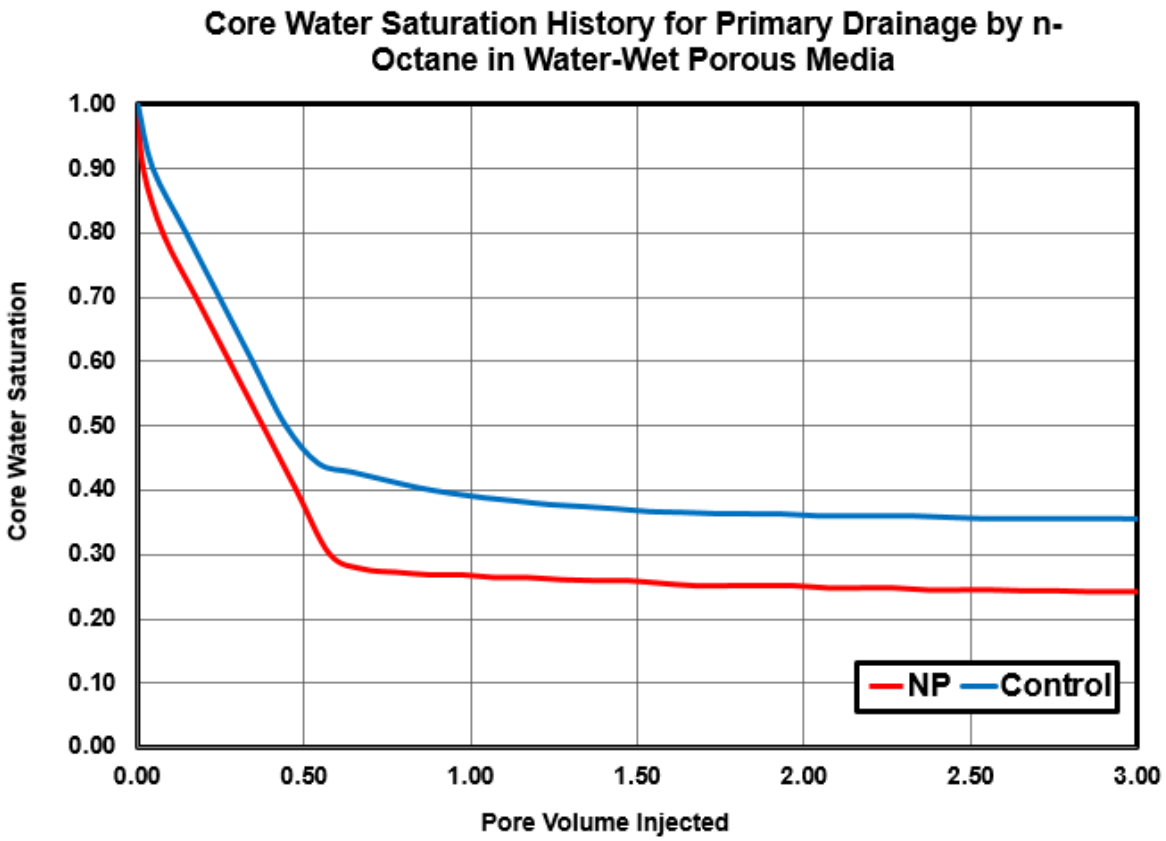


Figure 5.3: Average core water saturation history as a function of pore volume injected for primary drainage using n-octane in water-wet core-B for both control (blue) and nanoparticle case (red).

Figure 5.4 shows the pressure drop ratio of the nanoparticles case compared to the control case. The ratio was calculated by dividing the measured pressure drop at each point in time for nanoparticles case by the measured pressure drop at each point in time for the control case. This pressure drop was consistently 1.2 to 2.5 times greater than that of the control case and remained twice as much as that of the control for the rest of the displacement.

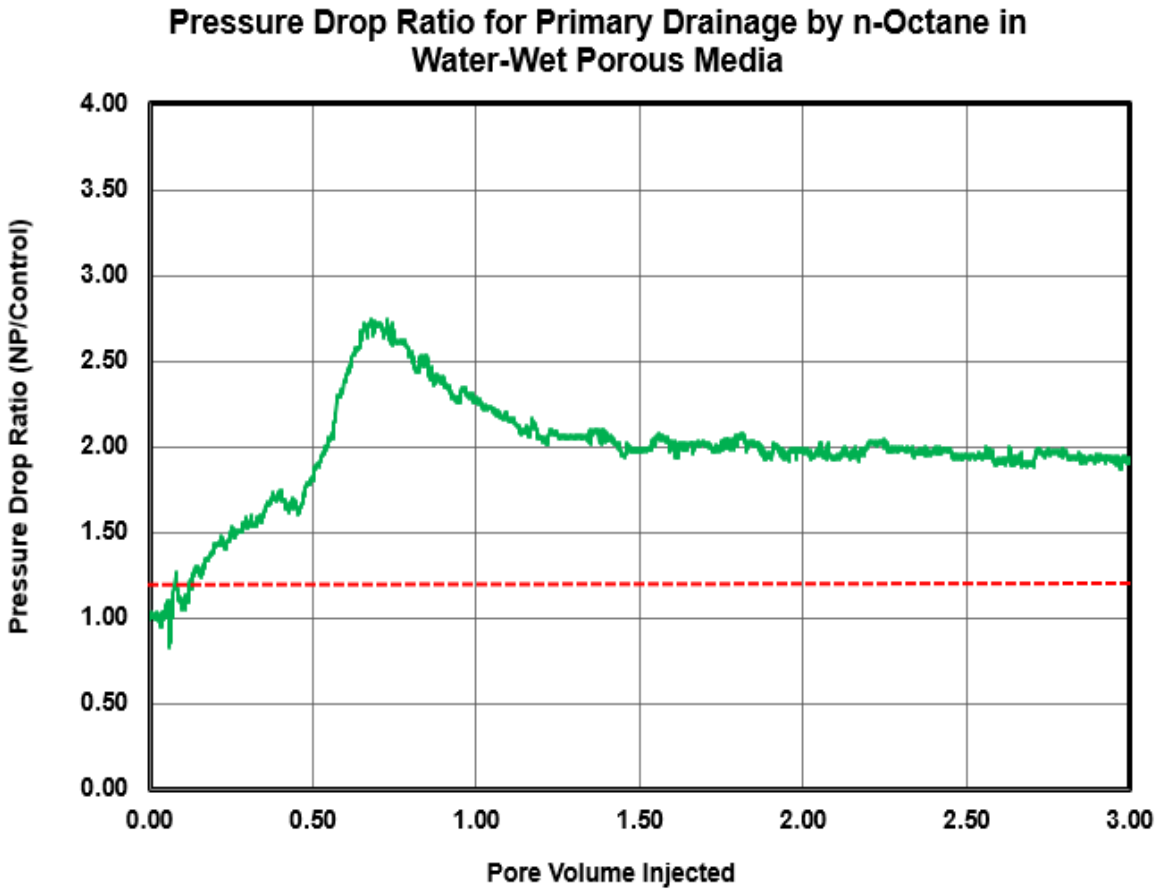


Figure 5.4: Pressure drop ratio calculated by dividing pressure drop measured at each point in time during nanoparticle case over the pressure drop for control case measured at each point in time as well. Ratio is expressed as a function of time for primary drainage using n-octane in water-wet core-B. Red dashed line represents the value of the viscosity ratio between the aqueous nanoparticle dispersion and brine solution.

Another useful quantity that can be obtained from pressure drop measurements and fluid viscosities is the endpoint relative permeability for the hydrocarbon phase ($k_{ro}^{o}$) which is given by:

$$k_{ro}^{o} = \frac{\Delta P_w \, \mu_o}{\Delta P_o \, \mu_w}$$

In the equation above, $\mu$ is the viscosity of the fluid represented by either *w* for the aqueous phase or *o* for the hydrocarbon phase. $\Delta P_o$ represents the pressure drop for single phase n-octane flowing at steady state at residual aqueous phase saturation while $\Delta P_w$ is the value of steady state pressure drop of the aqueous phase flowing as single phase at 100% aqueous phase saturation. In all cases, the flow rate was kept the same at 1 ml/min. The calculated value of endpoint relative permeability was 0.40 for the control case and 0.18 for the nanoparticle case indicating a reduction of 54%.

The observations found during this experimental protocol had shown that nanoparticles had caused the pressure drop to increase sharply compared to the control case with pressure drop ratio being consistently 2 to 2.5 times greater than that of the control case and by far greater than the viscosity ratio of nanoparticle-brine solution and brine solution which is 1.18. The pressure drop ratio is maximum at the breakthrough and gradually decrease afterward. Since it is hypothesized that this pressure drop ratio is caused by relevant pore-scale displacement events of Haines jump and Roof snap-off, the increase in pressure drop ratio should be greatest when these mechanisms are the most prevalent pore-scale events. Haines jump process requires the wetting phase to be present in the pore and therefore, this event is most likely to be active at the displacement front where the contact between both non-wetting phase and wetting phase is greatest. As a result, the displacement front moves along the core stabilizing more droplets and pressure drop ratio increases until it reached its maximum value of 2.5 by the time of breakthrough. In summary, this indicate a development of a more viscous phase that n-octane is trying to displace and/or flow around causing pressure drop increase resulting in lowering the invading phase (n-octane) mobility. This reduction in phase mobility was also confirmed by the 54% reduction in the end point relative permeability for the nanoparticle case as shown before. Also, it was shown nanoparticles had caused the

residual aqueous phase saturation to decrease with an average reduction of 11 saturation units. In addition, the observed behavior of the displacement showed that nanoparticle case had a later breakthrough of 0.18 PV with frequents bumps in the water cut trend. This small and sudden increase in water cut values may be due to recovering additional aqueous phase by viscous drag against the aqueous film layers covering the grains. This can be correlated by the observed increase in pressure drop ratio. Another possibility regarding those bumps is the flow out of some of the stabilized droplets. This argument is supported by observing some of the unstable emulsions leaving the core which broke to their pure phases by the time they reached the fraction collector. All of these observations support the hypothesis that pore scale processes such as Haines jump and Roof snap off will provide enough energy to bring the nanoparticles to the interface and armor the droplets of non-wetting phase forming nanoparticle-stabilized emulsion inside the pores which will generally force the non-wetting phase to flow out of its preferred flow paths and stabilize flow. As different processes occur during imbibition and drainage displacement, we next evaluate the primary imbibition displacement under the same wettability and viscous stability conditions.

***Primary Imbibition (Core-G)***

A core flooding experiment was conducted on Core-G to evaluate nanoparticles impact on primary imbibition process in water-wet Boise sandstone core. The core was initially saturated with n-octane prior to injecting brine in the control case and nanoparticle-brine dispersion in the second case. For both cases, a secondary drainage of post flush with n-octane followed the primary imbibition displacement and is presented in the next section.

Figure 5.5 shows the pressure drop trend as a function of pore volume injected. The blue curve represents the pressure drop for the control experiment while the red curve shows the pressure drawdown behavior for the nanoparticles case. The dashed lines show the breakthrough time for both displacements. As shown in the plot, both experiments show a similar pattern where pressure drop builds up almost linearly with pore volume at the beginning of the displacement followed by a plateau after breakthrough.

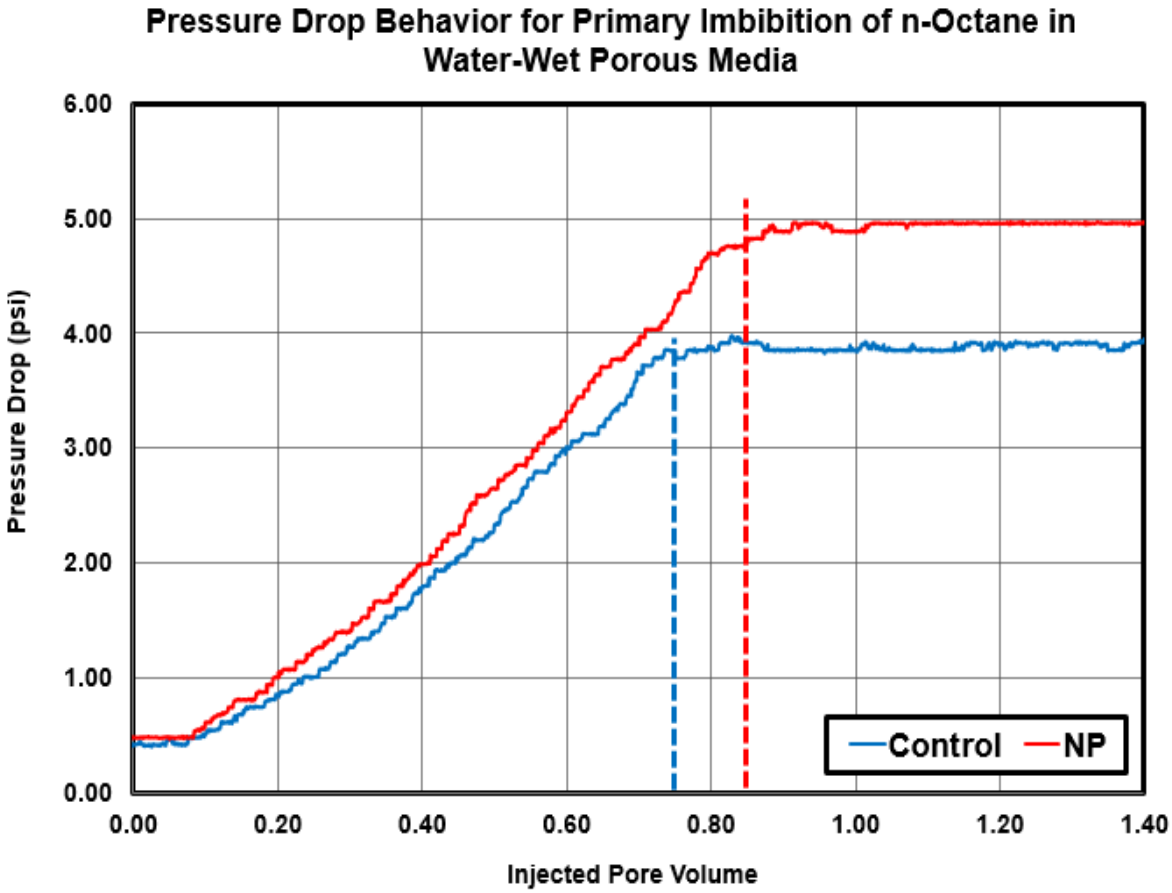


Figure 5.5: Measured pressure drop as a function of pore volume injected for control (blue) and nanoparticle case (red) into Boise sandstone for primary imbibition in water-wet core-G using n-octane. The dashed lines indicate breakthrough time.

Before we address the facts on the pressure drop behavior, it is important to mention that IPA treatment after completing the control experiment did not restore the core to its original petrophysical condition. In particular, single phase pressure drop data indicated a reduction in core permeability by nearly 24% post IPA treatment. The suspected cause of this reduction may be due to the fact that some of the flow paths which used to be available for flow is now occupied by IPA filling up some of the void space inside the core that was not flushed out after the miscible flow of n-octane back into the core. Another possibility is that some of the flow path and void spaces were not reached and accessed during the miscible IPA flush resulting in leaving some of the residual brine and/or n-octane behind resulting in the core not being fully flushed. As a result and to allow fair comparison reflecting all changes to the core's permeability and porosity, pressure drop normalization was performed. For the control case, raw pressure drawdown data presented in Figure 5.5 were divided by 0.42 psi which is the single phase pressure drop of n-octane flowing at 1 ml/min at a saturation of 100% n-octane. For the nanoparticle case, a pressure drop value of 0.48 psi was used to normalize the raw data. This pressure drop value corresponds to the single phase pressure drop of n-octane flowing at the same flow rate of 1 ml/min post IPA treatment. Also, pore volume correction was applied. Based on the measured reduction in permeability, the core porosity was reduced, as detailed in Appendix A2 based on Pittman permeability-porosity correlation, by 3% of the original value for this core. Again, the material suspected of occupying the previously open pore space is either IPA and/or residual brine or n-octane occupying some hard to access sites during the miscible flow of IPA post the primary imbibition stage. Normalized pressure drop curves for both control and nanoparticle case are shown in Figure 5.6.

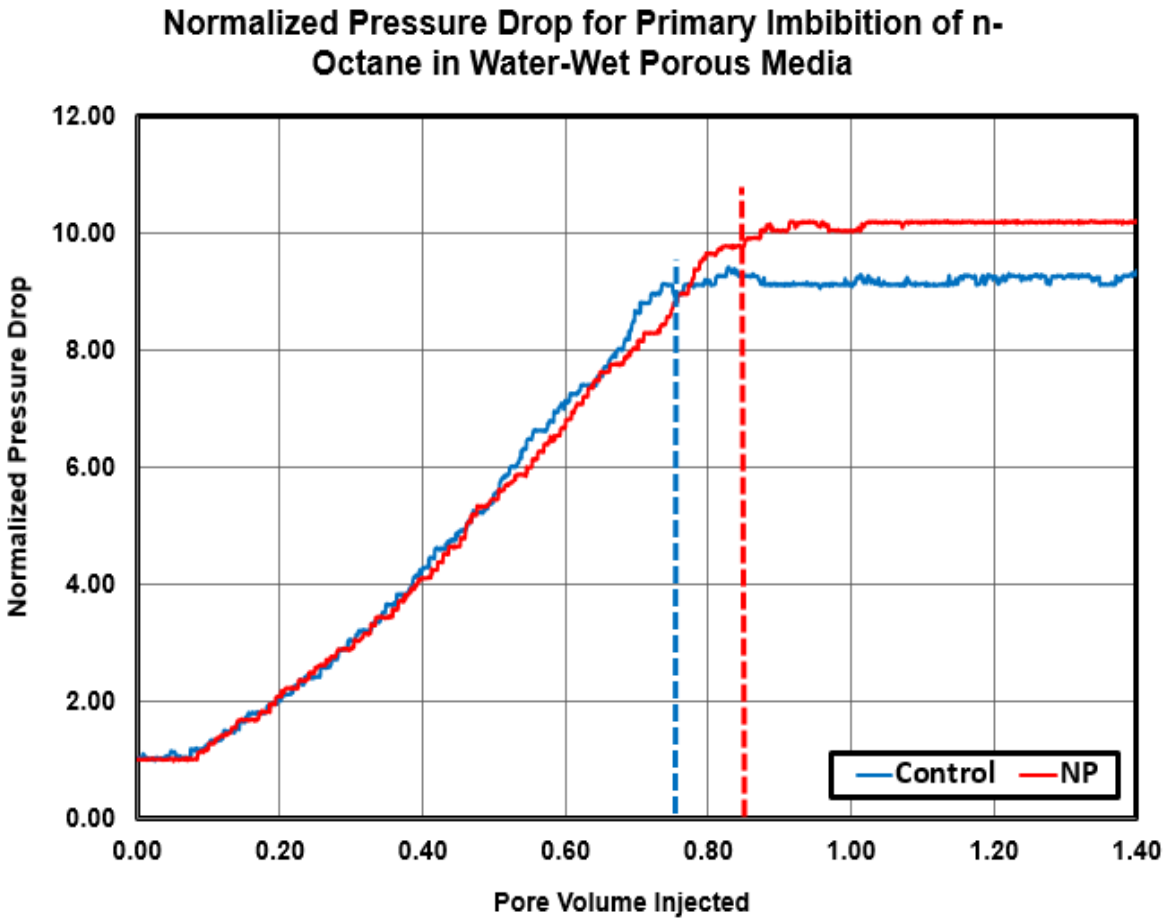


Figure 5.6: Normalized pressure drop as a function of pore volume injected for control (blue) and nanoparticle case (red) into Boise sandstone for primary imbibition in water-wet core-G using n-octane. The dashed lines indicate breakthrough time.

For the control experiment as shown in Figure 5.6 by the blue curve, the normalized pressure drop was increasing in a linear fashion with injected pore volume before it started to plateau around 9.1 after the breakthrough time of 0.76 PV. After that, the pressure drop maintained a value of 9.1 with little fluctuation until the end of the displacement. As for the nanoparticle case as illustrated in Figure 5.6 by the red curve, the normalized pressure drop showed comparable performance to that of the control case as pressure drop was increasing in a linear fashion with injected pore volume before it

started to plateau around 10.2 after the breakthrough time of 0.85 PV. After that, the pressure drop maintained a value of 10.2 with little fluctuation until the end of the displacement. It can be seen from Figure 5.6 that the nanoparticle case had a later breakthrough time that is 0.09 PV more compared to the control case (0.85 PV compared to 0.76 PV). In addition, nanoparticle experiment ended up with a slightly higher pressure drop that was nearly 13 % larger than that of the control case (10.2 compared to 9.1).

Figure 5.7 shows the water cut data which was collected during this displacement process. The blue curve shows the water cut values measured as a function of pore volume injected for the control experiment while the red curve shows the water cut for the nanoparticle case. For the control case, the water cut value maintained a value of 0.0 until the breakthrough time of 0.76 PV at which the water cut started to increase and reached 1.0 by the end of the displacement. As for the nanoparticle case, the water cut value maintained a value of 0.0 until the breakthrough time of 0.85 PV at which the water cut started to increase and reached 1.0 by displacement end. Comparing both control and nanoparticle experiments, we see that the water cut increase for the nanoparticle run occurred at later pore volume injected time that was 0.09 PV more compared to the control.

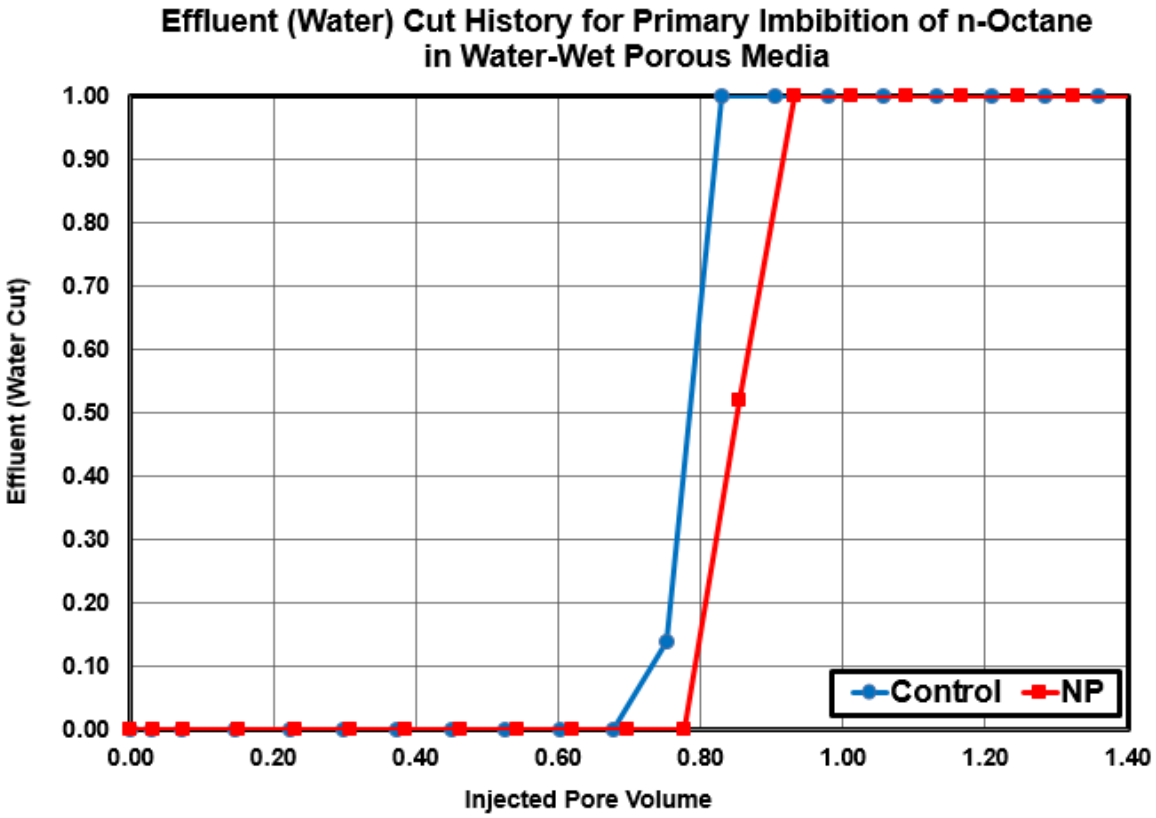


Figure 5.7: Effluent (water) cut as a function of pore volume injected for primary imbibition in water-wet core-G for both control (blue) and nanoparticle case (red).

The saturation of brine or brine containing nanoparticles was calculated based on the water cut measured in the effluent samples collected during the displacement. The core water saturation histories are shown in blue for the control case and in red for the nanoparticle case as clearly illustrated in Figure 5.8. The water saturation was calculated by comparing the total volume of water recovered and the pore volume of the core. The steady state aqueous phase saturation for the control case was 80%. As for the nanoparticles run, the steady state saturation was increased to 87% indicating an average increase of 7 saturation units.

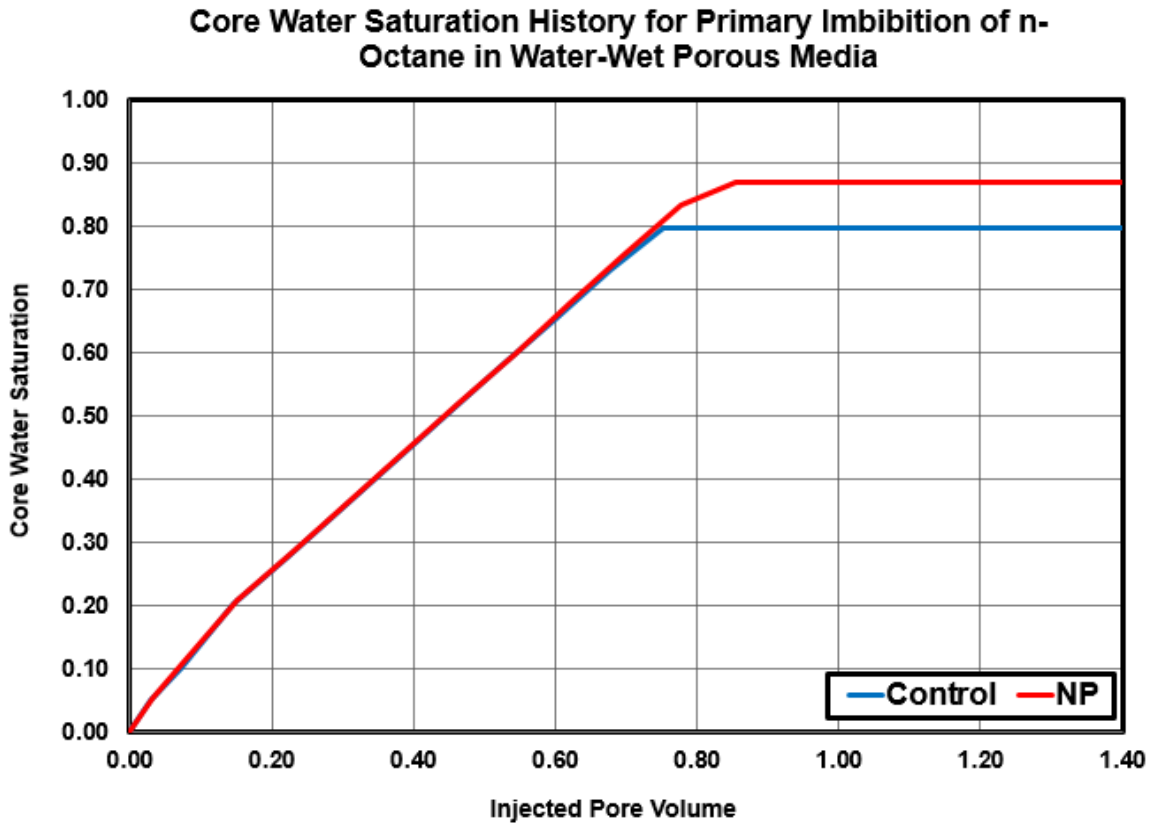


Figure 5.8: Average core water saturation history as a function of pore volume injected for primary imbibition in water-wet core-G for both control (blue) and nanoparticle case (red).

Figure 5.9 shows the pressure drop ratio of nanoparticles case compared to the control case. The ratio was calculated by dividing the normalized pressure drop of nanoparticles case at each moment of time by the normalized pressure drop for the control case at the same moment (measured by pore volume injected). As shown in the figure, the pressure drop ratio was initially around an average value of 1 for the first 0.76 PV injected and fluctuated around values close to 1.18 afterward.

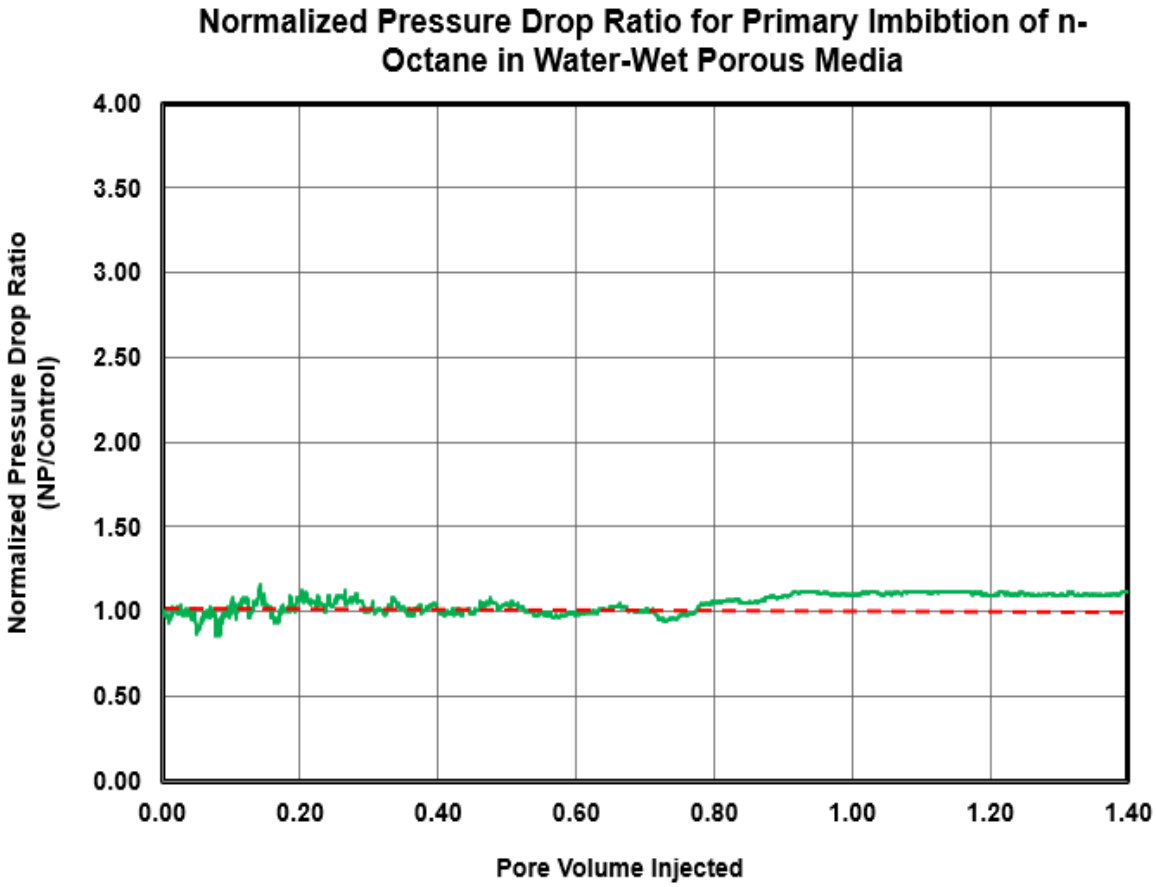


Figure 5.9: Pressure drop ratio calculated by dividing pressure drop measured at each point in time during nanoparticle case over that of the control case measured at the same moment. Ratio is expressed as a function of time for primary imbibition displacement in water-wet core-G using n-octane. Red dashed line represents the value of the normalized viscosity ratio between the aqueous nanoparticle dispersion and brine solution.

Another useful quantity that can be obtained from pressure drop measurements and fluid viscosities is the endpoint relative permeability for the aqueous phase ($k_{rw}^{o}$) which is given by:

$$k_{rw}^{o} = \frac{\Delta P_o \, \mu_w}{\Delta P_w \, \mu_o}$$

In the equation above, $\mu$ is the viscosity of the fluid represented by either *w* for the aqueous phase or *o* for the hydrocarbon phase. $\Delta P_o$ represents the pressure drop for single phase n-octane flowing at steady state while $\Delta P_w$ is the value of steady state pressure drop of the aqueous phase flowing at residual hydrocarbon saturation. In all cases, the flow rate was kept the same at 1 ml/min. The calculated endpoint relative permeability was 0.21 for the control case and 0.22.indicating a slight increase of nearly 4% for the nanoparticle case.

The observations found during this experimental protocol had shown that nanoparticles had caused almost no significant impact on the pressure drop performance as no excessive increase in pressure drawdown was observed. The pressure drop ratio was ranging between 1 and 1.20 throughout the entire experiment. In fact, this ratio was close to the viscosity ratio of 1.18 which is the viscosity ratio between brine solution and nanoparticle-brine dispersion. This suggests that the displacement behavior was just impacted only by the fact that nanoparticle dispersion was 18% more viscous compared to the control case. As a result, a 0.09 PV delay was seen in the breakthrough time for the nanoparticle case. Also, the increase in invading phase viscosity has helped in making an already a stable displacement into a more stable one which in turns may help in improving recovery as a result of the additional viscous forces applied by the aqueous phase. Despite the slight increase in the aqueous phase viscosity for the nanoparticle case, we see that the increase of 7 saturation units in the aqueous phase steady state saturation (reduction of 7 saturation units in residual n-octane saturation) was remarkable given that only 0.01 was the difference in the endpoint relative permeability for the aqueous phase. The slight difference in the endpoint relative permeability values shows no significant reduction in the mobility of the invading aqueous phase. The only difference we have in this case is that in this primary imbibition displacement, Haines jump and Roof snap off,

which are hypothesized to be responsible for generating nanoparticle-stabilized emulsion, are not expected to occur as other pore scale mechanisms will take place. As a result, those other processes under the conditions listed in this experiment will not help in creating the necessary conditions for nanoparticle-stabilized emulsion to form. Although there was no indirect indication of nanoparticle-stabilized emulsion generation inside porous media during nanoparticles run, it seems that nanoparticles have impacted the displacement in a different way contributing to the remarkable reduction of 8 saturation points for the residual n-octane saturation. The cause for such observed reduction in residual saturation might be a combination of the slight increase in phase viscosity but more importantly the chemical composition of nanoparticles dispersion. The hydrophilic dispersion of nanoparticle used in this experiment is received from the manufacturer (Nissan Chemicals) containing almost 9 wt. % ethylene glycol as surface-treated silica particles which was later reduced to nearly 3 wt. % prior to the experiment. The presence of ethylene glycol and/or the chemicals used for coating those particles to create stable dispersions may have been the reason to explain reduction in residual n-octane saturation, hence, the increase in the aqueous phase saturation. Recalling the definition of the capillary number introduced back at chapter 3, it seems that ethylene glycol and/or some of the chemicals used for surface coating may have created some miscibility sites during the displacement and the interfacial tension between the aqueous phase and n-octane was reduced causing the capillary number to go up which will result in lowering the residual saturation of n-octane as per capillary saturation curve relationship. In addition to that, the 18% increase in aqueous phase viscosity may have also contributed to that increase in capillary number.

In summary, this displacement scenario under the conditions listed above did not show enough indirect evidence to confirm the possibility of nanoparticle-stabilized

emulsion. Nonetheless, the presence of some chemicals such as ethylene glycol and those used for coating to create a stable nanoparticles dispersion may have impacted the aqueous phase steady state saturation and caused the observed increase. As emulsion symptoms were observed during primary drainage in water-wet case, we next evaluate the nanoparticle impact on the displacement for secondary drainage experiment.

***Secondary Drainage (Core-G)***

A post flush stage followed the primary imbibition displacement with n-octane invading back to the core. Core-G is now saturated with either brine at 20% residual n-octane saturation for the control case or nanoparticle-brine dispersion at 13% residual n-octane saturation. This displacement stage is known as a secondary drainage as the core is not saturated completely with aqueous phase. The displacement flow rate was kept at 1 ml/min and data were recorded and effluent samples were collected

Figure 5.10 shows the pressure drop trend as a function of pore volume injected. The blue curve represents the pressure drop for the control experiment while the red curve shows the pressure drawdown behavior for the nanoparticles case. The dashed lines show the breakthrough time for both displacements. As shown in the plot, both displacement cases showed a similar pattern of pressure build up behavior where pressure drawdown was increasing with more pore volume injected until a peak pressure drop value is reached followed by a general decline trend reaching a certain leveling off values by the displacement end. However, there was some quite differences in pressure drop trends between control and nanoparticle case as will be addressed next.

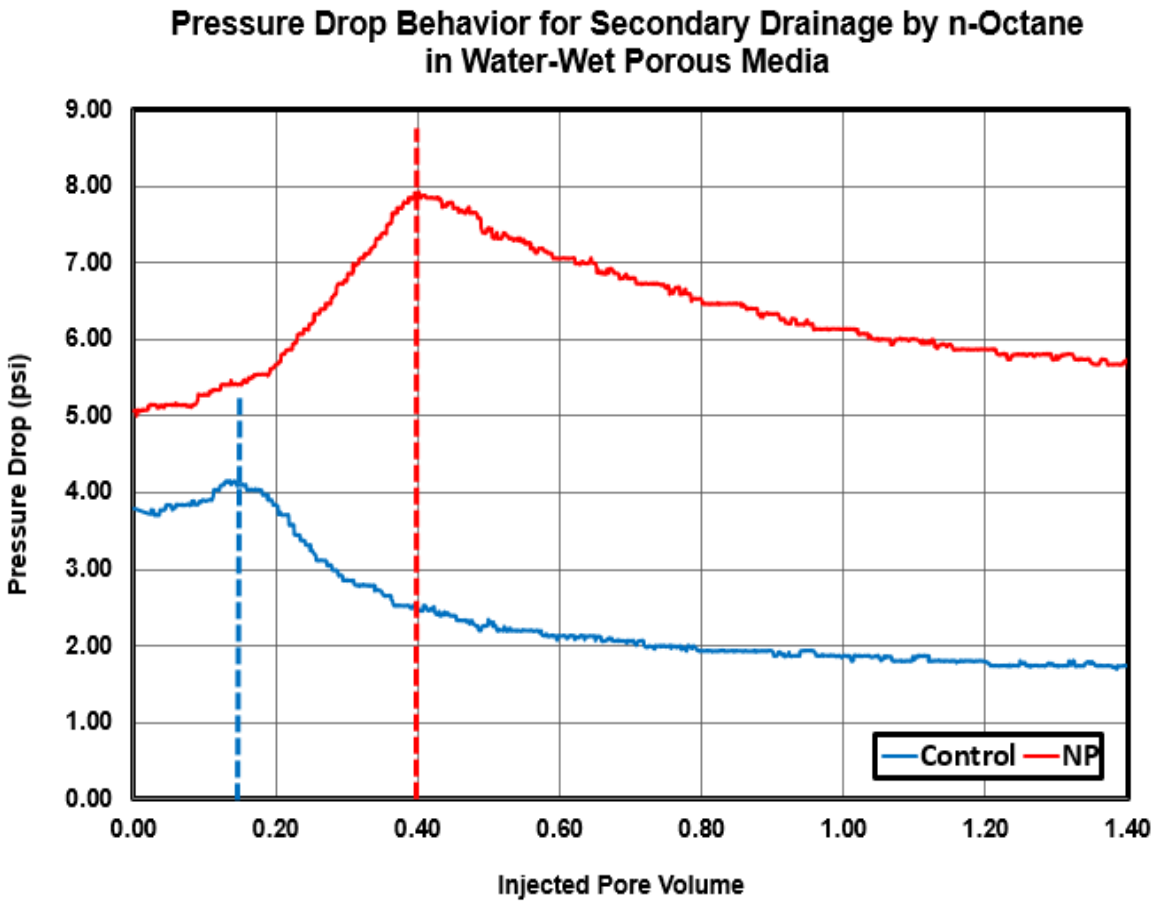


Figure 5.10: Measured pressure drop as a function of pore volume injected for control (blue) and nanoparticle case (red) into Boise sandstone for secondary drainage in water-wet core-G using n-octane. The dashed lines indicate breakthrough time.

Pressure normalization was carried in response to correcting for reduction in pore volume and permeability post IPA treatment. This was detailed before when primary imbibition case was presented. Normalized pressure drop curves for both control and nanoparticle case are shown in Figure 5.11.

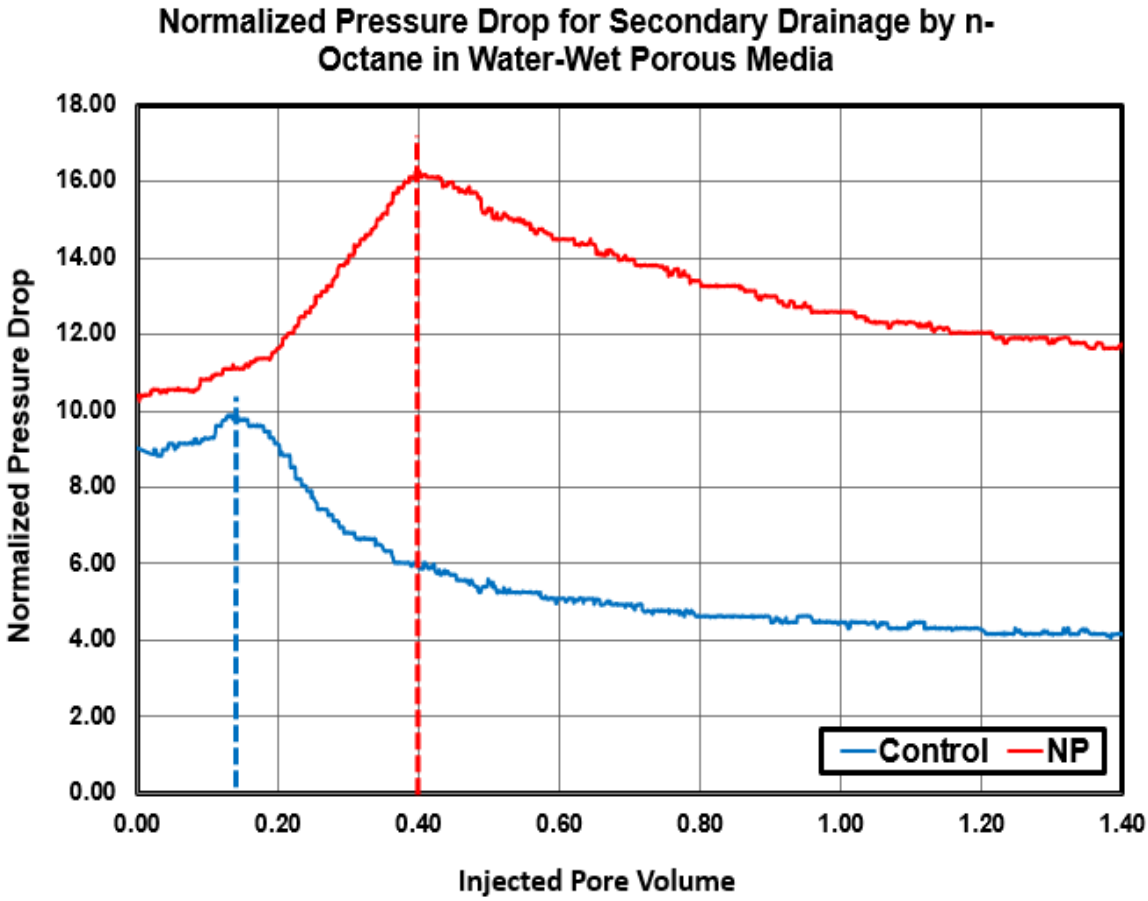


Figure 5.12: Normalized pressure drop as a function of pore volume injected for control (blue) and nanoparticle case (red) into Boise sandstone for secondary drainage in water-wet core-G using n-octane. The dashed lines indicate breakthrough time.

For the control experiment as shown in Figure 5.12 by the blue curve, the normalized pressure drop was increasing and reached a maximum value of 9.9 at 0.16 PV. After that, the pressure drop started to gradually decline and reached an asymptote value of about 4.1 at 1.4 PV. In this case, the pressure drop peak value corresponds to the breakthrough of n-octane from the core outlet as observed in the fraction collector. As for the nanoparticle case as illustrated in Figure 5.12 by the red curve, the normalized pressure drop showed comparable performance to that of the control case as pressure

drop reached a maximum value of 16.1 at 0.40 PV. After that, the pressure drop started to decline and reached an asymptote value of about 11.6 at 1.4 PV. In this case, the pressure drop peak value corresponds to the breakthrough of n-octane from the core outlet as observed in the fraction collector. It can be seen from Figure 5.12 that the nanoparticle case had a later breakthrough time that is 0.24 PV more compared to the control case (0.40 PV compared to 0.16 PV). In addition, nanoparticle experiment ended up with a higher normalized pressure drop that was nearly 39 % larger than that of the control case (16.1 compared to 11.6).

Figure 5.13 shows the water cut data which was collected during this displacement process. The blue curve shows the water cut values measured as a function of pore volume injected for the control experiment while the red curve shows the water cut for the nanoparticle case. For the control case, the water cut value maintained a value of 1 until the breakthrough time of 0.16 PV after which the water cut started to decrease until it reached an average of 0.02. As for the nanoparticle case, the water cut value maintained a value of 1 until the breakthrough time of 0.4 PV after which the water cut started to decrease until it reached values ranging between 0.04 and 0. Comparing both control and nanoparticle experiments, we see that the water cut reduction for the nanoparticle run occurred at later pore volume injected time that was 0.24 PV more compared to the control. Also, water cut trend after the time of breakthrough for the nanoparticle case showed a higher water cut values compared to the control case at the same time of injected pore volume.

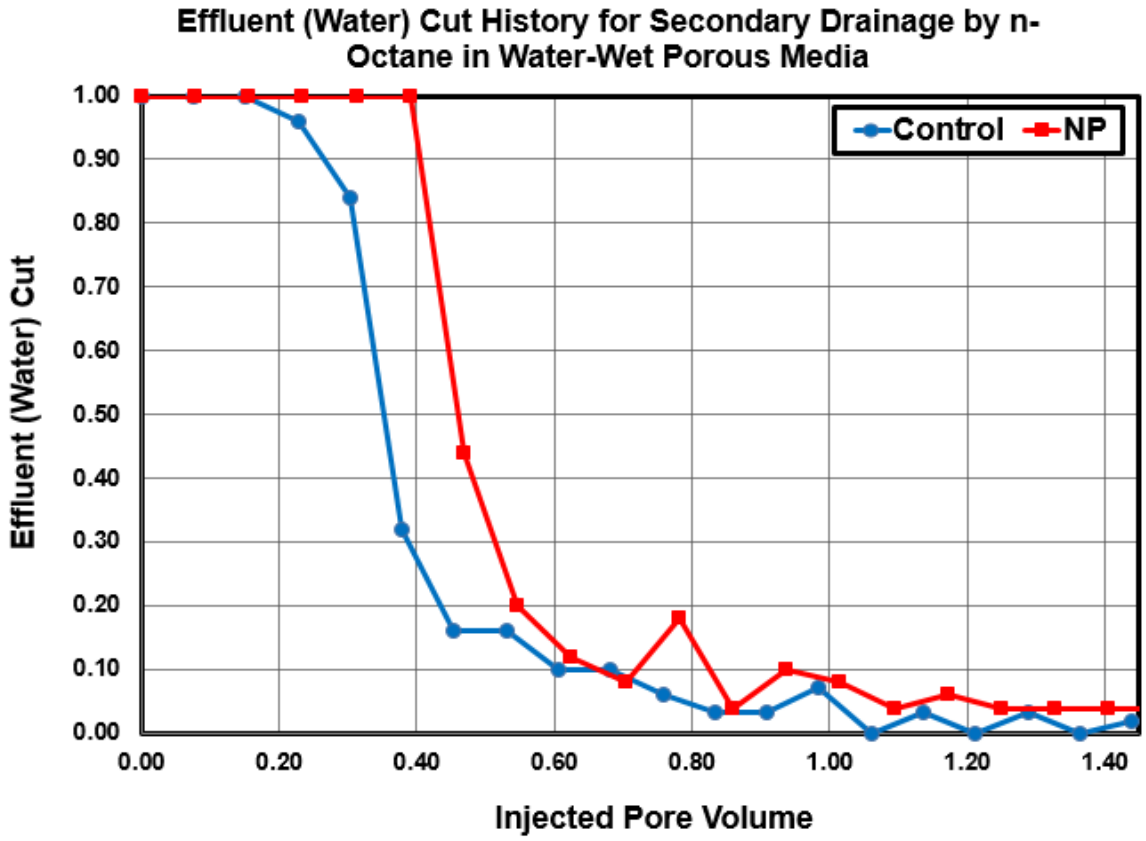


Figure 5.13: Effluent (water) cut as a function of pore volume injected for secondary drainage in water-wet core-G for both control (blue) and nanoparticle case (red).

The residual saturation of brine or brine containing nanoparticles was calculated based on the water cut measured in the effluent samples collected during the displacement. The core water saturation profiles are shown in blue for the control case and in red for the nanoparticle case as clearly illustrated in Figure 5.14. The water saturation was calculated by comparing the total volume of water recovered and the pore volume of the core. For the control run, the initial water saturation calculated at the beginning of this displacement stage is 80 % and it decreased until it reached a residual aqueous phase saturation of 42 %. As for the nanoparticles run, initial water saturation

calculated at the beginning of this displacement stage is 87 % and it decreased until it reached a residual aqueous phase saturation of 36 % as well. This suggest displacing an additional 13 saturation units of the aqueous phase for the nanoparticle case.

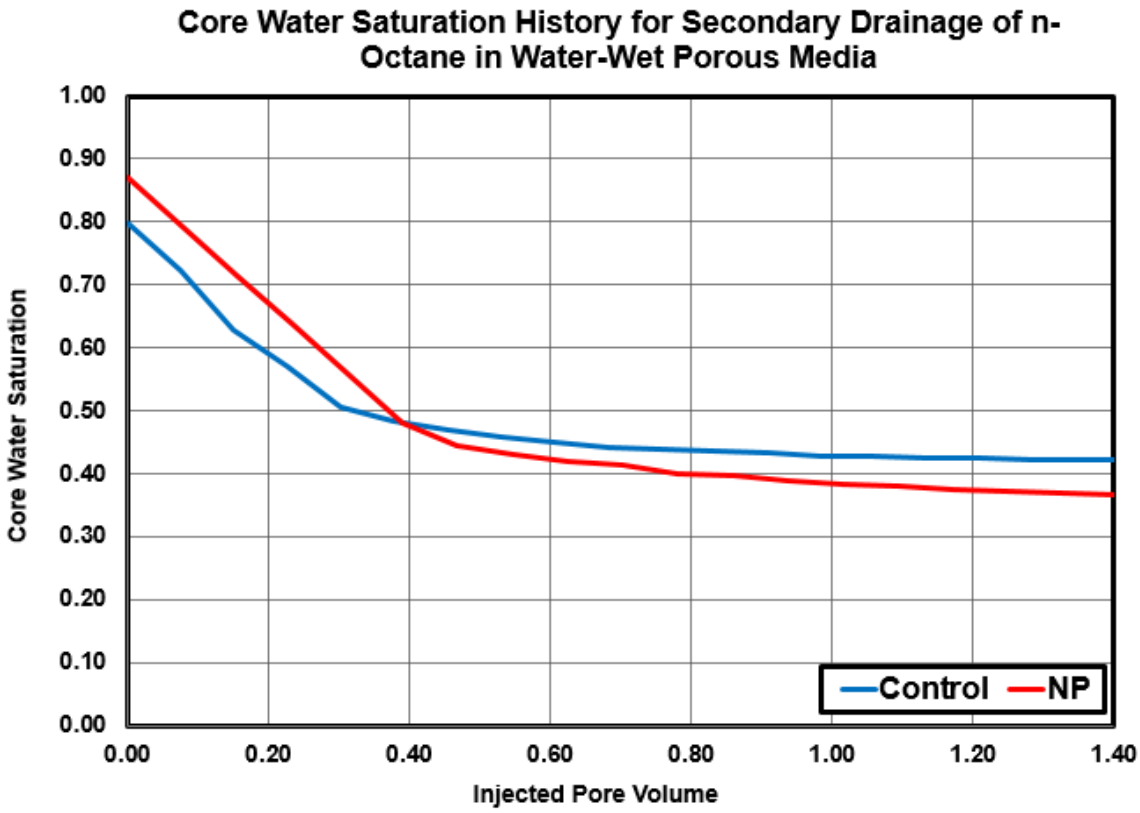


Figure 5.14: Average core water saturation history as a function of pore volume injected for secondary drainage in water-wet core-G for both control (blue) and nanoparticle case (red).

Figure 5.15 shows the pressure drop ratio of nanoparticles case compared to the control case. The ratio was calculated by dividing the normalized pressure drop measured at each point in time for nanoparticles case by the normalized pressure drop measured at the same moment in time for the control case. This pressure drop ratio was consistently 1.2 to 2.7 times greater than that of the control case. This large difference is despite the

fact that nanoparticles dispersion was only slightly more viscous compared to brine solution in the control case. That viscosity ratio was only 1.18 and is by far less than the observed ratios ranging from 1.2 to 2.7 highlighted before.

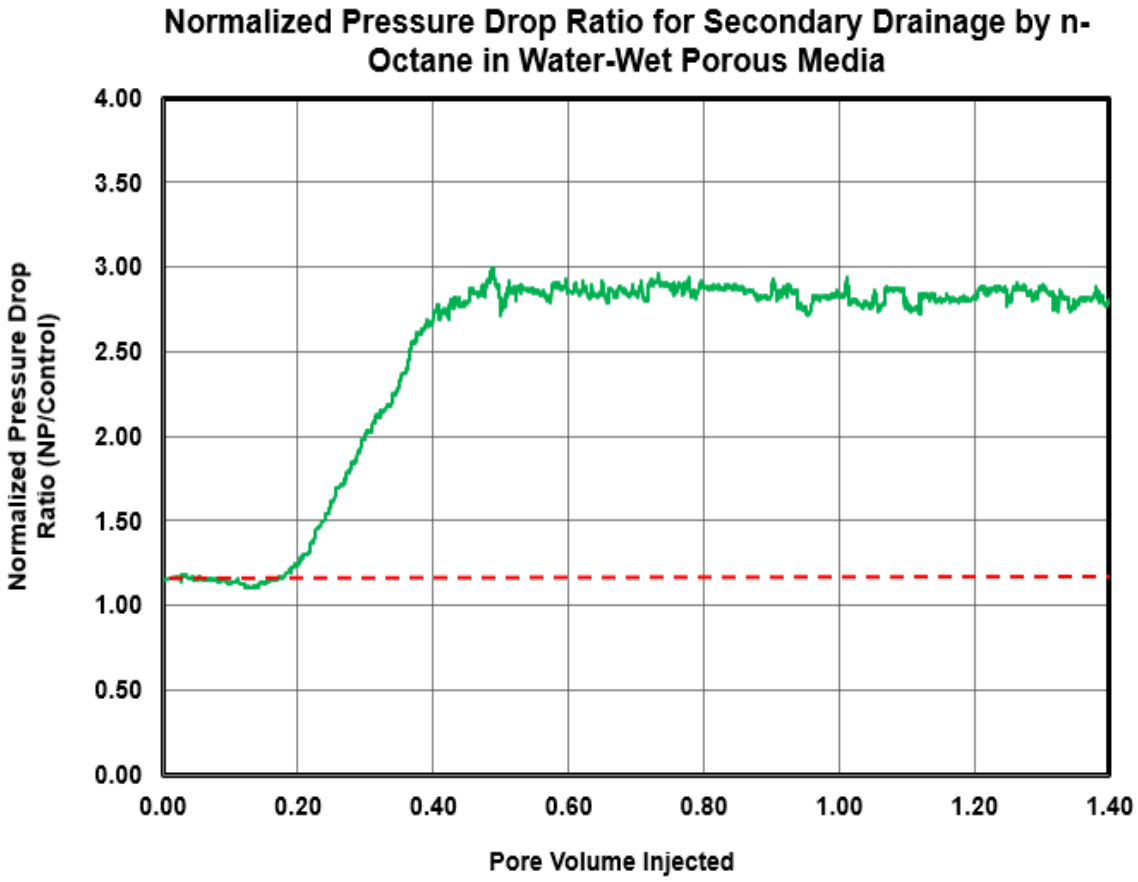


Figure 5.16: Pressure drop ratio calculated by dividing pressure drop measured at each point in time during nanoparticle case over that of the control case measured at the same moment. Ratio is expressed as a function of time for secondary drainage displacement in water-wet core-G using n-octane. Red dashed line represents the value of the viscosity ratio between the aqueous nanoparticle dispersion and brine solution.

Another important observation was the calculated endpoint relative permeability for the hydrocarbon phase ($k_{ro}^{o}$) which is given by:

$$k_{ro}^{o} = \frac{\Delta P_{o1}}{\Delta P_{o2}}$$

In the equation above, $\Delta P_{o1}$ represents the pressure drop for single phase n-octane flowing at steady state while $\Delta P_{o2}$ is the value of steady state pressure drop of n-octane phase flowing at residual aqueous phase saturation by the end of secondary drainage. In all cases, the flow rate was kept the same at 1 ml/min. The calculated endpoint relative permeability was 0.25 for the control case and 0.09 for the nanoparticle indicating a reduction of 64 % for the nanoparticle case.

The observations found during this experimental protocol had shown that nanoparticles had caused the pressure drop to increase sharply compared to the control case with pressure drop ratio being ranging from 1.2 to 2.7 times greater than that of the control case. Although nanoparticles dispersion was slightly more viscous and 1.18 times that of brine solution, the pressure drop ratio observed showed that this ratio is by far less than the observed pressure drop ratio of 2.7 seen with the nanoparticle case. Based on the hypothesis being tested, this increase in pressure drop for nanoparticles case may be attributed the fact that n-octane is now facing more resistance to flow as its path is being affected by the presence of nanoparticles armored droplets of oil-in-water emulsions as they intersect the path and may be plugging some pores This indicate a development of a more viscous phase that resulted in lower invading phase (n-octane) mobility.

This reduction in phase mobility was also confirmed by the 64% reduction in the end point relative permeability for the nanoparticle case as shown before. Also, it was shown nanoparticles had caused the residual aqueous phase saturation to decrease with an

average reduction of 13 saturation points units. In addition, the observed behavior of the displacement showed that nanoparticle case had a later breakthrough of 0.20 PV. All of these observations support the hypothesis that pore scale processes such as Haines jump and Roof snap off will provide enough energy to bring the nanoparticles to the interface and armor the droplets of non-wetting phase forming nanoparticle-stabilized emulsion inside the pores.

It is important here to address the effect of core initial conditions to the displacement behavior. In other words, despite the similarities in observing emulsion forming symptoms between primary drainage and secondary drainage in water-wet core with displacement involving a lower viscosity n-octane, yet, it can be seen that initial trapping of n-octane inside the core in the secondary drainage displacement process has affected the displacement when nanoparticles were present in a way that is different from the primary drainage. For example, the pressure drop trend for the nanoparticle was nearly flat for the first 0.15 PV before it started to slowly increase case and reached a peak value that is nearly 60 % larger compared to the initial starting pressure. Comparing this to primary drainage under the same experimental conditions, we see that pressure drop increase was observed right at the beginning of the displacement and it was increasing sharply reaching a peak value that was nearly 500 % larger compared to the initial stating pressure. This difference between both cases is govern by fluid distribution inside the core initially. Since it is hypothesized that the excessive increase in pressure drop for the nanoparticle case is mainly related to the development of nanoparticle-stabilized emulsion formed by Haines jump and Roof snap-off events, the severity of the pressure drop increase should be greatest when Haines jump and Roof snap-off are the most prevalent mechanisms during pore scale displacement. Those events require the wetting phase to be fully occupying the pore bodies. Therefore, the likelihood for these

events to occur will generally translate into forming more droplets inside pore space for nanoparticles to stabilize. Since the void space in this primary drainage case is mainly filled by the wetting phase, the chance for the Haines jump and Roof snap-off to occur and for nanoparticle-stabilized emulsion to form is greatest. This may explain 500 % increase that was observed during primary drainage case compared to only 60 % increase for the secondary drainage experiment. Not all the pores are filled with wetting phase during the secondary drainage experiment as the presence of some the non-wetting phase in residual form inside some of these pore bodies may prevent Haines jump and Roof snap-off from occurring or effect the process of nanoparticles to stabilize disconnected droplet of non-wetting phase.

Another notable difference between nanoparticles impact on primary drainage and secondary drainage is the nearly flat trend observed in pressure drop behavior for the first 0.15 PV injected. It might be that the presence of n-octane as a trapped phase has interrupted the sequence of events for the hypothesized Haines jump and Roof snap-off processes as n-octane has started to become connected when it invades pores where n-octane was initially trapped. Also the value of residual n-octane saturation may play a role in postponing the hypothesized emulsion generation process. In other words, the higher the residual saturation of a certain phase (n-octane in this case) means that the other phase will be less connected and more isolated. However, in this experiment, the core residual n-octane saturation was as low as 20% or even 13% for the nanoparticle case which means that the aqueous phase is more connected and less isolated. Yet even with that, the separation between both control and nanoparticle case did take place after nearly 0.19 PV which suggests that by that time, n-octane phase become connected with all of the trapped n-octane and now it started to displace those pores filled with aqueous phase only in a manner described by the suggested hypothesis presented back in chapter

3. The next section will discuss both primary imbibition and secondary drainage again with the same displacement sequence except that the rock's wettability is now oil-wet.

### 5.2.2 Displacement in Oil-Wet Porous Media

***Primary Imbibition (Core-D)***

A core flooding experiment was conducted on Core-D to evaluate nanoparticles impact on primary imbibition process in oil-wet Boise sandstone core. The core was initially saturated with n-octane prior to injecting brine in the control case and nanoparticle-brine dispersion in the second case. For both cases, a secondary drainage of post flush with n-octane followed the primary imbibition displacement and is presented in the next section.

Figure 5.17 shows the pressure drop trend as a function of pore volume injected. The blue curve represents the pressure drop for the control experiment while the red curve shows the pressure drawdown behavior for the nanoparticles case. The dashed lines show the breakthrough time for both displacements. As shown in the plot, both experiments show a similar pattern where pressure drop builds up with pore volume at the beginning of the displacement reaching a peak value by the time of breakthrough. After that, it started to slowly decline until it levelled off by the end of the displacement.

For the control experiment as shown in Figure 5.17 by the blue curve, the pressure drop was increasing and reached a maximum value of 1.47 psi at 0.63 PV. After that, the pressure drop started to slowly decline and reached an asymptote value of about 1.33 psi at 1.4 PV. In this case, the pressure drop peak value corresponds to the breakthrough of brine from the core outlet as observed in the fraction collector. As for the nanoparticle case as illustrated in Figure 5.17 by the red curve, the pressure drop showed comparable

performance to that of the control case as pressure drop reached a maximum value of 1.80 psi at 0.63 PV. After that, the pressure drop started to slowly decline and reached an asymptote value of about 1.66 psi at 1.4 PV. In this case, the pressure drop peak value corresponds to the breakthrough of nanoparticle-brine solution from the core outlet as observed in the fraction collector. It can be seen from Figure 5.17 that the nanoparticle case had a similar breakthrough time compared to the control case (0.63 PV for both cases). However, nanoparticle experiment ended up with a slightly higher pressure drop that was 0.33 psi larger than that of the control case (1.66 psi compared to 1.33 psi).

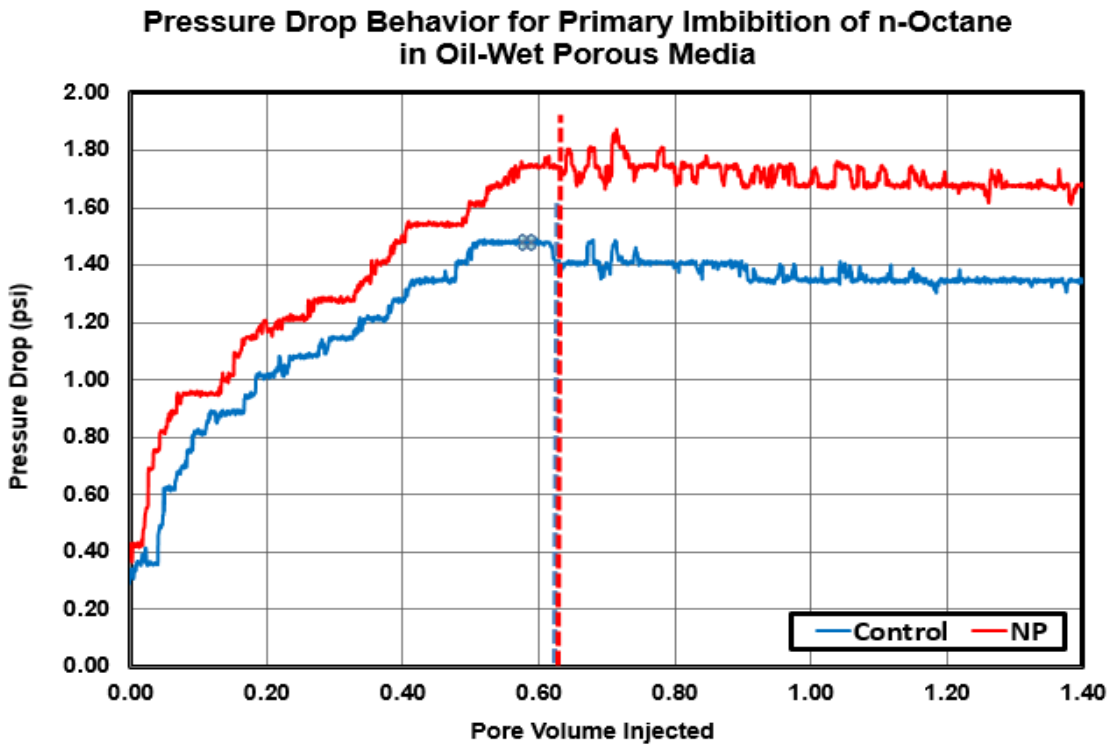


Figure 5.17: Measured pressure drop as a function of pore volume injected for control (blue) and nanoparticle case (red) into Boise sandstone for primary imbibition in oil-wet core-D using n-octane. The dashed lines indicate breakthrough time.

Figure 5.18 shows the water cut data which was collected during this displacement process. The blue curve shows the water cut values measured as a function of pore volume injected for the control experiment while the red curve shows the water cut for the nanoparticle case. For the control case, the water cut value maintained a value of 0 until the breakthrough time of 0.63 PV at which the water cut sharply increased to 0.96 and reached 1 as brine was the only phase flowing at residual n-octane saturation. As for the nanoparticle case, the water cut value maintained a value of 0 until the breakthrough time of 0.63 PV at which the water cut increased to 0.4 and reached 1 as nanoparticle-brine solution was only flowing at residual n-octane saturation. Comparing both control and nanoparticle experiments, we see that the water cut rise for the nanoparticle run occurred at the same pore volume injected time when compared to the control.

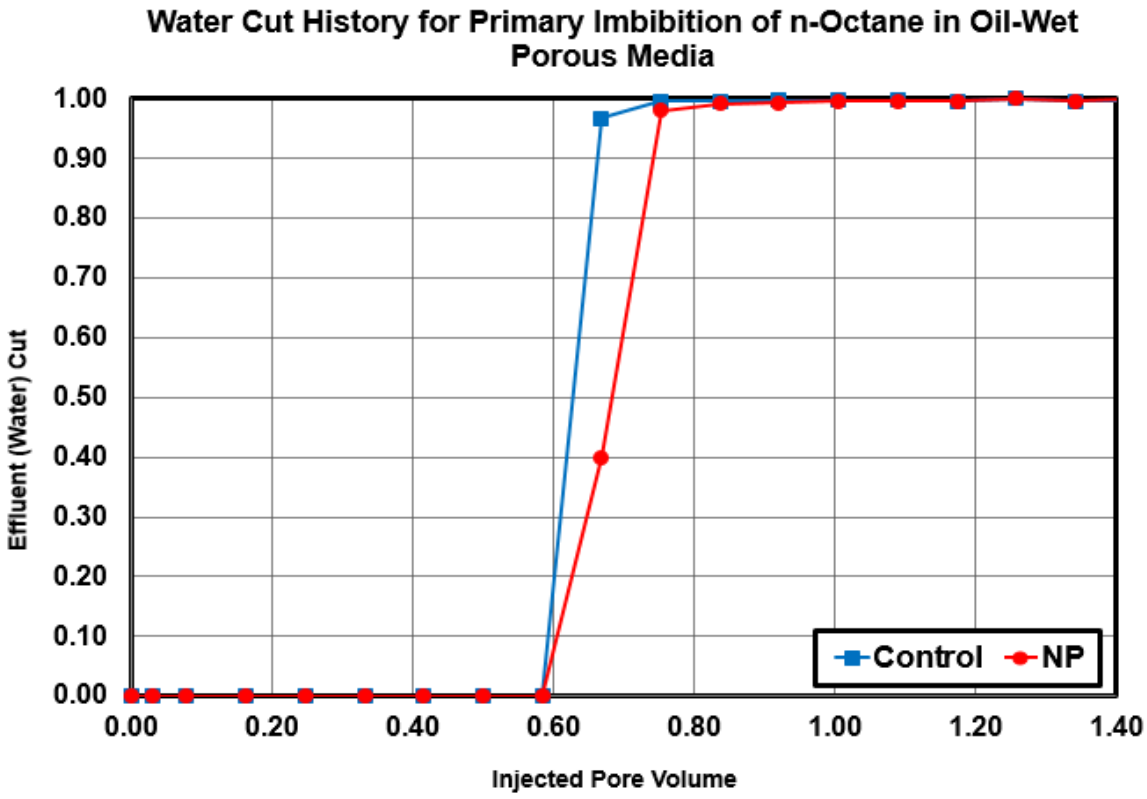


Figure 5.18: Effluent (water) cut as a function of pore volume injected for primary imbibition in oil-wet core-D for both control (blue) and nanoparticle case (red)

The saturation of brine or brine containing nanoparticles was calculated based on the water cut measured in the effluent samples collected during the displacement. The core water saturation histories are shown in blue for the control case and in red for the nanoparticle case as clearly illustrated in Figure 5.19. The water saturation was calculated by comparing the total volume of water recovered and the pore volume of the core. The steady state aqueous phase saturation for the control case was 65%. As for the nanoparticles run, the steady state saturation was increased to 70% indicating an average increase of 5 saturation unit.

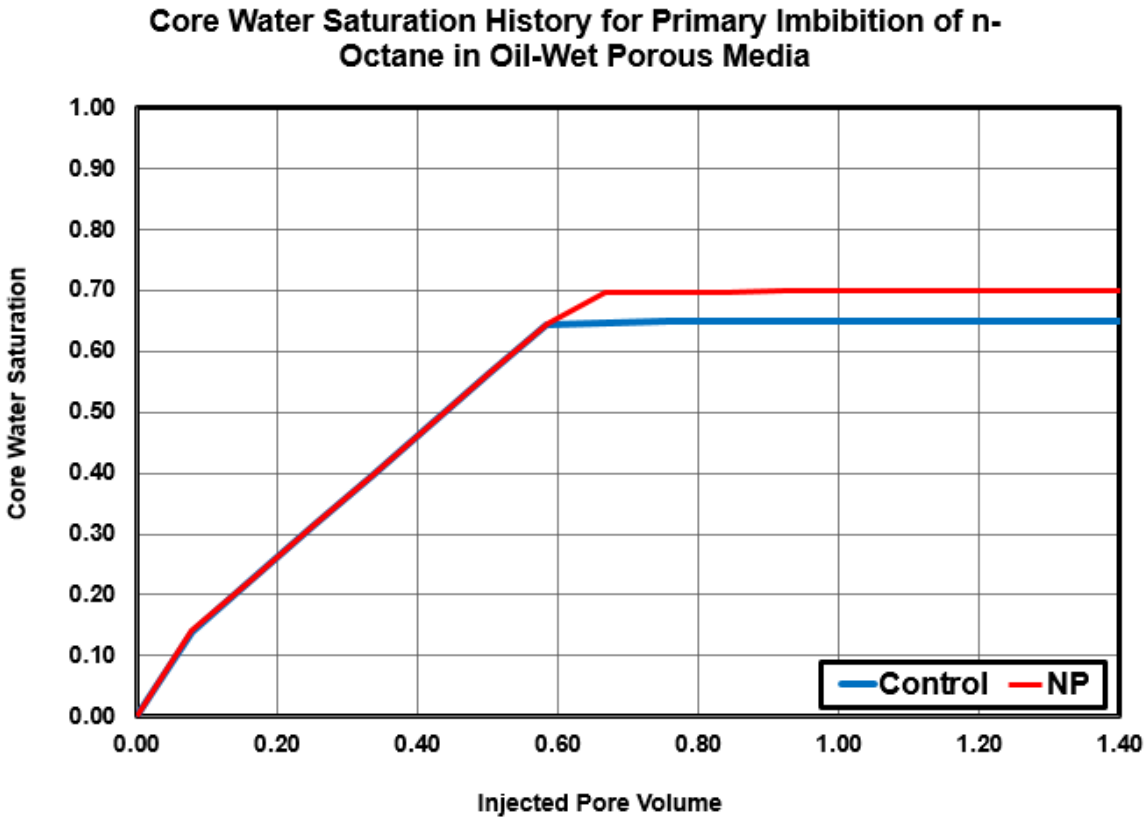


Figure 5.19: Average core water saturation history as a function of pore volume injected for primary imbibition in oil-wet core-D for both control (blue) and nanoparticle case (red).

Figure 5.20 shows the pressure drop ratio of nanoparticles case compared to the control case. The ratio was calculated by dividing the pressure drop of nanoparticles case measured at each point in time by the pressure drop for the control case measured at the same moment. As shown in the figure, the pressure drop ratio was initially around an average value of 1.20 for the first 0.63 PV injected and fluctuated from 1.20 to 1.30 afterward.

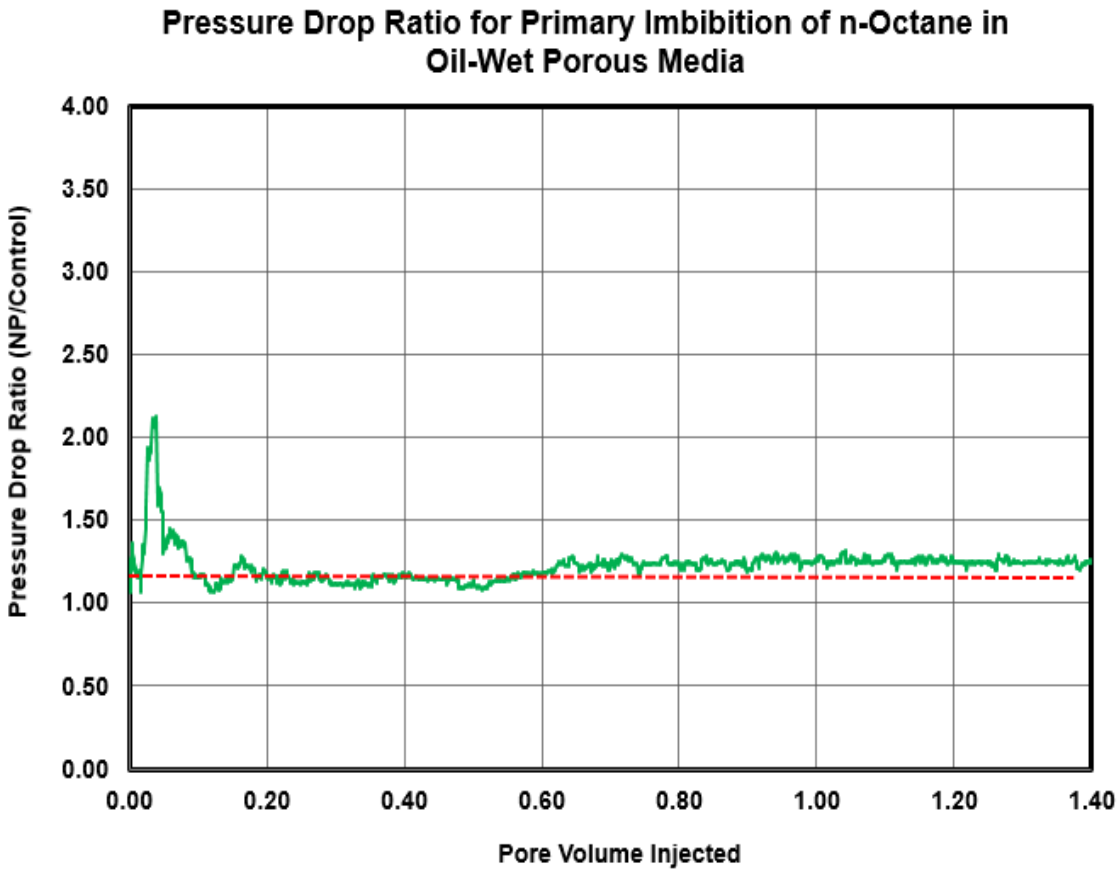


Figure 5.20: Pressure drop ratio calculated by dividing pressure drop measured at each point in time during nanoparticle case over that of the control case measured at the same moment. Ratio is expressed as a function of time for primary imbibition displacement in oil-wet core-D using n-octane. Red dashed line represents the value of the viscosity ratio between the aqueous nanoparticle dispersion and brine solution.

The endpoint relative permeability for the aqueous phase ($k_{rw}^{o}$) is given by:

$$k_{rw}^{o} = \frac{\Delta P_o \, \mu_w}{\Delta P_w \, \mu_o}$$

In the equation above, $\mu$ is the viscosity of the fluid represented by either $w$ for the aqueous phase or $o$ for the hydrocarbon phase. $\Delta P_o$ represents the pressure drop for single phase n-octane flowing at steady state while $\Delta P_w$ is the value of steady state

pressure drop of the aqueous phase flowing at residual hydrocarbon saturation. In all cases, the flow rate was kept the same at 1 ml/min. The calculated endpoint relative permeability was 0.57 for the control case and 0.53 for the nanoparticle indicating a reduction of 7 % for the nanoparticle case.

The observations found during this experimental protocol had shown that nanoparticles had caused almost no significant impact on the pressure drop performance as no excessive increase in pressure drawdown was observed. The pressure drop ratio was ranging between 1 and 1.30 throughout the entire experiment. In fact, this ratio was close to the viscosity ratio of 1.18 which is the viscosity ratio between brine solution and nanoparticle-brine dispersion. This suggests that the displacement behavior was impacted by the fact that nanoparticle dispersion was 18% more viscous compared to the control case. As a result, a 0.07 PV delay was seen in the breakthrough time for the nanoparticle case.

Despite the fact that the core is oil-wet, the displacement was viscously stable and nanoparticle-brine solution was likely to displace n-octane in a piston like manner. Even with that stability, wettability effect and pore geometrical changes may have caused some local preferential paths for some sites inside the core leading n-octane to snap-off as disconnected droplets or be left behind as a trapped lamellae. As the saturation of n-octane was declining as the front was reaching the breakthrough time, the pressure drop ratio was fluctuating around 1.30 to show that the trapped and isolated n-octane had restricted the flow of the aqueous phase.

Also, the increase in invading phase viscosity may have helped in making an already a stable displacement into a more stable one resulting in improving some additional oil. However, this slight increase in the aqueous phase viscosity may not be the primary reason for the reduction of the additional 5 saturation units in the residual

saturation of n-octane observed during the nanoparticle case. Similar to what was discussed during the primary imbibition displacement under water-wet condition, the presence of ethylene glycol and/or the chemicals used for coating those particles to create a stable aqueous nanoparticle dispersion may have been the reason to explain reduction in residual n-octane saturation, hence, the increase in the aqueous phase saturation Despite similarities in terms of the viscous stability of the displacement for both oil-wet and water-wet cases, the residual n-octane saturation values calculated for oil-wet core were 10 to 15% higher indicating that the core retained more n-octane as a result of the rock being oil-wet in this case. The additional trapped n-octane is mainly covering rock surfaces in a form of oil film and filling smaller pores to maximize contact with grain surfaces. This generally creates stronger capillary barriers which make it hard to access these sites unless excessive viscous forces are applied.

Despite the similarities between primary imbibition and primary drainage with respect to nanoparticle presence in general, the 0.04 difference (7% reduction) between the endpoint relative permeability values of the nanoparticle case and the control case shows no significant reduction in the mobility of the invading phase. In this displacement, the wetting phase is displaced by non-wetting phase and therefore, pore scale events of Haines jump and Roof snap-off are expected to occur. However, no indications as highlighted before to support that nanoparticle-stabilized emulsion formed during this displacement. Several reasons could have played a role in preventing the generation of nanoparticles-stabilized emulsion. Those factors include the viscous stability of the displacement as well as the fact that nanoparticles used in this experiments are hydrophilic and are placed in the aqueous phase may have hinder the possibility of generating water in oil emulsion as the wetting nature of those particles would generally tend to make oil in water emulsion. Also, another possibility is that the phenomenon is

heavily dependent on fluid properties and on which fluid is displacing and which one is displaced. To confirm that, we next present the findings for the secondary drainage experiment in oil-wet core.

***Secondary Drainage (Core-D)***

A post flush stage followed the primary imbibition displacement with n-octane invading back to the core. Core-D is now saturated with either brine at 35% residual n-octane saturation for the control case or nanoparticle-brine dispersion at 30% residual n-octane saturation. This displacement stage is known as a secondary drainage as the core is not saturated completely with aqueous phase. The displacement flow rate was kept at 1 ml/min and data were recorded and effluent samples were collected

Figure 5.21 shows the pressure drop trend as a function of pore volume injected. The blue curve represents the pressure drop for the control experiment while the red curve shows the pressure drawdown behavior for the nanoparticles case. The dashed lines show the breakthrough time for both displacements. As shown in the plot, both displacement cases showed a different pattern of pressure build up behavior where drawdown was increasing with more pore volume injected until a peak pressure drop value is reached followed by a general decline trend reaching a certain leveling off values by the displacement end.

For the control experiment as shown in Figure 5.21 by the blue curve, the pressure drop was increasing and reached a plateau value of 1.53 psi at 0.34 PV. After that, the pressure drop started to gradually decline and reached an asymptote value of about 1.14 psi at 1.4 PV. In this case, the pressure drop plateau value corresponds to the breakthrough of n-octane from the core outlet as observed in the fraction collector. As for the nanoparticle case as illustrated in Figure 5.21 by the red curve, the pressure drop

showed a dramatically different performance compared to that of the control case as pressure drop sharply increased reaching a maximum value of 3.57 psi at 0.46 PV. After that, the pressure drop started to gradually decline and reached an asymptote value of about 3.05 psi at 1.4 PV. In this case, the pressure drop peak value corresponds to the breakthrough of n-octane from the core outlet as observed in the fraction collector. It can be seen from Figure 5.21 that the nanoparticle case had a later breakthrough time that is 0.12 PV more compared to the control case (0.46 PV compared to 0.34 PV). In addition, nanoparticle experiment ended up with a higher pressure drop that was 1.91 psi larger than that of the control case (3.05 psi compared to 1.14 psi).

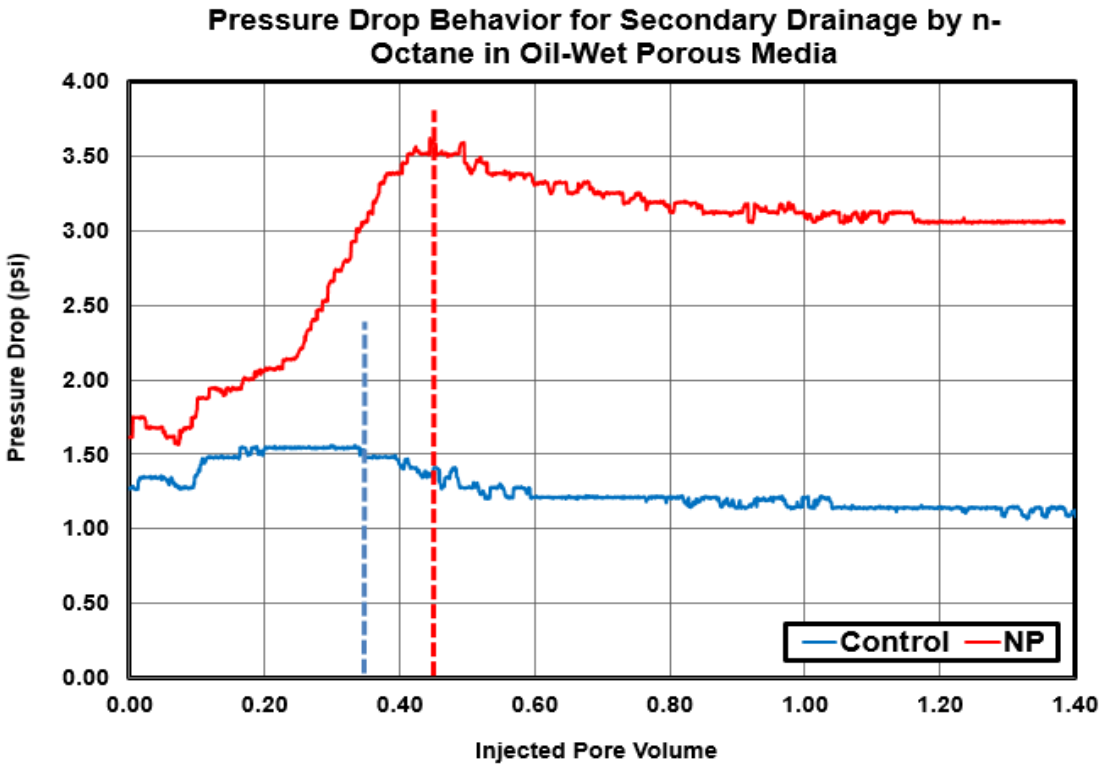


Figure 5.21: Measured pressure drop as a function of pore volume injected for control (blue) and nanoparticle case (red) into Boise sandstone for secondary drainage in oil-wet core-D using n-octane. The dashed lines indicate breakthrough time.

Figure 5.22 shows the water cut data which was collected during this displacement process. The blue curve shows the water cut values measured as a function of pore volume injected for the control experiment while the red curve shows the water cut for the nanoparticle case. For the control case, the water cut value maintained a value of 1 until the breakthrough time of 0.34 PV after which the water cut started to decrease until it reached almost 0 as n-octane was only flowing at residual aqueous phase saturation. As for the nanoparticle case, the water cut value maintained a value of 1 until the breakthrough time of 0.46 PV after which the water cut started to decrease until it reached nearly 0 as n-octane was only flowing at residual aqueous phase saturation. Comparing both control and nanoparticle experiments, we see that the water cut reduction for the nanoparticle run occurred at later pore volume injected time that was 0.12 PV more compared to the control.

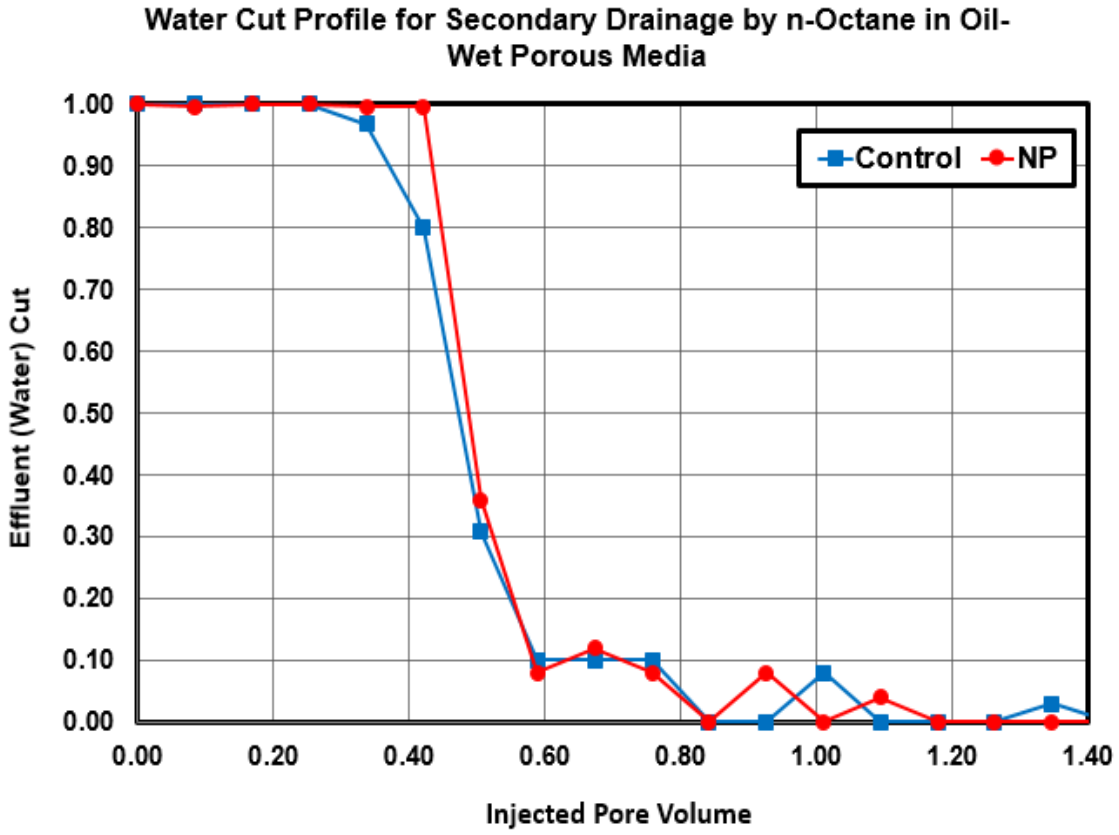


Figure 5.22: Effluent (water) cut as a function of pore volume injected for secondary drainage in oil-wet core-D for both control (blue) and nanoparticle case (red).

The residual saturation of brine or brine containing nanoparticles was calculated based on the water cut measured in the effluent samples collected during the displacement. The core water saturation histories are shown in blue for the control case and in red for the nanoparticle case as clearly illustrated in Figure 5.23. The water saturation was calculated by comparing the total volume of water recovered and the pore volume of the core. For the control run, the initial water saturation calculated at the beginning of this displacement stage is 65 % and it decreased until it reached a residual aqueous phase saturation of 18 %. As for the nanoparticles run, initial water saturation

calculated at the beginning of this displacement stage is 70 % and it decreased until it reached a residual aqueous phase saturation of 22 % as well. This suggest displacing an additional 1 saturation units of the aqueous phase for the nanoparticle case.

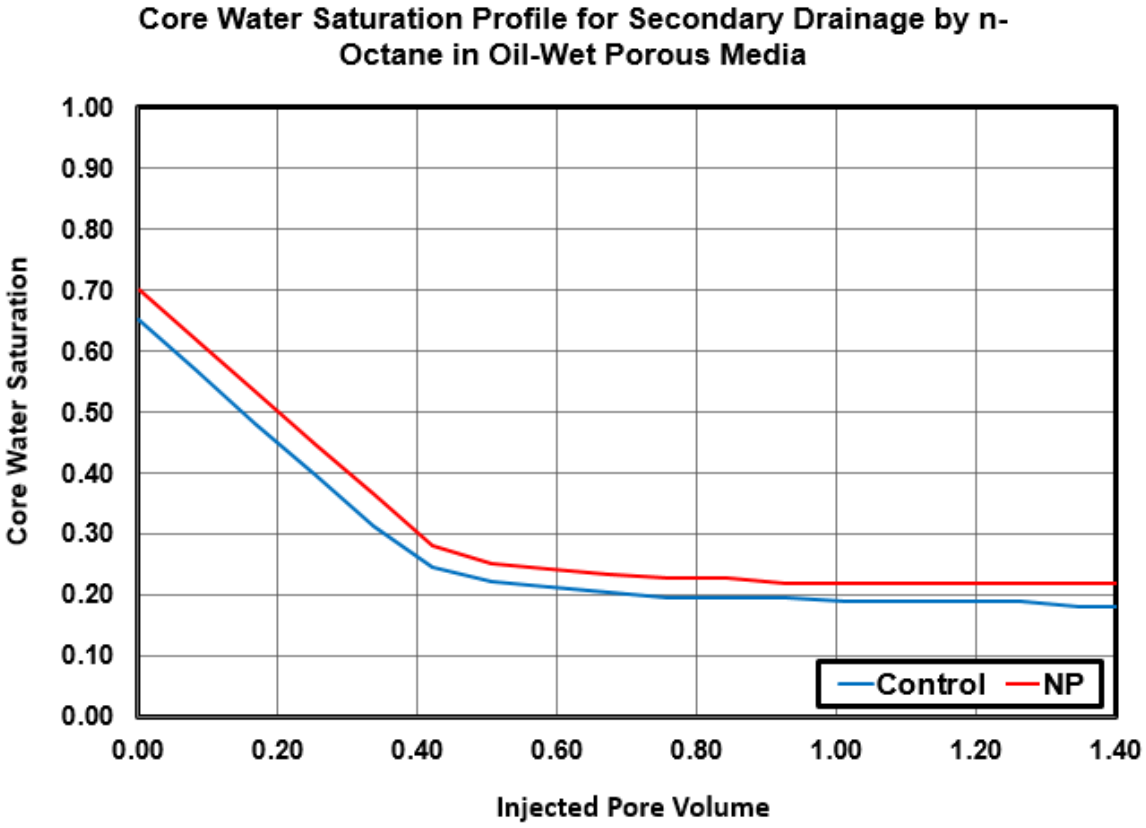


Figure 5.23: Average core water saturation history as a function of pore volume injected for secondary drainage in oil-wet core-D for both control (blue) and nanoparticle case (red).

Figure 5.24 shows the pressure drop ratio of nanoparticles case compared to the control case. The ratio was calculated by dividing the pressure drop of nanoparticles case measured at each point in time by the pressure drop for the control case measured at the

same moment. This pressure drop was consistently 1.2 to 2.7 times greater than that of the control case and was maintained at nearly 2.7 for almost the rest of the displacement.

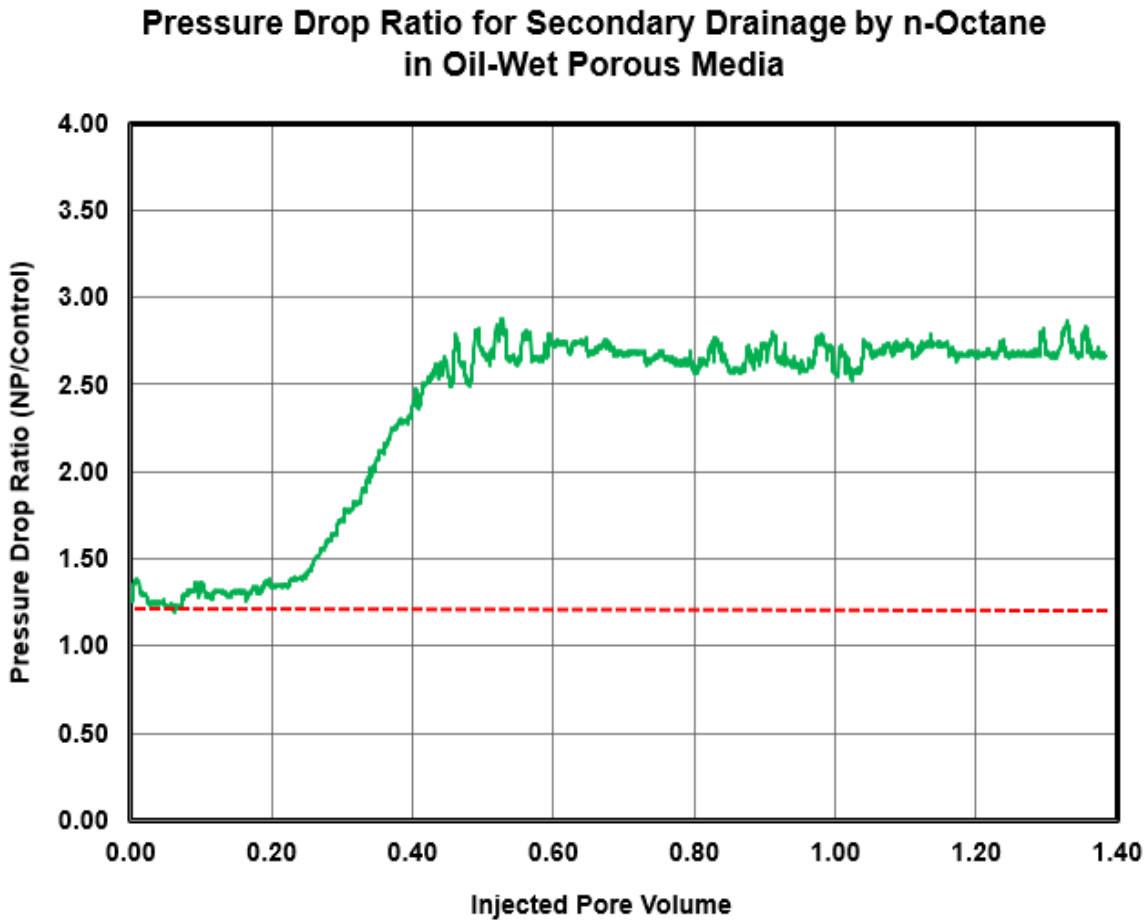


Figure 5.24: Pressure drop ratio calculated by dividing pressure drop measured at each point in time during nanoparticle case over that of the control case measured at the same moment. Ratio is expressed as a function of time for secondary drainage displacement in oil-wet core-D using n-octane. Red dashed line represents the value of the viscosity ratio between the aqueous nanoparticle dispersion and brine solution.

The calculated endpoint relative permeability for the hydrocarbon phase ($k_{ro}^{o}$) is given by:

$$k_{ro}^{o} = \frac{\Delta P_{o1}}{\Delta P_{o2}}$$

In the equation above, $\Delta P_{o1}$ represents the pressure drop for single phase n-octane flowing at steady state while $\Delta P_{o2}$ is the value of steady state pressure drop of tetradecane phase flowing at residual aqueous phase saturation by the end of secondary drainage. In all cases, the flow rate was kept the same at 1 ml/min. The calculated endpoint relative permeability was 0.33 for the control case and 0.12 for the nanoparticle indicating a reduction of 63 % for the nanoparticle case.

The observations found during this experimental protocol had shown that nanoparticles had caused the pressure drop to increase sharply compared to the control case with pressure drop ratio being ranging from 1.2 to 2.7 times greater than that of the control case. Although nanoparticles dispersion was slightly more viscous and 1.18 times that of brine solution, the pressure drop ratio observed showed that this ratio is by far less than the observed pressure drop ratio of 2.7 seen with the nanoparticle case. Based on the hypothesis being tested, this increase in pressure drop for nanoparticles case may be attributed the fact that n-octane is now facing more resistance to flow as its path is being affected by the presence of nanoparticles armored droplets of oil-in-water emulsions as they intersect the path and may be plugging some pores. This indicate a development of a more viscous phase that resulted in lowering the invading phase (n-octane) mobility. The emulsion generation process may be explain under one of the two arguments that will be discussed later. The reduction in phase mobility was also confirmed by the 63% reduction in the endpoint relative permeability for the nanoparticle case as shown before. Also, it

was shown nanoparticles had caused the residual aqueous phase saturation to decrease with an average drop of nearly 1 saturation unit. In addition, the observed behavior of the displacement showed that nanoparticle case had a later breakthrough of 0.20 PV. All of these observations present some indirect evidences for viscous phase development inside porous media. Those indicators are similar to those observed during the same displacement type under water-wet condition where it was hypothesized that nanoparticle-stabilized emulsion was generated. If this is the case, it is important then to understand how nanoparticles were able to help generating nanoparticle-stabilized emulsion in the absence of Haines jump and Roof snap-off mechanisms hypothetically assumed to be the essential events that would help in creating the conditions for the nanoparticle-stabilized emulsion to form.

The fact that emulsion generation symptoms were observed for secondary drainage process under both wettability suggests two interesting arguments. The first argument regarding the emulsion generation symptoms observed during the secondary drainage in oil-wet core is that the core started to act like a water-wet core. In this claim, it is hypothesized that nanoparticles have been brought to the interface between n-octane and the aqueous phase at the some sites inside the rock. As those particles generally stabilize the interface, this would suggest, if this happen, that nanoparticle dispersion is now covering the hydrocarbon layer previously attached to the rock through chemical means in the wettability alteration procedure. The layer of nanoparticles would form a hydrophilic coating attached to the oil layers covering the grains especially in the large pore spaces. In other words, the injected n-octane would now see the rock as if it were water-wet at least in those sites. As a result, the hypothesis of Haines jump and Roof snap-off being responsible for generating emulsion in porous media may still hold true in this case. This argument is supported by the fact that endpoint relative permeability for

the invading hydrocarbon phase was reduced by almost the same amount, if not slightly less, compared to that found during secondary drainage under water-wet condition (nearly 63 % reduction). Also, the residual aqueous phase saturation for the nanoparticle case was reduced by 1 saturation unit which may be an indication of improved sweep action resulted likely from the development of what seems to be nanoparticle-stabilized emulsion. As discussed before, since we assume that nanoparticles have somehow modified the wetting nature of some sites inside the core to be more hydrophilic, water in this case has become the new wetting phase inside those sites and that the invading n-octane is now acting as non-wetting phase. Under such condition, n-octane will jump and snap-off as explained by Haines jump and Roof snap-off and form droplets which will be stabilized by nanoparticles that are present in the aqueous phase. As the displacement front moves, those stabilized droplets will attempt to travel along the front but since they are more viscous and may attempt to plug some of the pore throats as they travel along, the mobility of the invading n-octane is then reduced as it is being forced out of its preferential paths. This will cause the displacement front to slow down and access more sites inside the rock displacing more of the aqueous phase out. Therefore, we see that we have a slight increase of 1 saturation unit in the residual aqueous phase saturation for the nanoparticle case compared to the control case. Compared to the increase in the aqueous phase saturation found during secondary drainage under water-wet condition (increase of 6 saturation units), we see a difference of 2 saturation units which suggest that actually agrees with our suggested argument that the wettability has only been modified in some sites (mainly large pore bodies) while some sites (smaller pores) are still oil-wet and may not have been accessed during the previous displacement stage. Having some sites to be hydrophobic suggest that n-octane (which is a preferred fluid by the rock in this case) was retained by the rock at those sites which explain the lower residual aqueous phase

saturation by the end of the secondary drainage under oil-wet condition. To further test this claim, a capillary pressure vs. saturation curve has to be established to quantify the wettability behavior of the rock.

The second argument is that rock wettability has no controlling effect on emulsion generation process and that there are other processes beside Haines jump and Roof snap-off which occurred during this secondary drainage displacement that might contribute to emulsion generation inside porous media. Assuming that the rock is still oil-wet, in this case, n-octane invades the core trying to displace the nanoparticle dispersion out. The difference in viscosity between both fluids create viscous instability which might lead n-octane to finger through the aqueous phase and/or forced to flow through the conductive hydrocarbon layer covering rock surfaces. During this displacement type where wetting phase attempt to displace non-wetting phase, it is expected for n-octane to travel faster compared to the more viscous aqueous dispersion of nanoparticles causing the non-wetting phase to snap-off inside pore bodies. The viscous instability would suggest bypassing the aqueous phase at some sites inside the porous media which will translate into having higher residual aqueous phase saturation. However, this is not the case here. Experimental observations suggesting the generation of nanoparticle-stabilized emulsion found during the secondary drainage experiment under water-wet condition are similar to those observations found here. Given that no Haines jump and Roof snap-off to occur under oil-wet conditions, it seems that nanoparticle-stabilized emulsion will form regardless of the existence of those pore scale events. In this case and under oil-wet conditions, it seems that as long as nanoparticles of suitable wettability are placed in the displaced fluid inside porous media and then was displaced by another displacing fluid, nanoparticle-stabilized emulsion will form. In this case, any pore scale event that may lead to the snap-off of the displacing fluid may cause nanoparticle-stabilized emulsion to

form. This argument may also explain why nanoparticle-stabilized emulsion was not observed during the primary imbibition displacement under both oil and water-wet condition since nanoparticles were present in the displacing phase instead of the displaced fluid.

It is important here to address the effect of core initial conditions to the displacement behavior. It can be seen that initial trapping of n-octane inside the core in the secondary drainage displacement process has affected flow path and displacement patterns in a way that is different from the primary drainage in the water-wet case but similar to that of secondary drainage in water-wet case. The similarities between secondary drainage in both oil-wet and water-wet were observed by looking at the pressure drop response, breakthrough time, and the residual n-octane saturation history. Under both wettability conditions, the pressure drop behavior for both control and nanoparticle run during secondary drainage flood were comparable during the first portion of the displacement when nearly 0.18 or 0.19 PV was injected into the core. After that, the core may have reached a certain critical saturation where both control and nanoparticle experiments started to show different displacement pattern where rapid increase in pressure drawdown was observed in the nanoparticle case. The pressure drop rise continued until it reached its maximum at the breakthrough time for both experiments then was followed by decline in pressure drop until steady state flow of n-octane at residual aqueous phase was reached.

Another similarity between the oil-wet and water-wet secondary drainage displacement is the later breakthrough time compared to the control case. In water-wet, the secondary drainage breakthrough time was 0.2 PV later than that of the control run. As for the oil-wet, the breakthrough was 0.1 PV later than that of the control case. The delay difference between both experiments is resulted from the fact that the oil-wet

experiment had later breakthrough (0.34 PV) compared to the water-wet one (0.19 PV). The difference in breakthrough time for the secondary drainage process involving n-octane injection to displace the aqueous phase is due to the difference in how phases are distributed inside porous media under different wettability conditions. After primary imbibition process, the morphology of n-octane inside the core is different between the water-wet and oil-wet. In water-wet, n-octane is mainly trapped inside large pores in a form of large blobs. By filling larger pores as a non-wetting phase, it is easier for the injected n-octane to establish connection with these disconnected blobs of trapped n-octane inside porous media where flow paths are more conductive. However, in the oil-wet case, the n-octane is mainly filling smaller pores to maximize contact with rock surfaces. As for larger pores, n-octane will mainly cover the grains in the form of thin oil layer covering the grains while aqueous phase is filling large pore bodies. Under such condition of fluid distribution, flow paths for n-octane in this case are less conductive as n-octane faces more resistance to displace the more viscous aqueous phase occupying larger pore bodies or simply occupying the high conductive paths inside the core. As a result, the invading n-octane will generally have later breakthrough time for the oil-wet case compared to water-wet case. Yet, both cases showed similar behavior of later breakthrough and symptoms for nanoparticle-stabilized emulsion forming inside porous media when nanoparticles are present in the system.

Similar to secondary drainage in water-wet, the value of residual n-octane saturation may play a role in postponing the hypothesized emulsion generation process. In other words, the higher the residual saturation of a certain phase (n-octane in this case) means that the other phase will be less connected and more isolated. However, in this experiment, the core residual n-octane saturation was as low as 35% or even 30% for the nanoparticle case which means that the aqueous phase is somewhat connected and less

isolated. Yet even with that, the separation between both control and nanoparticle case did take place after nearly 0.18 PV which suggests that by that time, n-octane phase become connected with all of the trapped n-octane and now it started to displace those pores filled with aqueous phase only in a manner described by the suggested hypothesis.

## 5.3 HIGHER-OIL VISCOSITY DISPLACEMENT

### 5.3.1 Displacement in Water-Wet Porous Media

This section focuses on all experimental tests conducted on water-wet porous media where the impact of nanoparticle presence in the system of the displacement is evaluated. The hydrocarbon phase that will be used for these tests is tetradecane which has higher viscosity than that of either brine or nanoparticle-brine dispersion.

***Primary Drainage (Core-J)***

A core flooding experiment was conducted on Core-J to evaluate nanoparticles impact on primary drainage process in water-wet Boise sandstone core. Tetradecane is used as a more viscous hydrocarbon phase. Prior to tetradecane injection into the core, the core was initially saturated with brine for the control case and nanoparticle-brine dispersion for the second case.

Figure 5.25 shows the pressure drop trend as a function of pore volume injected. The blue curve represents the pressure drop for the control experiment while the red curve shows the pressure drawdown behavior for the nanoparticles case. The dashed lines show the breakthrough time for both displacements. As shown in the plot, both displacement cases showed a similar pattern of pressure build up behavior where drawdown was increasing with more pore volume injected until a peak pressure drop

value is reached followed by a general decline trend reaching a certain leveling off values by the displacement end.

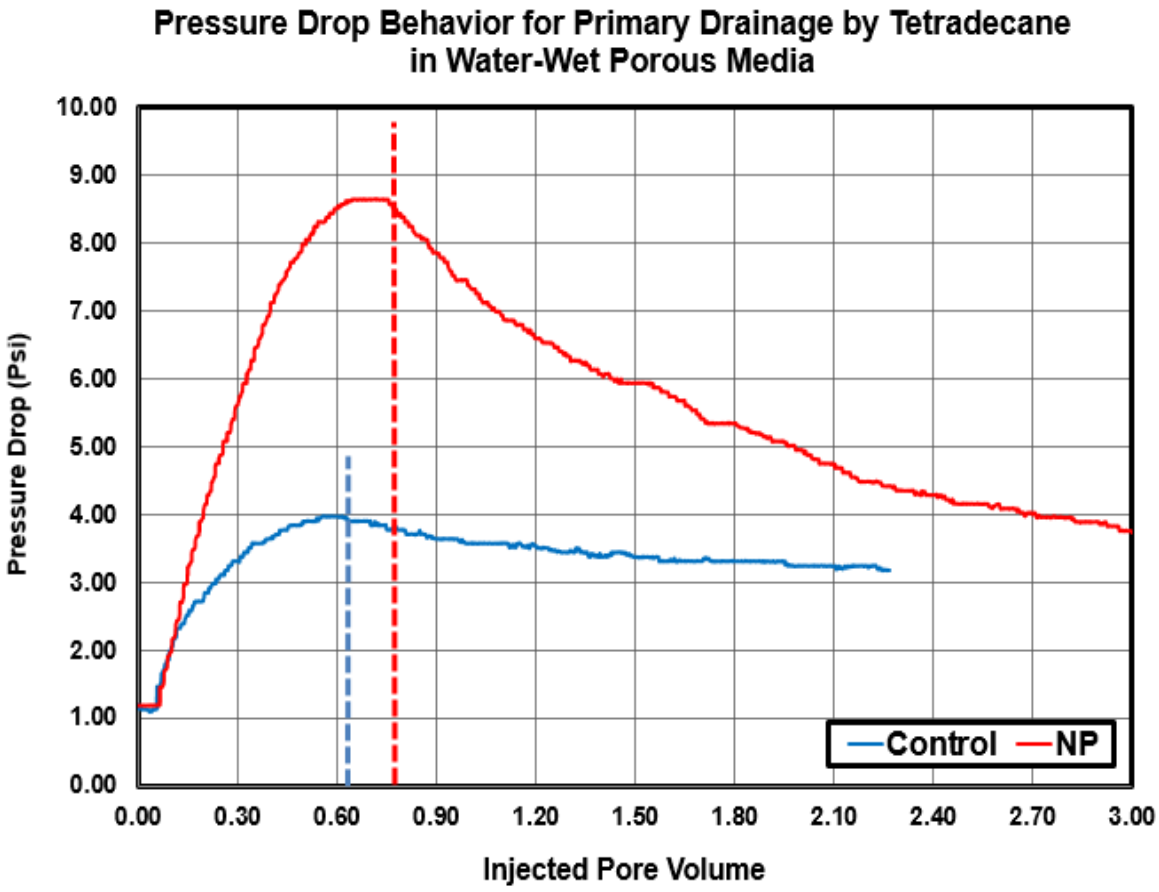


Figure 5.25: Measured pressure drop as a function of pore volume injected for control (blue) and nanoparticle case (red) for primary drainage into water-wet core-J using tetradecane. The dashed lines indicate breakthrough time.

For the control experiment as shown in Figure 5.25 by the blue curve, the pressure drop was increasing and reached a peak value of 4 psi at 0.62 PV. After that, the pressure drop started to gradually decline and reached an asymptote value of about 3.18 psi at 2.25 PV. In this case, the pressure drop peak value corresponds to the breakthrough of tetradecane from the core outlet as observed in the fraction collector. As for the

nanoparticle case as illustrated in Figure 5.25 by the red curve, the pressure drop showed a similar performance to that of control case with sharp increasing trend as pressure drop reached a maximum value of 8.55 psi at 0.76 PV. After that, the pressure drop started to decline and reached an asymptote value of about 3.75 psi at 3.0 PV. In this case, the pressure drop peak value corresponds to the breakthrough of tetradecane from the core outlet as observed in the fraction collector. It can be seen from Figure 5.25 that the nanoparticle case had a later breakthrough time that is 0.14 PV more compared to the control case (0.76 PV compared to 0.62 PV). In addition, nanoparticle experiment ended up with a higher pressure drop that was 0.57 psi larger than that of the control case (3.75 psi compared to 3.18 psi). We next present the water cut and core saturation profiles.

Figure 5.26 shows the water cut data which was collected during this displacement process. The blue curve shows the water cut values measured as a function of pore volume injected for the control experiment while the red curve shows the water cut for the nanoparticle case. For the control case, the water cut value maintained a value of 1 until the breakthrough time of 0.62 PV after which the water cut started to drop rapidly to 0.12 and reached 0 as tetradecane was only flowing at residual aqueous phase (brine) saturation. As for the nanoparticle case, the water cut value maintained a value of 1 until the breakthrough time of 0.76 PV after which the water cut started to drop rapidly to 0.8 and reached 0 as tetradecane was only flowing at residual aqueous phase (brine-nanoparticle solution) saturation. Comparing both control and nanoparticle experiments, we see that the water cut reduction for the nanoparticle run occurred at later pore volume injected time that was 0.14 PV more compared to the control.

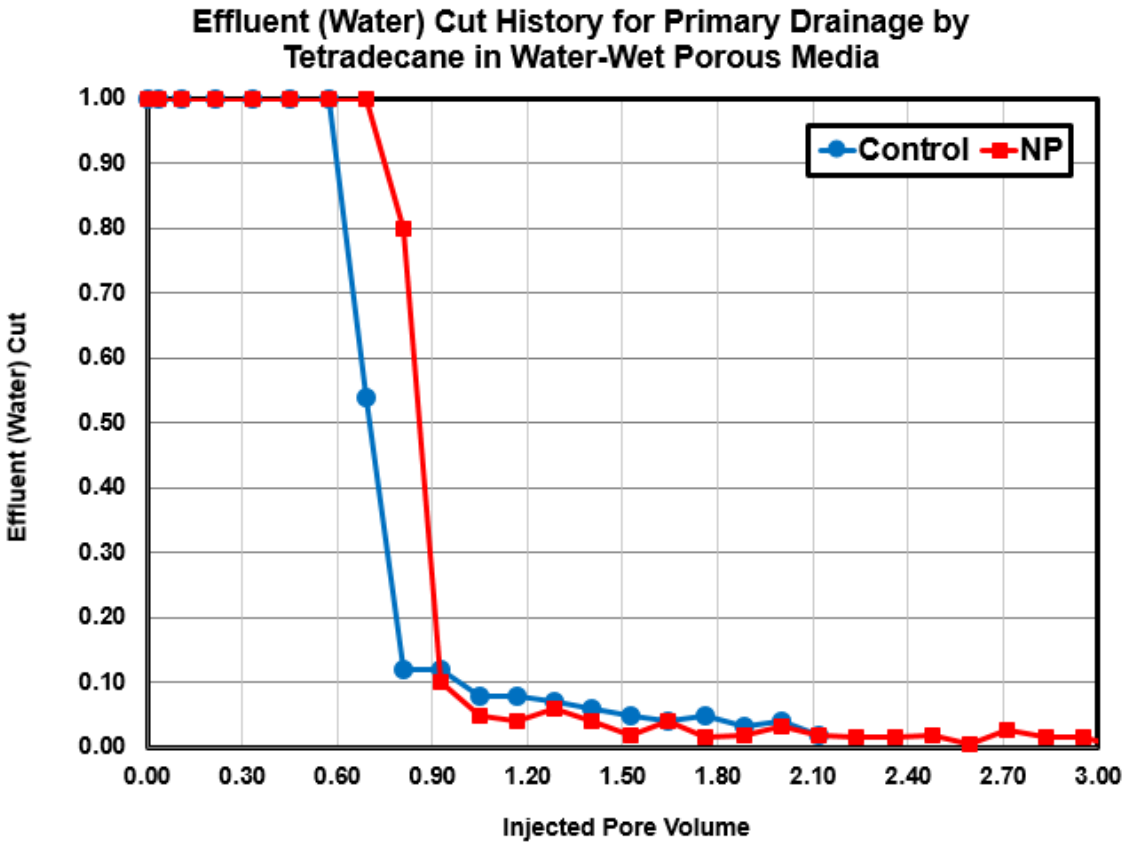


Figure 5.26: Effluent (water) cut data as a function of pore volume injected for primary drainage using tetradecane in water-wet core-J for both control (blue) and nanoparticle case (red).

The residual saturation of brine or brine containing nanoparticles was calculated based on the water cut measured in the effluent samples collected during the displacement. The core water saturation histories are shown in blue for the control case and in red for the nanoparticle case as clearly illustrated in Figure 5.27. The water saturation was calculated by comparing the total volume of water recovered and the pore volume of the core. The residual aqueous phase saturation for the control case was nearly 17%. As for the nanoparticles run, the residual core water saturation was almost 6%

indicating an average reduction of 11 saturation units for the same period of pore volume injection of 2.10 PV.

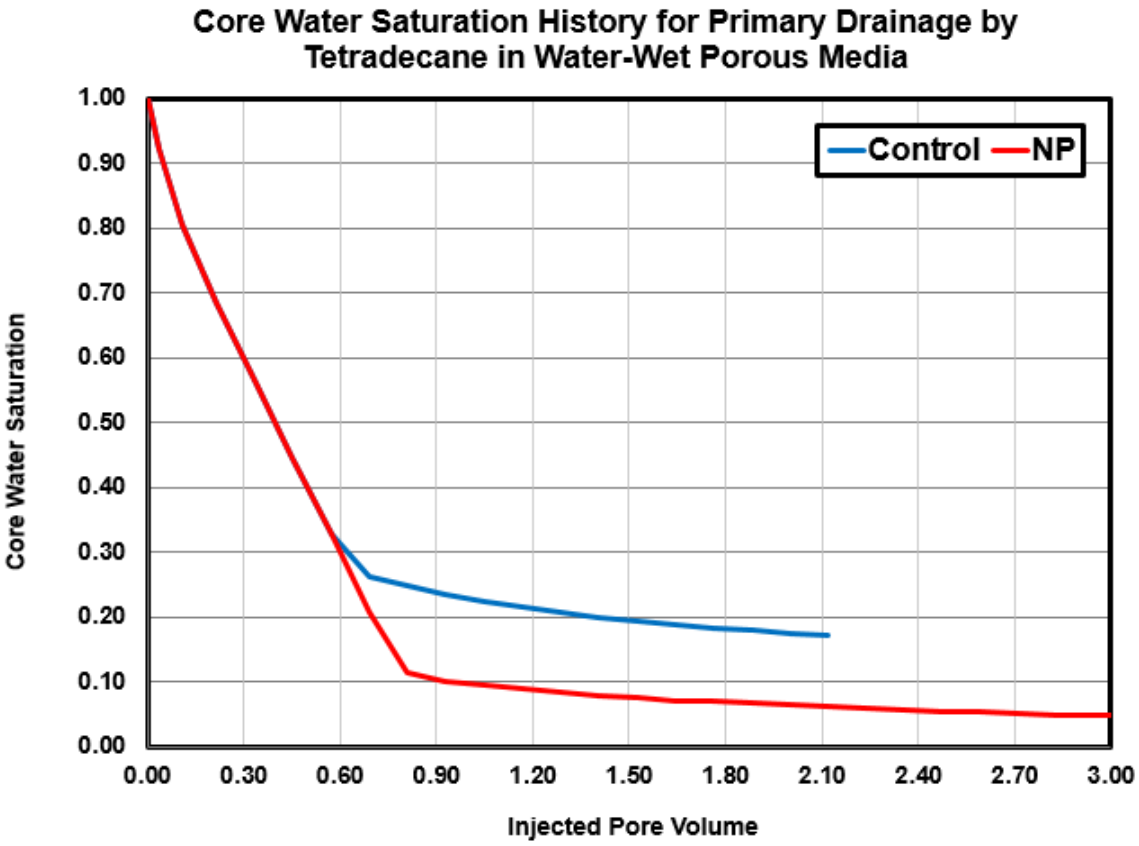


Figure 5.27: Average core water saturation history as a function of pore volume injected for primary drainage using tetradecane in water-wet core-J for both control (blue) and nanoparticle case (red).

Figure 5.28 shows the pressure drop ratio of the nanoparticles case compared to the control case. The ratio was calculated by dividing the pressure drop of nanoparticles case measured at each point in time by the pressure drop for the control case measured at the same moment. This pressure drop was generally 1.2 to 2.25 times greater than that of the control case with a peak value of 2.25 at nearly the time of breakthrough for both

cases. The ratio showed a slow declining trend which leveled off by the end of the displacement at a ratio of 1.39.

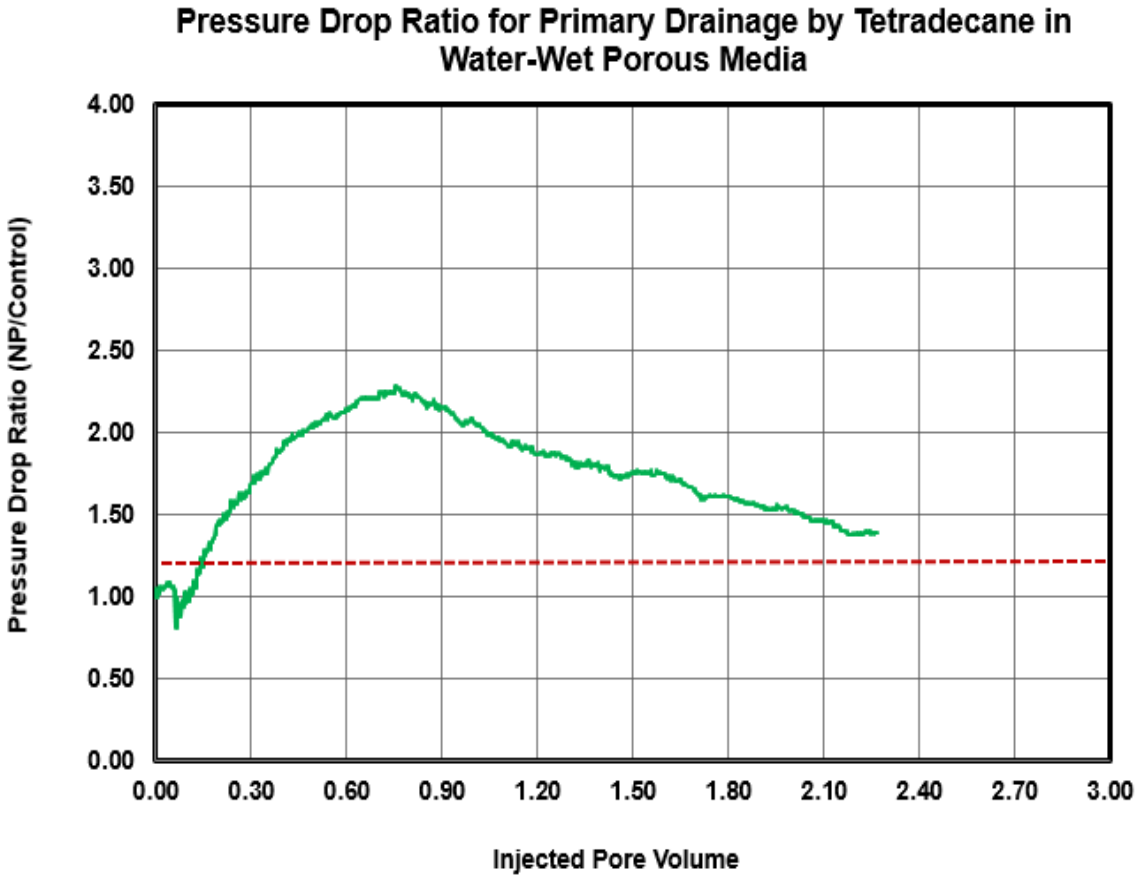


Figure 5.28: Pressure drop ratio calculated by dividing pressure drop measured at each point in time during nanoparticle case over that of the control case measured at the same moment. Ratio is expressed as a function of time for primary drainage using tetradecane in water-wet core-J. Red dashed line represents the value of the viscosity ratio between the aqueous nanoparticle dispersion and brine solution.

The endpoint relative permeability for the hydrocarbon phase $(k_{ro}^{o})$ is given by:

$$k_{ro}^{o} = \frac{\Delta P_w \, \mu_o}{\Delta P_o \, \mu_w}$$

In the equation above, $\mu$ is the viscosity of the fluid represented by either *w* for the aqueous phase or *o* for the hydrocarbon phase. $\Delta P_o$ represents the pressure drop for single phase tetradecane flowing at steady state at residual aqueous phase saturation while $\Delta P_w$ is the value of steady state pressure drop of the aqueous phase flowing as single phase. In all cases, the flow rate was kept the same at 1 ml/min. The calculated value was 0.75 for the control case and 0.66 for the nanoparticle case indicating a reduction of 14%.

The previously listed observations show indicators of nanoparticle-stabilized emulsion forming during aqueous phase displacement by tetradecane in porous media. Symptoms like the lower residual saturation of brine-nanoparticle solution and the pressure drop ratio, which was almost ranging from 1.20 to 2.25 times that of control case, correlate well with the 0.14 PV delay in breakthrough time. Since it is hypothesized that the increase in pressure drop ratio is caused by relevant pore-scale displacement events of Haines jump and Roof snap-off, the increase in pressure drop ratio should be greatest when these mechanisms are the most prevalent pore-scale events. Haines jump process requires the wetting phase to be present in the pore and therefore, this event is most likely to be active at the displacement front where the contact between both non-wetting phase and wetting phase is greatest. As a result, the displacement front moves along the core stabilizing more droplets and pressure drop ratio increases until it reached its maximum value of 2.25 by the time of breakthrough. In summary, this indicate a development of a more viscous phase that tetradecane was trying to displace and/or flow around causing pressure drop increase resulting in lowering the invading phase (tetradecane) mobility.

This increase in apparent viscosity translated into 14 % reduction in the endpoint relative permeability with a lower mobility of the invading hydrocarbon phase which correlate to emulsion formation symptoms for the nanoparticle case. All of these observations support the hypothesis that pore scale processes such as Haines jump and Roof snap off will provide enough energy to bring the nanoparticles to the interface and armor the droplets of non-wetting phase forming nanoparticle-stabilized emulsion inside the pores which will generally force the non-wetting phase (tetradecane) out of its preferred flow paths and stabilize flow, hence, the reduction in its mobility as confirmed by endpoint relative permeability data.

The observations of water displacement by tetradecane in water-wet system suggest that nanoparticles has impacted the displacement by possibly armoring tetradecane droplets as they snap off inside pore body after their pore scale jump. Those small scale events are typical in non-wetting phase displacing wetting phase scenario. Compared to the same displacement scenario involving n-octane as the hydrocarbon phase, it seems that the viscous stability of the displacement may have lowered the reduction in the mobility of the invading hydrocarbon phase as tetradecane is four times more viscous than n-octane. This explains the 11 % reduction observed when comparing the maximum pressure drop ratio observed with tetradecane (2.25) compared to that observed with n-octane (2.5) under the same wettability conditions

The difference in phase mobility reduction calculated for n-octane case and that of tetradecane case can be attributed to two arguments. One argument is that it may be easier to generate emulsion with n-octane as it may require less adsorption energy to bring the nanoparticle to the interface. Also, it seems that the physics governing Haines jump and Roof snap-off mechanisms provide the necessary work to cause such adsorption which may be a function of viscosity. A second argument is that the viscous

stability of the displacement will somehow dominate the displacement performance and that any other pore scale events are likely to be surpassed. The symptoms of nanoparticle-stabilized emulsion observed involving both n-octane and tetradecane were quite similar despite differences in terms of phase mobility reduction which can be related to the higher viscosity of tetradecane and the general overall viscous stability of the displacement.

***Secondary Imbibition (Core-J)***

A post flush stage followed the primary drainage displacement with the aqueous phase injected back to the core. Core-J is now saturated with tetradecane at either 17% residual brine saturation for the control case or 6% residual saturation of nanoparticle-brine dispersion for the nanoparticle case. Figure 5.29 shows the pressure drop trend as a function of pore volume injected. The blue curve represents the pressure drop for the control experiment while the red curve shows the pressure drawdown behavior for the nanoparticles case. The dashed lines show the breakthrough time for both displacements. As shown in the plot, both experiments show a similar pattern where pressure drop builds up almost linearly with pore volume at the beginning of the displacement followed by a plateau after breakthrough.

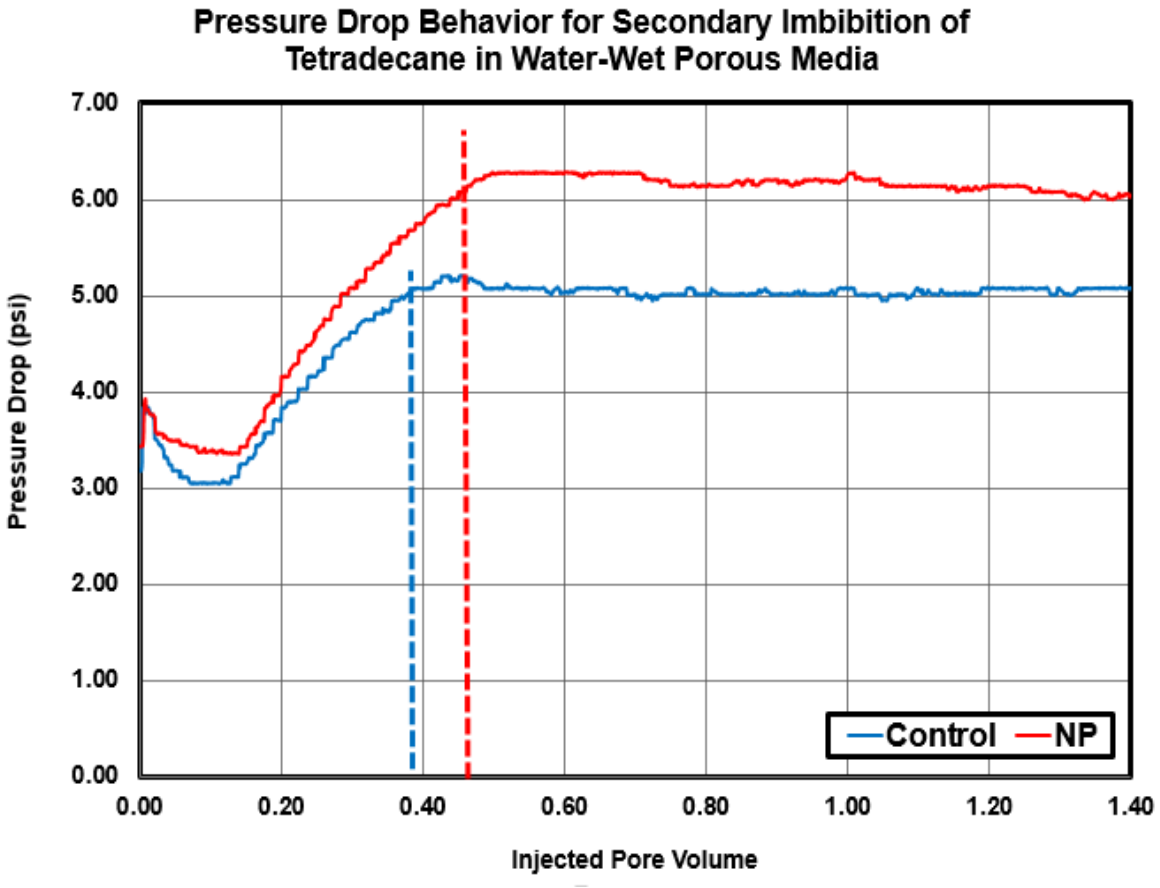


Figure 5.29: Measured pressure drop as a function of pore volume injected for control (blue) and nanoparticle case (red) for secondary imbibition into water-wet core-J using tetradecane. The dashed lines indicate breakthrough time.

For the control experiment as shown in Figure 5.29 by the blue curve, the pressure drop was increasing in a linear fashion with injected pore volume before it started to plateau around 5.15 psi after the breakthrough time of 0.38 PV. After that, the pressure drop maintained a value of 5.15 psi with little fluctuation until the end of the displacement. As for the nanoparticle case as illustrated in Figure 5.29 by the red curve, the pressure drop showed comparable performance to that of the control case as pressure drop was increasing in a linear fashion with injected pore volume before it started to plateau around 6.2 psi after the breakthrough time of 0.45 PV. After that, the pressure

drop showed a slow declining trend fluctuating around a value of 6.0 psi until the end of the displacement. It can be seen from Figure 5.29 that the nanoparticle case had a later breakthrough time that is 0.07 PV more compared to the control case (0.45 PV compared to 0.39 PV). In addition, nanoparticle experiment ended up with a slightly higher pressure drop that was nearly 1.0 psi larger than that of the control case (6.1 psi compared to 5.1 psi).

Figure 5.30 shows the water cut data which was collected during this displacement process. The blue curve shows the water cut values measured as a function of pore volume injected for the control experiment while the red curve shows the water cut for the nanoparticle case. For the control case, the water cut value maintained a value of 0 until nearly the breakthrough time of 0.37 PV after which the water cut started to increase until it reached 1 as brine was only flowing at residual tetradecane saturation. As for the nanoparticle case, the water cut value maintained a value of 0 until the breakthrough time of 0.45 PV after which the water cut started to increase until it reached 1 as brine-nanoparticle solution was only flowing at residual tetradecane saturation. Comparing both control and nanoparticle experiments, we see that the water cut increase for the nanoparticle run occurred at later pore volume injected time that was approximately 0.07 PV more compared to the control.

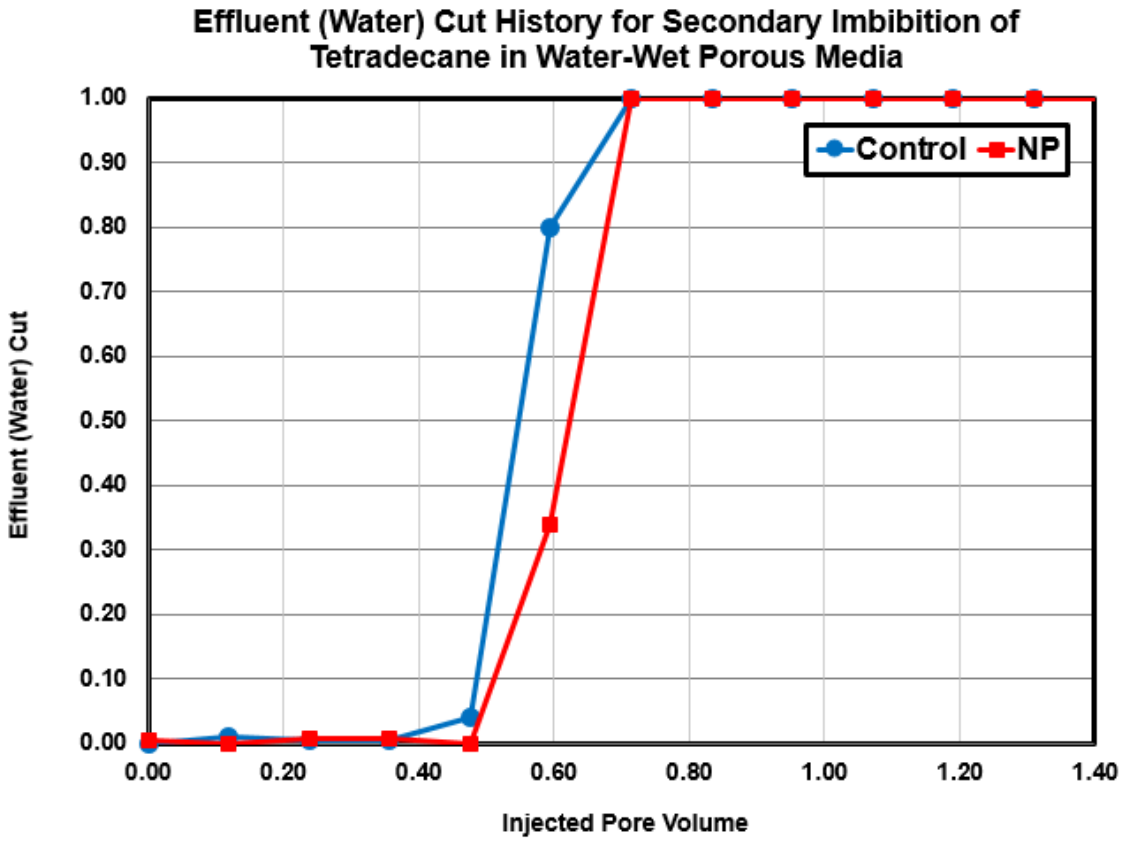


Figure 5.30: Raw effluent (water) cut data as a function of pore volume injected for secondary imbibition using tetradecane in water-wet core-J for both control (blue) and nanoparticle case (red).

The saturation of brine or brine containing nanoparticles was calculated based on the water cut measured in the effluent samples collected during the displacement. The core water saturation profiles are shown in blue for the control case and in red for the nanoparticle case as clearly illustrated in Figure 5.31. The water saturation was calculated by comparing the total volume of water recovered and the pore volume of the core. For the control run, the initial water saturation calculated at the beginning of this displacement stage is 17 % and it increased until it reached a steady state aqueous phase saturation of 67%. As for the nanoparticles run, initial water saturation calculated at the

beginning of this displacement stage is 5 % and it increased until it reached a steady state aqueous phase saturation of 60 %. This suggest displacing an additional 5 saturation units of the hydrocarbon phase for the nanoparticle case.

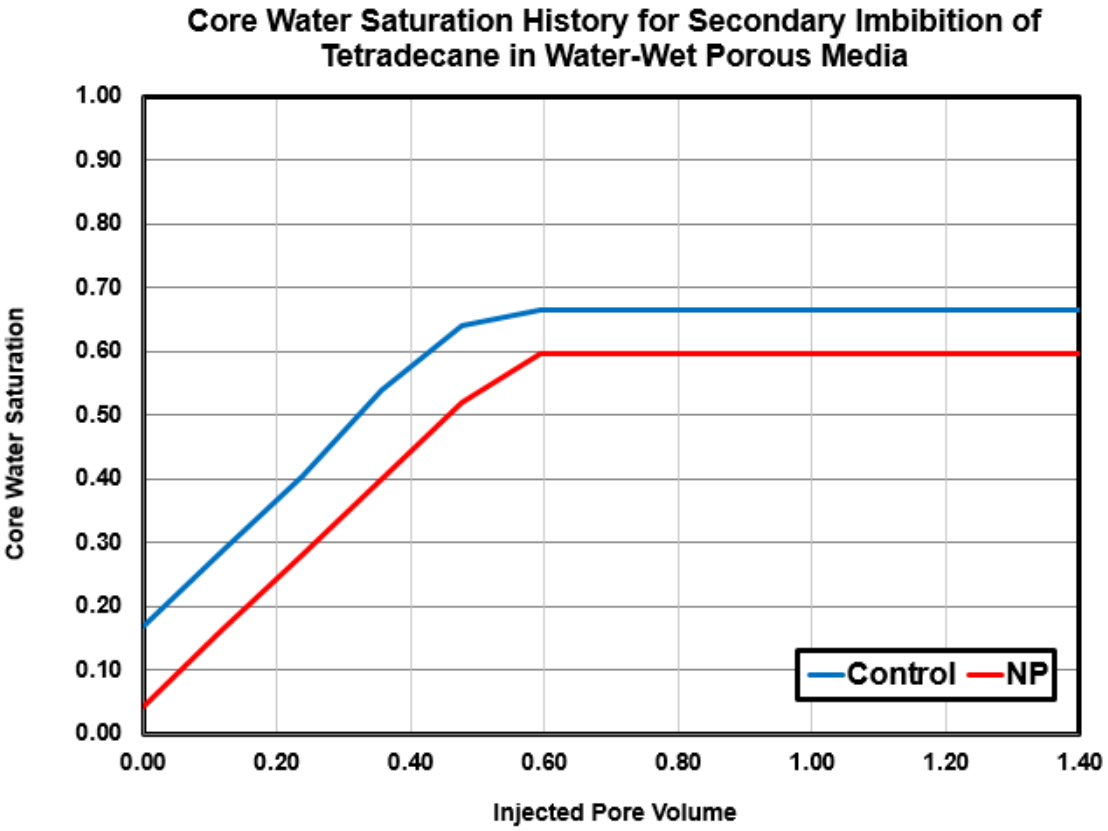


Figure 5.31: Average core water saturation history as a function of pore volume injected for secondary imbibition using tetradecane in water-wet core-J for both control (blue) and nanoparticle case (red).

Figure 5.32 shows the pressure drop ratio of nanoparticles case compared to the control case. The ratio was calculated by dividing the pressure drop of nanoparticles case measured at each point in time by the pressure drop for the control case measured at the same moment. The ratio was maintained around 1.10 for the first 0.47 PV injected into

the core. After that, it started to increase and maintained a ratio of nearly 1.22 times greater than that of the control run throughout the remainder of the displacement

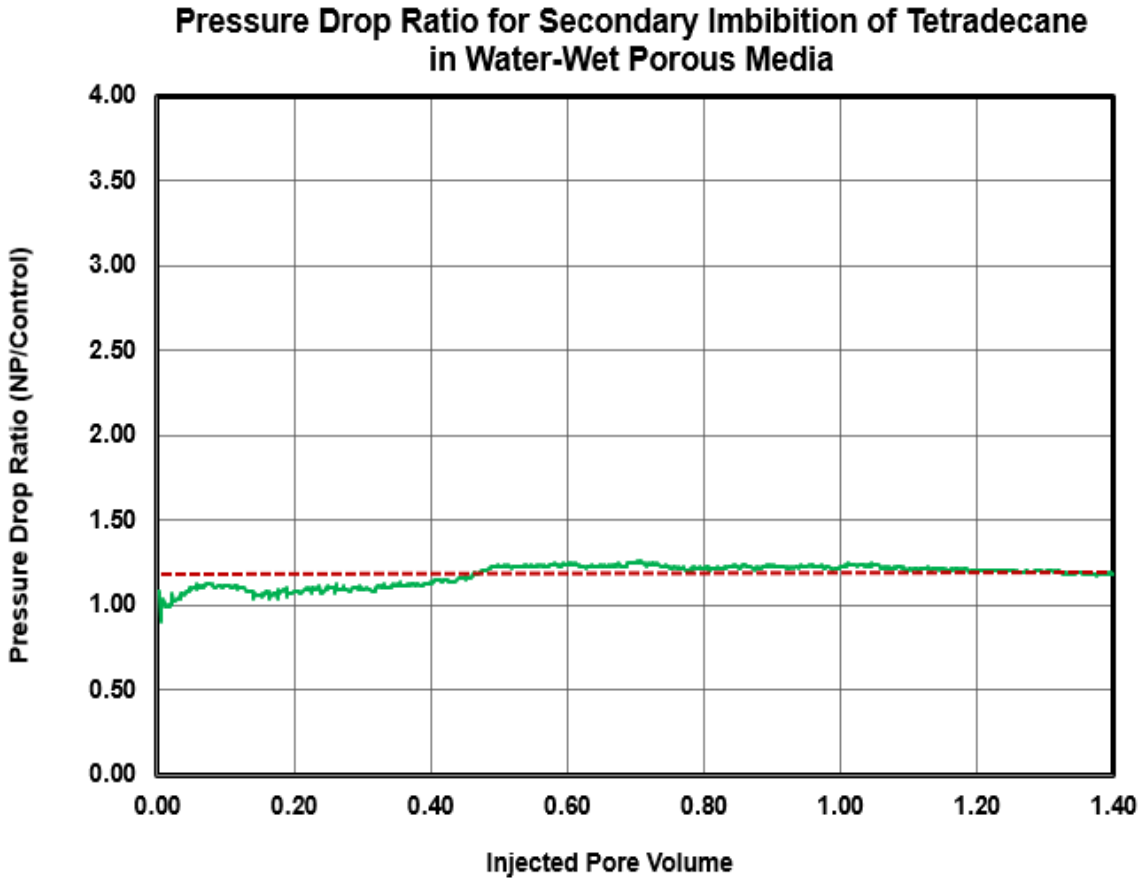


Figure 5.32: Pressure drop ratio calculated by dividing pressure drop measured at each point in time during nanoparticle case over that of the control case measured at the same moment. Ratio is expressed as a function of time for secondary imbibition displacement in water-wet core-J using tetradecane. Red dashed line represents the value of the viscosity ratio between the aqueous nanoparticle dispersion and brine solution.

The calculated endpoint relative permeability for the aqueous phase ($k_{rw}^{o}$) is given by:

$$k_{rw}^{o} = \frac{\Delta P_{w1}}{\Delta P_{w2}}$$

In the equation above, $\Delta P_{w1}$ represents the pressure drop for single phase aqueous solution flowing at steady state while $\Delta P_{w2}$ is the value of steady state pressure drop of the aqueous solution flowing at residual hydrocarbon phase saturation by the end of secondary imbibition. In all cases, the flow rate was kept the same at 1 ml/min. The calculated endpoint relative permeability was 0.20 for the control case and 0.19 for the nanoparticle indicating a slight reduction of 5 % for the nanoparticle case.

The observed behavior of this displacement suggests no significant outcome to be reported regarding nanoparticle presence in the displacement with respect to emulsion generation symptoms. The pressure drop behavior shows a slight drop at the beginning of the displacement which may be due to the hydrophilic wettability of the rock as it is easier for the aqueous phase to be absorbed. The pressure drop for the nanoparticle case showed an identical performance to that of the control and pressure drop ratio was maintained around 1.10 for the first 0.47 PV injected into the core. After that, it started to increase and maintained a ratio of nearly 1.22 times greater than that of the control run throughout the remainder of the displacement. It can be seen that this ratio is within the 1.18 viscosity ratio between nanoparticle-brine solution and brine solution. As a result, the increase in pressure observed for the nanoparticle case is most likely due to the nanoparticle-brine solution being 18% more viscous compared to the brine. Similarly, the increase in invading phase viscosity may have caused the slight reduction of 6 % in the aqueous phase endpoint relative permeability and overall mobility with breakthrough

time being delayed by 0.07 PV. Yet, in all of the reported observation, there was still no conclusive evidence that nanoparticle-stabilized emulsion was generated as all of the reported findings were primarily related to the increase in the viscosity of the invading phase. In fact, the values of delay in breakthrough time as well as reduction in the endpoint relative permeability are all close to those observed as well during the primary imbibition displacement in water-wet. However, one important thing to discuss is the 5 saturation units additional recovery of hydrocarbon phase measured at the end of this secondary imbibition displacement. Similar to primary imbibition experiments conducted using n-octane, it seems that the presence of ethylene glycol and/or the chemicals used for coating those particles to create a stable aqueous nanoparticle dispersion may have been the reason to explain reduction in residual tetradecane as there was some degree of miscibility which may have resulted in reducing interfacial tension and increasing the capillary number, hence, the decrease in the residual tetradecane saturation. We next attempt to see if the observations found here are going to be distinct for the primary imbibition case.

***Primary Imbibition (Core-I)***

A core flooding experiment was conducted on Core-I to evaluate nanoparticles impact on primary imbibition process in water-wet Boise sandstone core. The core was initially saturated with tetradecane to evaluate viscous instability condition prior to injecting brine to the core in the control case and nanoparticle-brine dispersion in the second case. For both cases, a secondary drainage of post flush with tetradecane followed the primary imbibition displacement and is presented in the next section.

Figure 5.33 shows the pressure drop trend as a function of pore volume injected. The blue curve represents the pressure drop for the control experiment while the red curve shows the pressure drawdown behavior for the nanoparticles case. The dashed lines show the breakthrough time for both displacements. As shown in the plot, both experiments show a similar pattern where pressure drop builds up almost linearly with pore volume at the beginning of the displacement followed by a plateau after breakthrough.

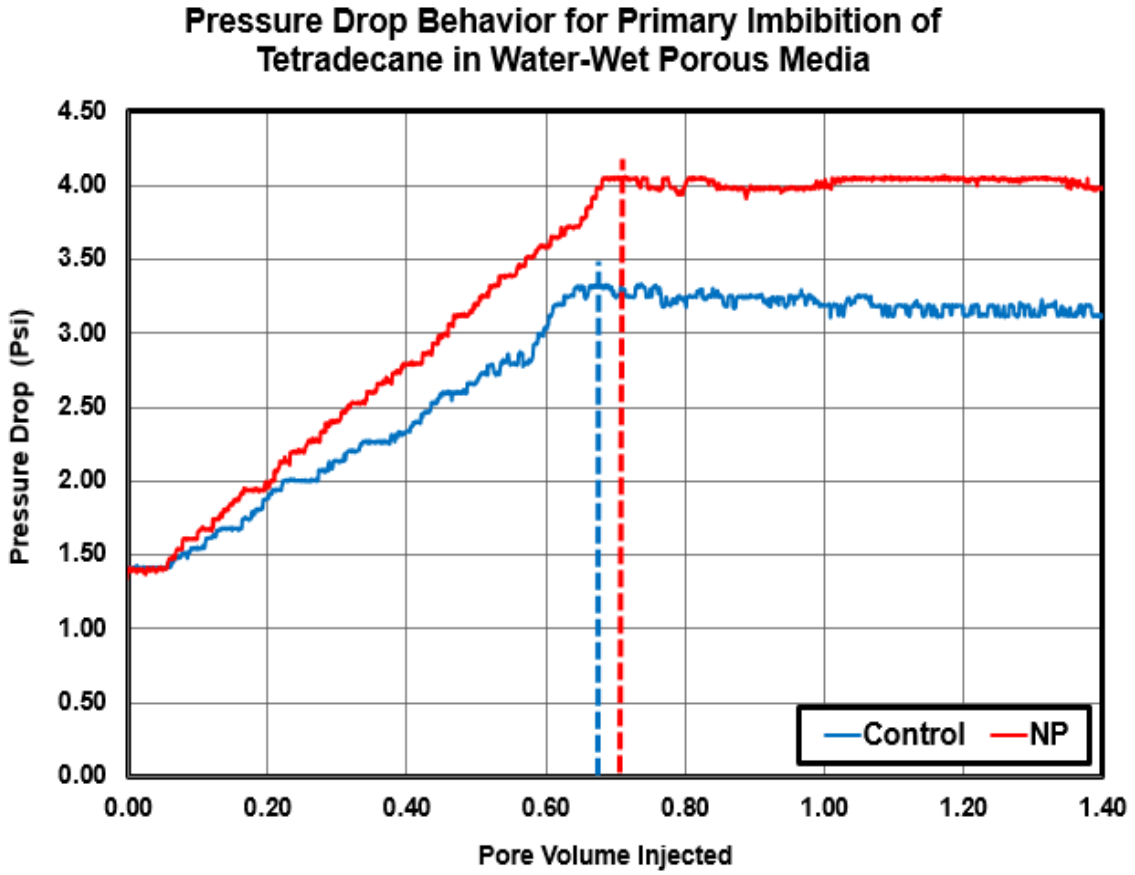


Figure 5.33: Measured pressure drop as a function of pore volume injected for control (blue) and nanoparticle case (red) into Boise sandstone for primary imbibition in water-wet core-I using tetradecane. The dashed lines indicate breakthrough time.

For the control experiment as shown in Figure 5.33 by the blue curve, the pressure drop was increasing almost in a linear fashion with injected pore volume before it started to plateau around 3.15 psi after the breakthrough time of 0.67 PV. After that, the pressure drop maintained a value of 3.15 with little fluctuation until the end of the displacement. As for the nanoparticle case as illustrated in Figure 5.33 by the red curve, the pressure drop showed comparable performance to that of the control case as pressure drop was increasing in almost a linear fashion with injected pore volume before it started to plateau around 4.1 psi after the breakthrough time of 0.73 PV. After that, the pressure drop maintained a value of 4.1 with little fluctuation until the end of the displacement. It can be seen from Figure 5.33 that the nanoparticle case had a later breakthrough time that is 0.06 PV more compared to the control case (0.73 PV compared to 0.67 PV). In addition, nanoparticle experiment ended up with a slightly higher pressure drop that was nearly 1 psi larger than that of the control case (4.1 compared to 3.1).

Figure 5.34 shows the water cut data which was collected during this displacement process. The blue curve shows the water cut values measured as a function of pore volume injected for the control experiment while the red curve shows the water cut for the nanoparticle case. For the control case, the water cut value maintained a value of 0.0 until the breakthrough time of 0.67 PV at which the water cut started to sharply increase and reached 1.0. As for the nanoparticle case, the water cut value maintained a value of 0.0 until the breakthrough time of 0.73 PV at which the water cut started to sharply increased and reached 1.0 by displacement end. Comparing both control and nanoparticle experiments, we see that the water cut increase for the nanoparticle run occurred at later pore volume injected time that was 0.06 PV more compared to the control.

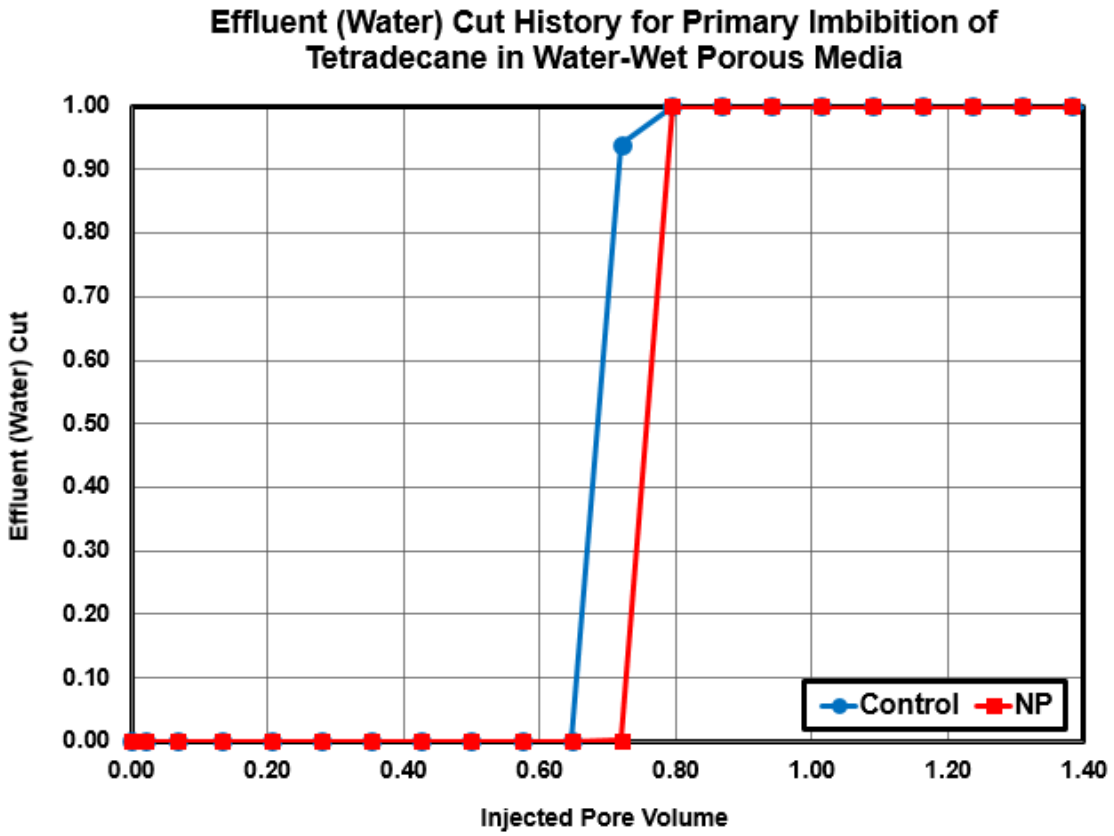


Figure 5.34: Effluent (water) cut as a function of pore volume injected for primary imbibition in water-wet core-I using tetradecane for both control (blue) and nanoparticle case (red).

The saturation of brine or brine containing nanoparticles was calculated based on the water cut measured in the effluent samples collected during the displacement. The core water saturation histories are shown in blue for the control case and in red for the nanoparticle case as clearly illustrated in Figure 5.35. The water saturation was calculated by comparing the total volume of water recovered and the pore volume of the core. The steady state aqueous phase saturation for the control case was 70%. As for the nanoparticles run, the steady state saturation was 78% indicating an average increase of 8 saturation units.

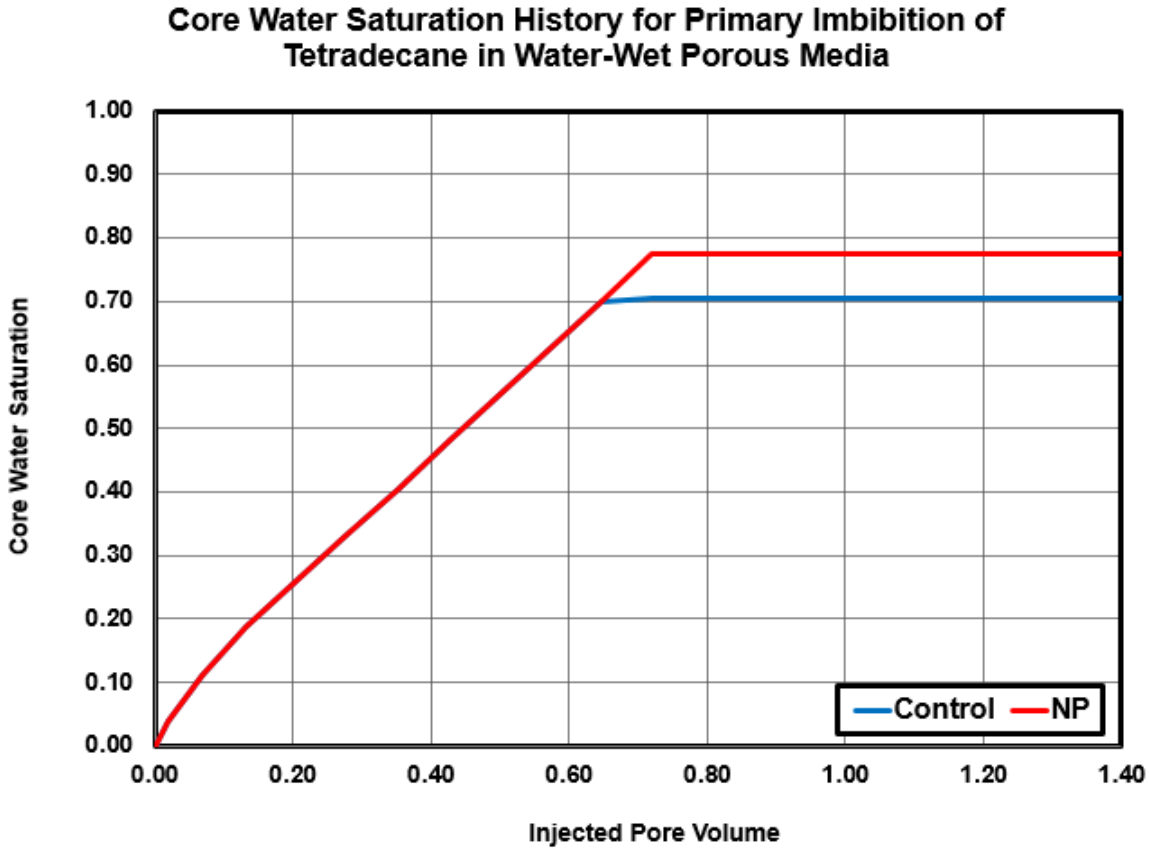


Figure 5.35: Average core water saturation history as a function of pore volume injected for primary imbibition in water-wet core-I for both control (blue) and nanoparticle case (red).

Figure 5.36 shows the pressure drop ratio of nanoparticles case measured at each point in time compared to the control case measured at the same moment. The ratio was calculated by dividing the pressure drop of nanoparticles case by the pressure drop for the control case. As shown in the figure, the pressure drop ratio was initially ranging between 1 and 1.2 for the first 0.67 PV injected. After that, the pressure drop ratio increased to an average of 1.30 for the reminder of the displacement. The red dashed horizontal line represents the line of the viscosity ratio between nanoparticle-brine solution and brine

solution which is equal to the ratio of 1.18. Generally and as can been seen by Figure 5.36, this ratio is within the observed pressure drop ratio range shown as the line generally overlaps the calculated pressure drop ratio for this displacement with no major differences.

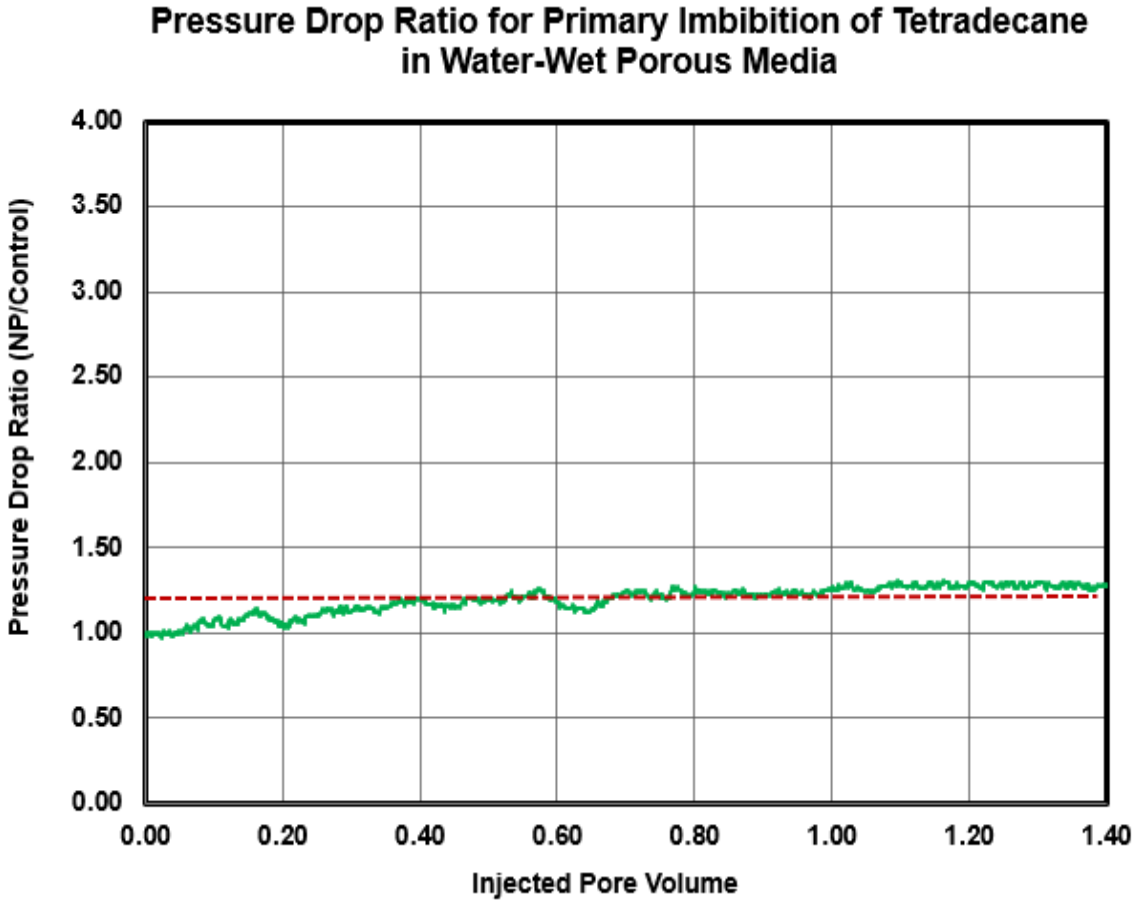


Figure 5.36: Pressure drop ratio calculated by dividing pressure drop measured at each point in time during nanoparticle case over that of the control case measured at the same moment. Ratio is expressed as a function of time for primary imbibition displacement in water-wet core-I using tetradecane. Red dashed line represents the value of the viscosity ratio between the aqueous nanoparticle dispersion and brine solution.

Another useful quantity that can be obtained from pressure drop measurements and fluid viscosities is the endpoint relative permeability for the aqueous phase ($k_{rw}^{o}$) which is given by:

$$k_{rw}^{o} = \frac{\Delta P_o \, \mu_w}{\Delta P_w \, \mu_o}$$

In the equation above, $\mu$ is the viscosity of the fluid represented by either *w* for the aqueous phase or *o* for the hydrocarbon phase. $\Delta P_o$ represents the pressure drop for single phase tetradecane flowing at steady state while $\Delta P_w$ is the value of steady state pressure drop of the aqueous phase flowing at residual hydrocarbon saturation. In all cases, the flow rate was kept the same at 1 ml/min. The calculated end point relative permeability was 0.19 for the control case and 0.18 indicating a slight decrease of nearly 5 % (only 0.01) for the nanoparticle case.

For this displacement case, the pressure drop for the nanoparticle case showed a comparable performance to that of the control case with pressure drop ratio ranging generally from 1.0 to 1.20 for the first 0.7 PV injected before it started to fluctuate around 1.30 afterward. Reduction in tetradecane saturation has caused the pressure drop increase to slow down and level off after the breakthrough of the aqueous phase. Overall, the observed and measured data during this displacement indicates no significant nanoparticle impact on the displacement behavior with respect to emulsion generation process. This is supported by the calculated pressure drop ratio range which was close to the viscosity ratio value of 1.18 (viscosity ratio between nanoparticle dispersion and brine solution). In addition, the endpoint relative permeability of the invading aqueous phase has been reduced by nearly 6 % indicating no significant change in the mobility of the invading phase which goes parallel with other reported observations that nanoparticle

presence in this displacement scenario had no major impact on the displacement. It is important to highlight that this displacement is viscously instable especially when breakthrough time is compared to that of the primary imbibition displacement involving n-octane under the same wettability conditions. In this experiment, tetradecane is more viscous than the aqueous phase which may cause water to finger through the more viscous tetradecane in some sites. As a result, water will generally breakthrough earlier under such conditions. Looking at the control case for primary imbibition displacement under water-wet conditions, we see that the breakthrough time was nearly 0.76 PV when n-octane was used as a hydrocarbon phase. As for the experiment conducted with tetradecane as the oil-phase fluid, we see an earlier breakthrough for the aqueous phase at around 0.67 PV. This indicate that there is less fingering and more stable displacement conditions when n-octane was used. The same argument can be expanded for the nanoparticle case as well.

Although there was no indirect indication of nanoparticle-stabilized emulsion generation inside porous media during nanoparticles run of this experiment, it seems that nanoparticles have impacted the displacement in a different way contributing to the remarkable reduction of 8 saturation points for the residual tetradecane saturation. The cause for such observed reduction in residual saturation might be a combination of the slight increase in the aqueous phase viscosity but more importantly the chemical composition of nanoparticles dispersion. Similar to what was discussed before in all of the imbibition displacement cases, the presence of ethylene glycol and/or the chemicals used for coating those particles to create stable dispersions may have been the reason to explain reduction in residual tetradecane saturation, hence, the increase in the aqueous phase saturation. Recalling the definition of the capillary number introduced back at chapter 3, it seems that ethylene glycol and/or some of the chemicals used for surface

coating may have created some miscibility sites during the displacement and the interfacial tension between the aqueous phase and tetradecane was reduced causing the capillary number to go up and eventually lead to reducing residual saturation of tetradecane. In addition to that, the 18% increase in aqueous phase viscosity may have also contributed to that increase in capillary number.

In summary, this displacement scenario under the conditions listed above did not show enough indirect evidence to confirm the possibility of nanoparticle-stabilized emulsion generation. Nonetheless, the presence of some chemicals such as ethylene glycol and those used for coating to create a stable nanoparticles dispersion may have impacted the aqueous phase steady state saturation and caused the observed increase in its value. We next present the observations for the secondary drainage case and evaluate the impact of nanoparticle presence, viscous stability, and initial fluid saturation impact on the displacement.

***Secondary Drainage (Core-I)***

A post flush stage followed the primary imbibition displacement with n-octane invading back to the core. Core-I is now saturated with either brine at 30% residual tetradecane saturation for the control case or nanoparticle-brine dispersion at 22% residual tetradecane saturation. This displacement stage is known as a secondary drainage as the core is not saturated completely with aqueous phase. The displacement flow rate was kept at 1 ml/min and data were recorded and effluent samples were collected

Figure 5.37 shows the pressure drop trend as a function of pore volume injected. The blue curve represents the pressure drop for the control experiment while the red curve shows the pressure drawdown behavior for the nanoparticles case. The dashed lines show the breakthrough time for both displacements. As shown in the plot, both

displacement cases showed a similar pattern of pressure build up behavior where pressure drawdown was increasing with more pore volume injected until a peak pressure drop value is reached followed by a general decline trend reaching a certain leveling off value by the displacement end. However, there was some quite differences in pressure drop trends between control and nanoparticle case as will be addressed next.

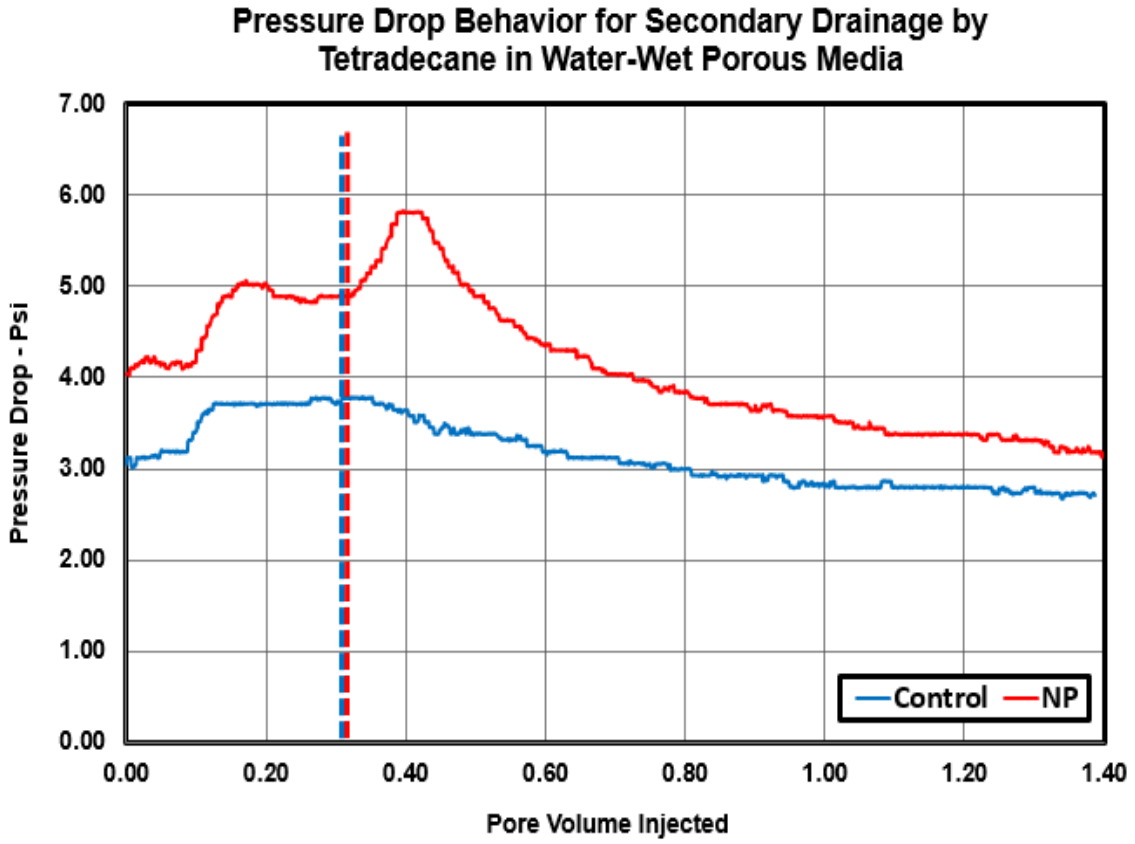


Figure 5.37: Measured pressure drop as a function of pore volume injected for control (blue) and nanoparticle case (red) into Boise sandstone for secondary drainage in water-wet core-I using tetradecane. The dashed lines indicate breakthrough time.

For the control experiment as shown in Figure 5.37 by the blue curve, the pressure drop was increasing and reached a maximum value of 3.75 at nearly 0.32 PV. After that,

the pressure drop started to gradually decline and reached an asymptote value of about 2.75 at 1.4 PV. In this case, the pressure drop plateau value corresponds to the breakthrough of tetradecane from the core outlet as observed in the fraction collector. As for the nanoparticle case as illustrated in Figure 5.37 by the red curve, the pressure drop showed comparable performance to that of the control case until 0.32 PV. After that, the pressure drop started to increase sharply reaching a maximum value of 5.8 at 0.41 PV. After that, the pressure drop started to decline and reached an asymptote value of about 3.15 at 1.4 PV. In this case, the pressure drop peak value did not correspond to the breakthrough of tetradecane from the core outlet as the time of breakthrough for the nanoparticle case is 0.32. It can be seen from Figure 5.37 that the nanoparticle case had the same breakthrough time that is 0.32 PV. In addition, nanoparticle experiment ended up with slightly higher pressure drop that was 0.40 larger than that of the control case (3.15 compared to 2.75).

Figure 5.38 shows the water cut data which was collected during this displacement process. The blue curve shows the water cut values measured as a function of pore volume injected for the control experiment while the red curve shows the water cut for the nanoparticle case. For the control case, the water cut value maintained a value of 1 until the breakthrough time of 0.32 PV after which the water cut started to decrease to 0.20 and reached an average of 0 by the end of displacement. As for the nanoparticle case, the water cut value maintained a value of 1 until the breakthrough time of 0.32 PV after which the water cut started to decrease to 0.75 and reached 0 by the end of the displacement. Comparing both control and nanoparticle experiments, we see that the water cut reduction for the nanoparticle run occurred nearly at the same pore volume injected time that was.

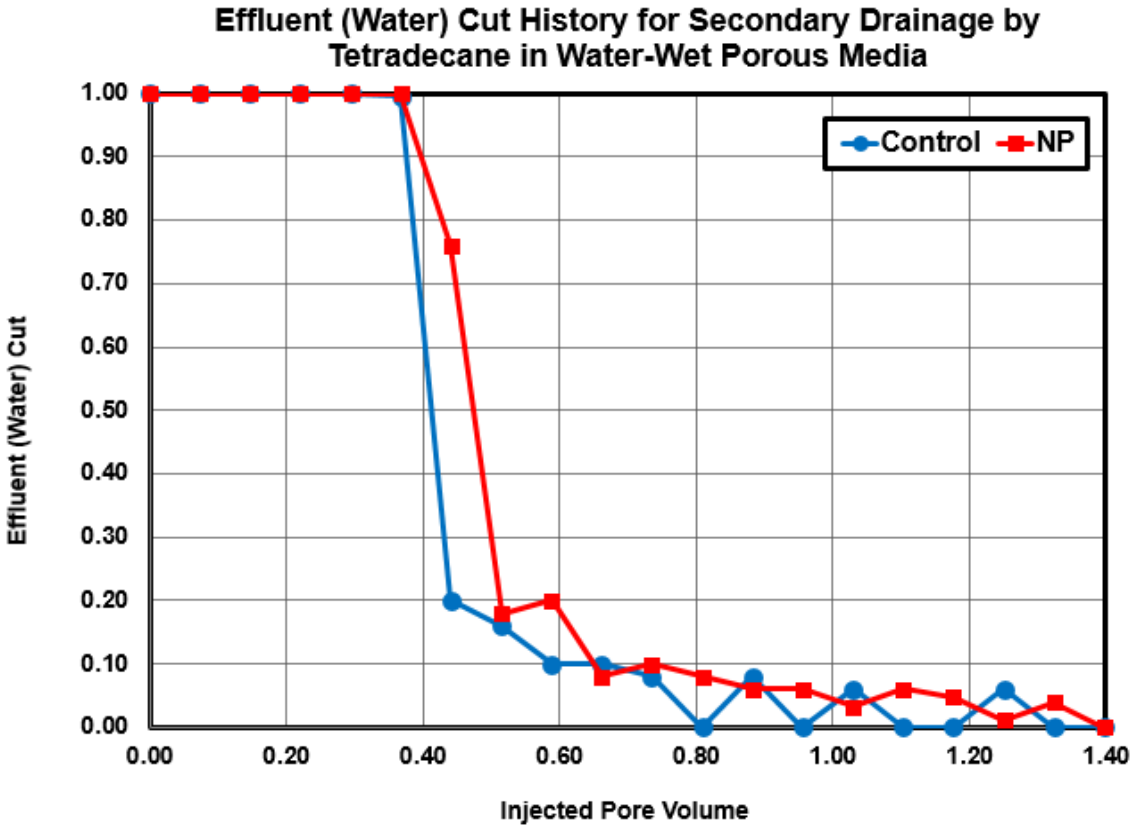


Figure 5.38: Effluent (water) cut as a function of pore volume injected for secondary drainage in water-wet core-I using tetradecane for both control (blue) and nanoparticle case (red).

The residual saturation of brine or brine containing nanoparticles was calculated based on the water cut measured in the effluent samples collected during the displacement. The core water saturation histories are shown in blue for the control case and in red for the nanoparticle case as clearly illustrated in Figure 5.39. The water saturation was calculated by comparing the total volume of water recovered and the pore volume of the core. For the control run, the initial water saturation calculated at the beginning of this displacement stage is 70 % and it decreased until it reached a residual aqueous phase saturation of 28%. As for the nanoparticles run, initial water saturation

calculated at the beginning of this displacement stage is 78 % and it decreased until it reached a residual aqueous phase saturation of 28 % as well. This suggest displacing an additional 8 saturation units of the aqueous phase for the nanoparticle case.

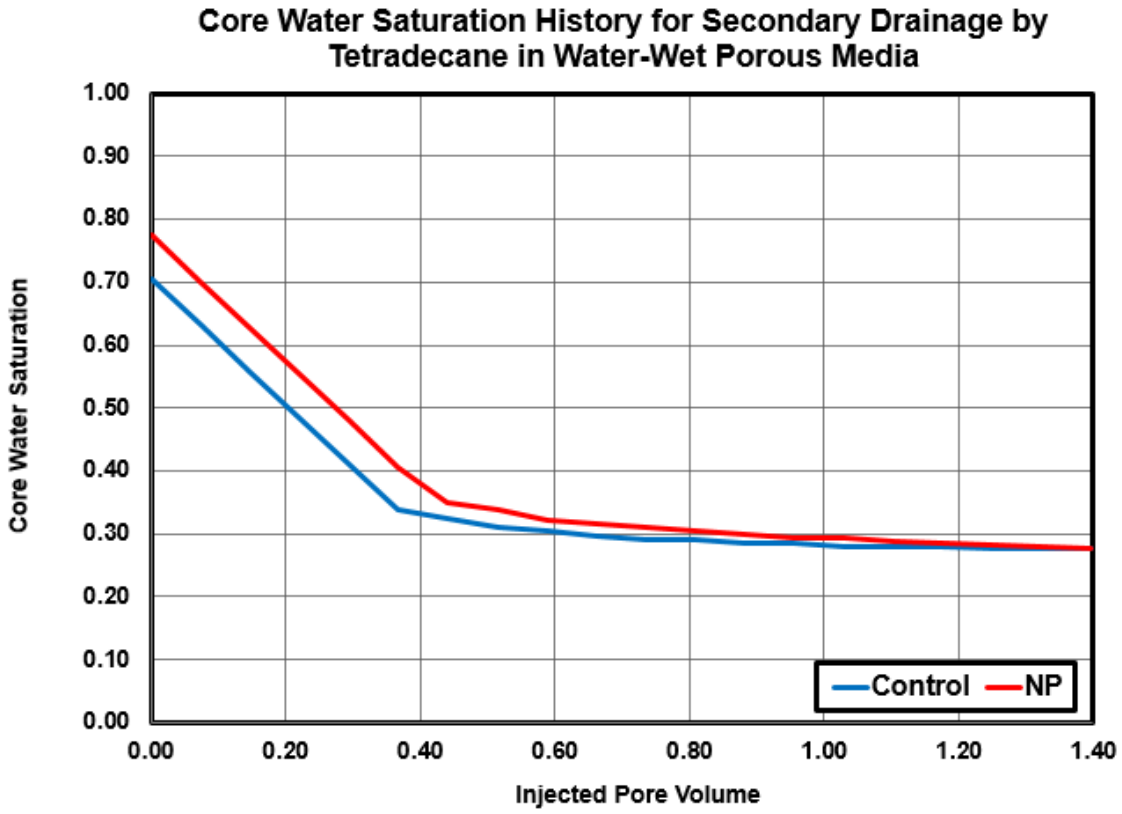


Figure 5.39: Average core water saturation history as a function of pore volume injected for secondary drainage in water-wet core-I using tetradecane for both control (blue) and nanoparticle case (red).

Figure 5.40 shows the pressure drop ratio of nanoparticles case compared to the control case. The ratio was calculated by dividing the pressure drop for the nanoparticle case measured at each point in time by the pressure drop of the control case measured at the same moment. The ratio was fluctuating around 1.30 throughout the first 0.32 PV injection period. After that, it started to increase rapidly to 1.62 times greater than that of

the control run until 0.44 PV when it started to decrease slowly reaching 1.18 at steady state flow of tetradecane at residual aqueous phase saturation.

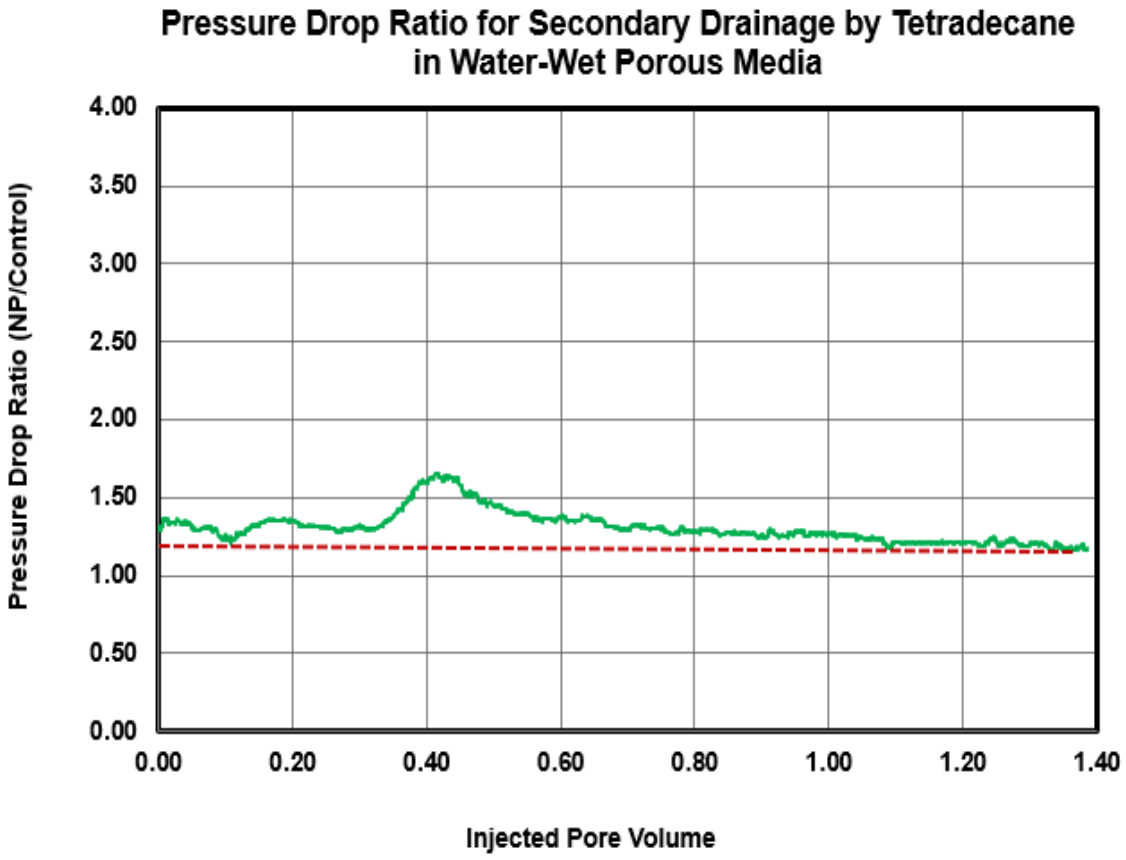


Figure 5.40: Pressure drop ratio calculated by dividing pressure drop measured at each point in time during nanoparticle case over that of the control case measured at the same moment. Ratio is expressed as a function of time for secondary drainage displacement in water-wet core-I using tetradecane. Red dashed line represents the value of the viscosity ratio between the aqueous nanoparticle dispersion and brine solution.

The calculated endpoint relative permeability for the hydrocarbon phase ($k_{ro}^{o}$) is given by:

$$k_{ro}^{o} = \frac{\Delta P_{o1}}{\Delta P_{o2}}$$

In the equation above, $\Delta P_{o1}$ represents the pressure drop for single phase n-octane flowing at steady state while $\Delta P_{o2}$ is the value of steady state pressure drop of tetradecane phase flowing at residual aqueous phase saturation by the end of secondary drainage. In all cases, the flow rate was kept the same at 1 ml/min. The calculated endpoint relative permeability was 0.50 for the control case and 0.41 for the nanoparticle indicating a reduction of 18 % for the nanoparticle case.

All in all, evaluating carefully the observations of this secondary drainage displacement indicate the generation of viscous phase inside porous media. The pressure drop was generally comparable to that of control with pressure drop ratio ranging from 1.30 to 1.60. The ratio started to drop by the end of the displacement to be almost 1.20. Despite having the same breakthrough time for both control and nanoparticle case, the sudden increase of 25 % in pressure drop for the nanoparticle case and the additional trapping of tetradecane (additional 8 saturation units) are all symptoms for emulsion generation inside porous media when nanoparticles are present. The reduction in tetradecane mobility may have been caused by the fact that tetradecane is facing more resistance to flow now as it was being forced out of its preferred paths. It is true that the viscous phase was generated after the time of breakthrough which explains why both control and nanoparticle case have the same breakthrough time. However, if for some reason, the emulsion generation were to occur prior to the time of breakthrough, it is high likely that the breakthrough time for nanoparticle case will be later. Unlike the water-wet secondary drainage displacement case involving a lower viscosity n-octane where the symptoms of emulsion generation were seen before breakthrough, the secondary drainage displacement conducted with more viscous tetradecane under the same wettability

condition required the core to reach higher tetradecane saturation for nanoparticle-stabilized emulsion processes to occur. In other words, it could be that the core had to be at higher tetradecane saturation for Haines jump and Roof snap-off to occur. This suggests that not only the amount of the initial residual saturation of hydrocarbon phase matters but also its properties such as the viscosity. In other words, the viscosity stability of the displacement plays an important part on how fluids are distributed inside porous media after the completion of the displacement. The key feature that matters the most, at least to the purpose of this research, is how well connected these phases are.

Based on the previous discussion, the fluid distribution after the primary imbibition involving more viscous tetradecane is different than the displacement involving a lower viscosity n-octane. As the aqueous phase was trying to displace tetradecane, it was fingering through tetradecane and flowing through the water layers coating the grains. This led to a higher residual saturation of tetradecane compared to primary imbibition involving n-octane as additional tetradecane was still trapped inside. However, based on the displacement performance seen during the secondary drainage conducted with tetradecane, the fact that the core required additional injection to reach the saturation needed for emulsion generation processes to take place suggest that the morphology of tetradecane phase distribution inside the porous media was more isolated and less connected compared to the morphology of trapped n-octane under the same displacement conditions. As a result, the morphology of fluid distribution inside porous media is a vital factor that may hinder pore scale processes responsible for the hypothesized emulsion generation process when nanoparticles are present. As discussed during secondary drainage displacement involving n-octane under water-wet condition, pore bodies may need to be completely filled with wetting phase for Haines jump and Roof snap-off to be highly active and occurring more frequently. Based on that, we can

see that the initial trapping of tetradecane in this case may explain the difference in the pressure drop increase trend observed in this experiment compared to the primary drainage case. For example, pressure drop increased by only 45 % compared to the initial staring value for the nanoparticle case during this secondary drainage experiment. If we were to compare this to the primary drainage under the same wettability condition, we see that the pressure drop increase was nearly 700 % compared to the initial value. It seems that the pressure drop increasing trend for tetradecane was higher than that of n-octane if we were to compare the same displacement type under same wettability condition. We next present the experimental results for using tetradecane under oil-wet condition evaluating both primary imbibition and secondary drainage.

### 5.3.2 Displacement in Oil-Wet Porous Media

Based on the findings discussed before for displacements that utilize the higher viscosity tetradecane in water-wet core, it is of primary importance to examine the impact of nanoparticles on primary imbibition and secondary drainage displacement when the rock is oil-wet. Because it is hypothesized that stabilized nanoparticle emulsion is high likely to be observed in the displacement scenario where wetting phase is displaced by non-wetting phase during which pore scale mechanisms like Haines jump and Roof snap-off are likely to occur, it is interesting to see if those mechanism are the only necessary processes for that phenomenon to occur. Otherwise, there are other controlling factors that govern those processes which has to be addressed to refine the hypothesis of this research.

***Primary Imbibition (Core-F)***

A core flooding experiment was conducted on Core-F to evaluate nanoparticles impact on primary imbibition process in oil-wet Boise sandstone core. The core was initially saturated with tetradecane prior to injecting brine in the control case and nanoparticle-brine dispersion in the second case. For both cases, a secondary drainage of post flush with tetradecane followed the primary imbibition displacement and is presented in the next section.

Figure 5.41 shows the pressure drop trend as a function of pore volume injected. The blue curve represents the pressure drop for the control experiment while the red curve shows the pressure drawdown behavior for the nanoparticles case. The dashed lines show the breakthrough time for both displacements. As shown in the plot, both experiments show a similar pattern where pressure drop builds up with injected pore volume at the beginning of the displacement followed by a peak pressure corresponding to the breakthrough time for each case. This peak pressure drop is then followed by a general slow decline in pressure drawdown before it almost started to level off.

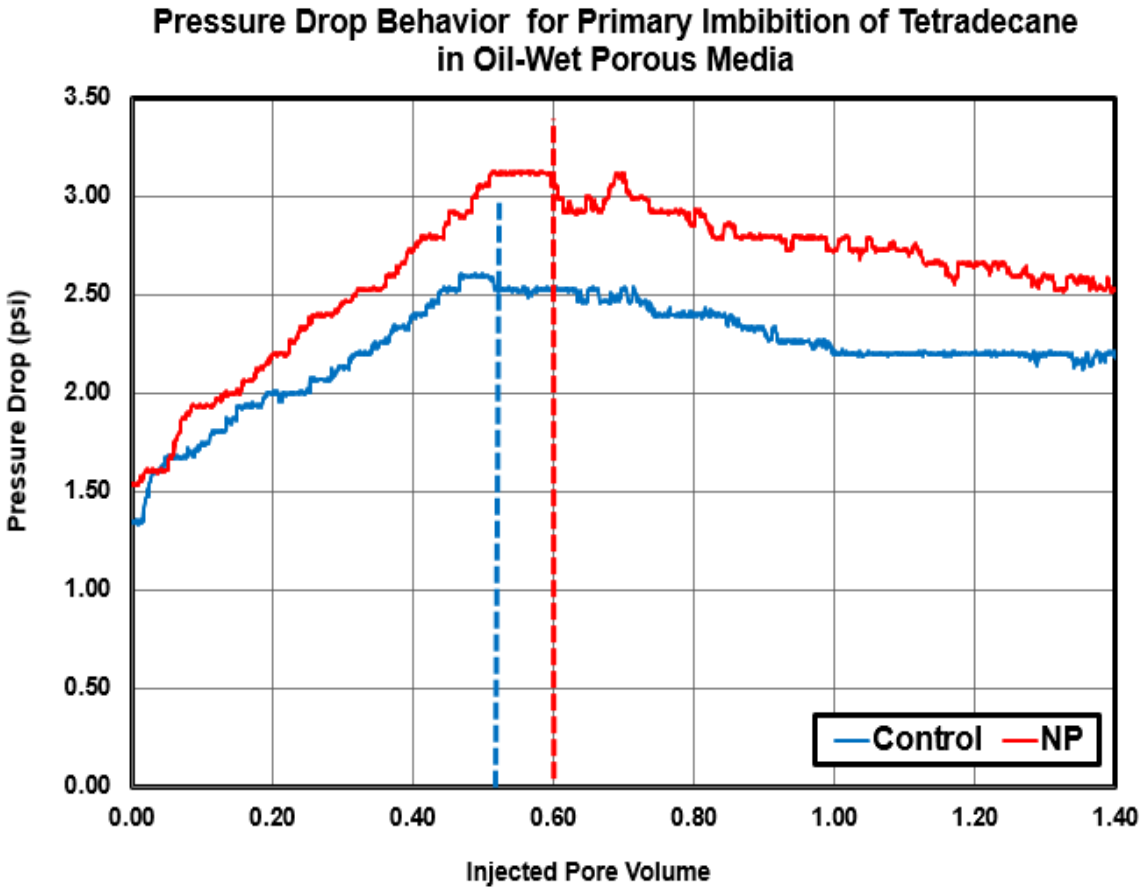


Figure 5.41: Measured pressure drop as a function of pore volume injected for control (blue) and nanoparticle case (red) into Boise sandstone for primary imbibition in oil-wet core-F using tetradecane. The dashed lines indicate breakthrough time.

It is important to mention that the core was not restored to its original conditions post IPA treatment after completing the control experiments. Single phase pressure drop data indicated a reduction in core permeability by nearly 9% post IPA treatment. As a result and to allow fair comparison reflecting all changes to the core's permeability and porosity, pressure drop normalization was performed. For the control case, raw drawdown data presented in Figure 5.41 were divided by 1.34 psi which is the single phase pressure drop of tetradecane flowing at 1 ml/min. As for the nanoparticle case, a

pressure drop value of 1.52 psi was used to normalize the raw data. This pressure drop value corresponds to the single phase pressure drop of tetradecane flowing at the same flow rate of 1 ml/min post IPA treatment. Also, pore volume correction was applied. The pore volume was reduced, as detailed in Appendix A2 based on Pittman permeability-porosity correlation, by 1.6% for this core. Normalized pressure drop curves for both control and nanoparticle case are shown in Figure 5.42.

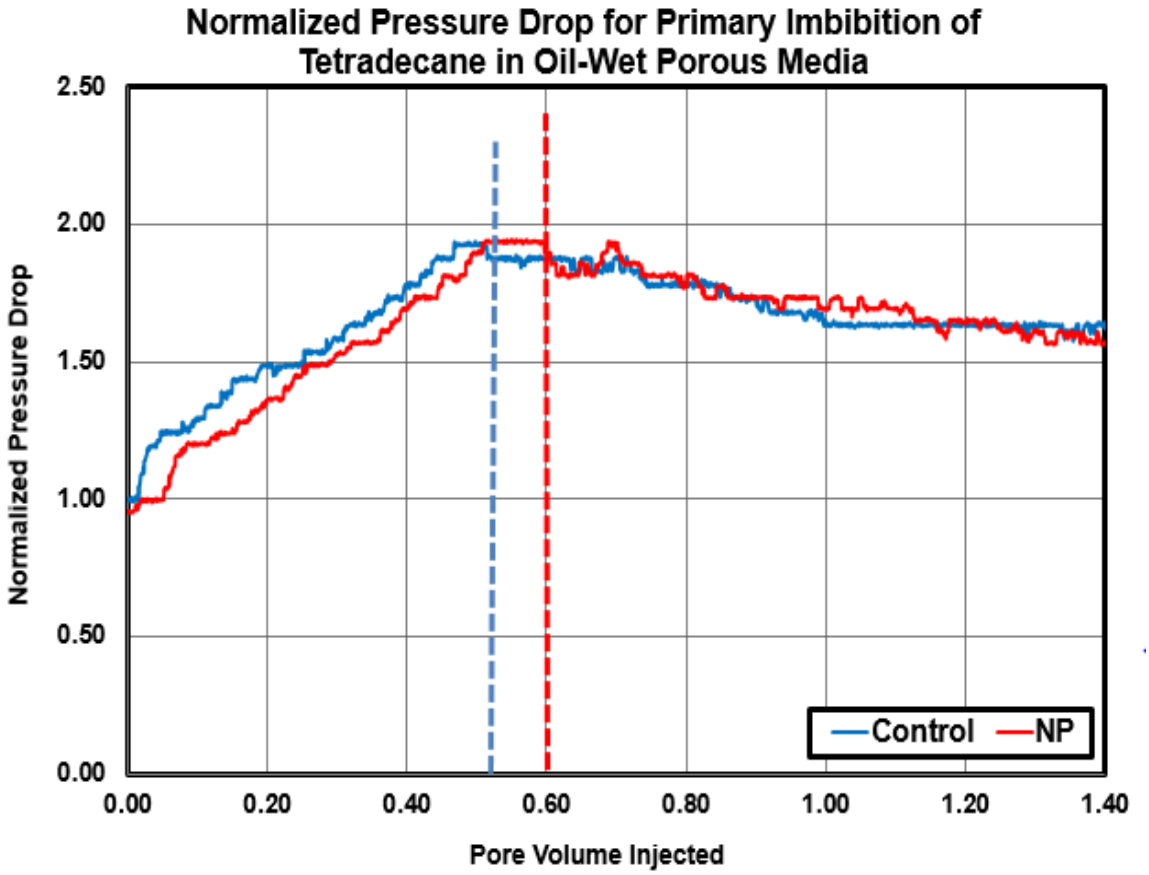


Figure 5.42: Normalized pressure drop as a function of pore volume injected for control (blue) and nanoparticle case (red) into Boise sandstone for primary imbibition in oil-wet core-F using tetradecane. The dashed lines indicate breakthrough time.

For the control experiment as shown in Figure 5.42 by the blue curve, the normalized pressure drop was increasing with injected pore volume before it started to reach a peak value of 1.88 after the breakthrough time of 0.52 PV. After that, the normalized pressure drop started to slowly decline and reached an asymptote value of 1.61 until the end of the displacement at 1.40 PV. As for the nanoparticle case as illustrated in Figure 5.42 by the red curve, the normalized pressure drop showed comparable performance to that of the control case as pressure drop was increasing in a with injected pore volume before it started to reach a maximum value around 1.94 at a breakthrough time of 0.60 PV. After that, the pressure drop started to slowly decline and reached an asymptote value of 1.56 until the end of the displacement at 1.40 PV. It can be seen from Figure 5.42 that the nanoparticle case had a later breakthrough time that is 0.08 PV more compared to the control case (0.60 PV compared to 0.52 PV). In addition, nanoparticle experiment ended up with a slightly lower normalized pressure drop that was nearly 0.05 lower than that of the control case (1.56 compared to 1.61).

Figure 5.43 shows the water cut data which was collected during this displacement process. The blue curve shows the water cut values measured as a function of pore volume injected for the control experiment while the red curve shows the water cut for the nanoparticle case. For the control case, the water cut value maintained a value of 0 until the breakthrough time of 0.52 PV at which the water cut started to increase to 0.17 until it reached 1 as brine was only flowing at residual tetradecane saturation. As for the nanoparticle case, the water cut value maintained a value of 0 until the breakthrough time of 0.60 PV at which the water cut started to increase to 0.8 and reached nearly 1 as nanoparticle-brine solution was only flowing at residual tetradecane saturation. Comparing both control and nanoparticle experiments, we see that the water cut rise for

the nanoparticle run occurred at later pore volume injected time that was 0.08 PV more compared to the control.

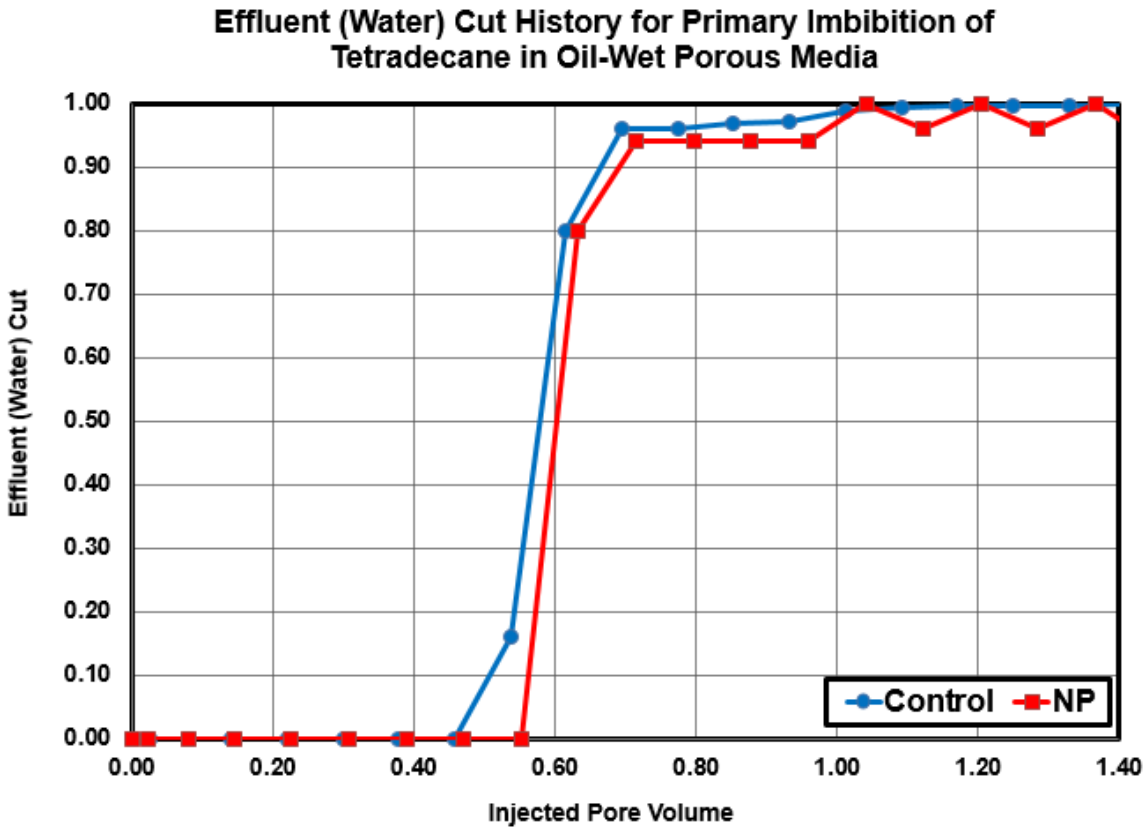


Figure 5.43: Effluent (water) cut as a function of pore volume injected for primary imbibition in oil-wet core-F using tetradecane for both control (blue) and nanoparticle case (red).

The saturation of brine or brine containing nanoparticles was calculated based on the water cut measured in the effluent samples collected during the displacement. The core water saturation histories are shown in blue for the control case and in red for the nanoparticle case as clearly illustrated in Figure 5.44. The water saturation was calculated by comparing the total volume of water recovered and the pore volume of the core. The steady state aqueous phase saturation for the control case was 61%. As for the

nanoparticles run, the steady state saturation nearly 66% indicating an average increase of 5 saturation units.

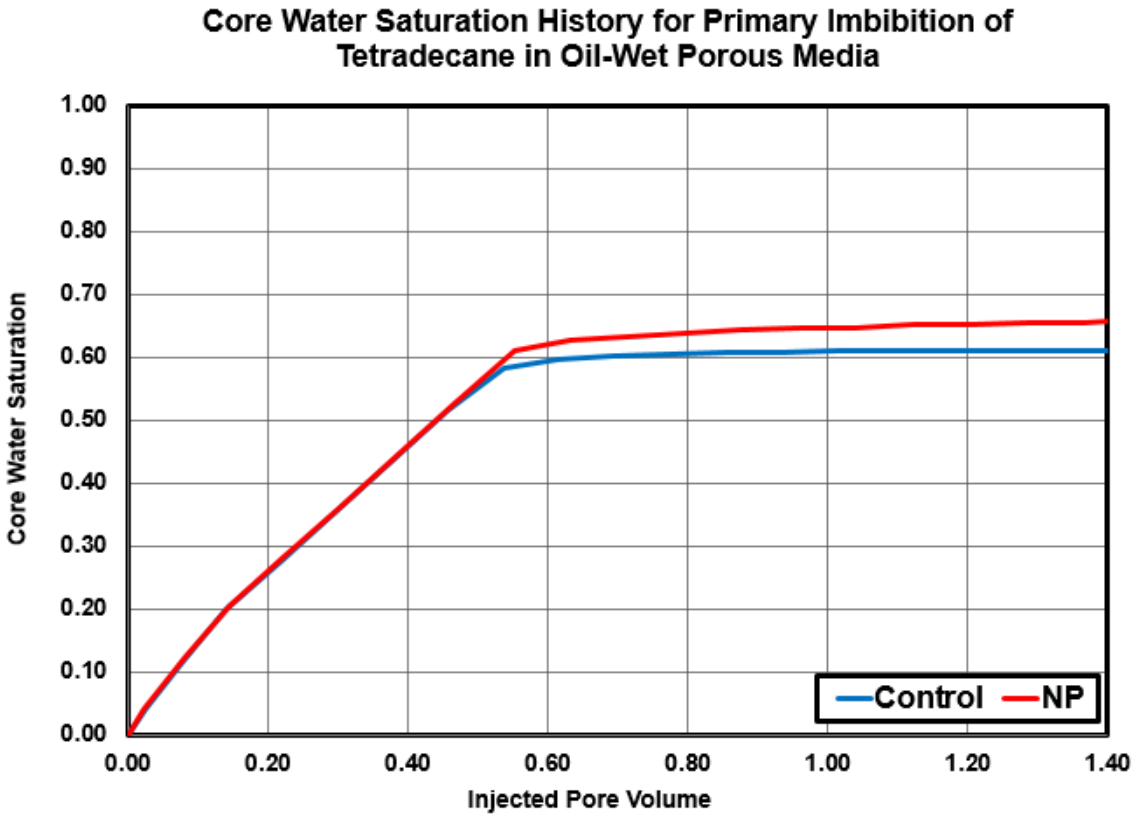


Figure 5.44: Average core water saturation history as a function of pore volume injected for primary imbibition in oil-wet core-F using tetradecane for both control (blue) and nanoparticle case (red).

Figure 5.45 shows the pressure drop ratio of nanoparticles case compared to the control case. The ratio was calculated by dividing the normalized pressure drop of nanoparticles case measured at each point in time by the normalized pressure drop for the control case measured at the same moment. As shown in the figure, the pressure drop ratio was initially around an average value of 0.97 for the first 0.52 PV injected and fluctuated around 1 afterward.

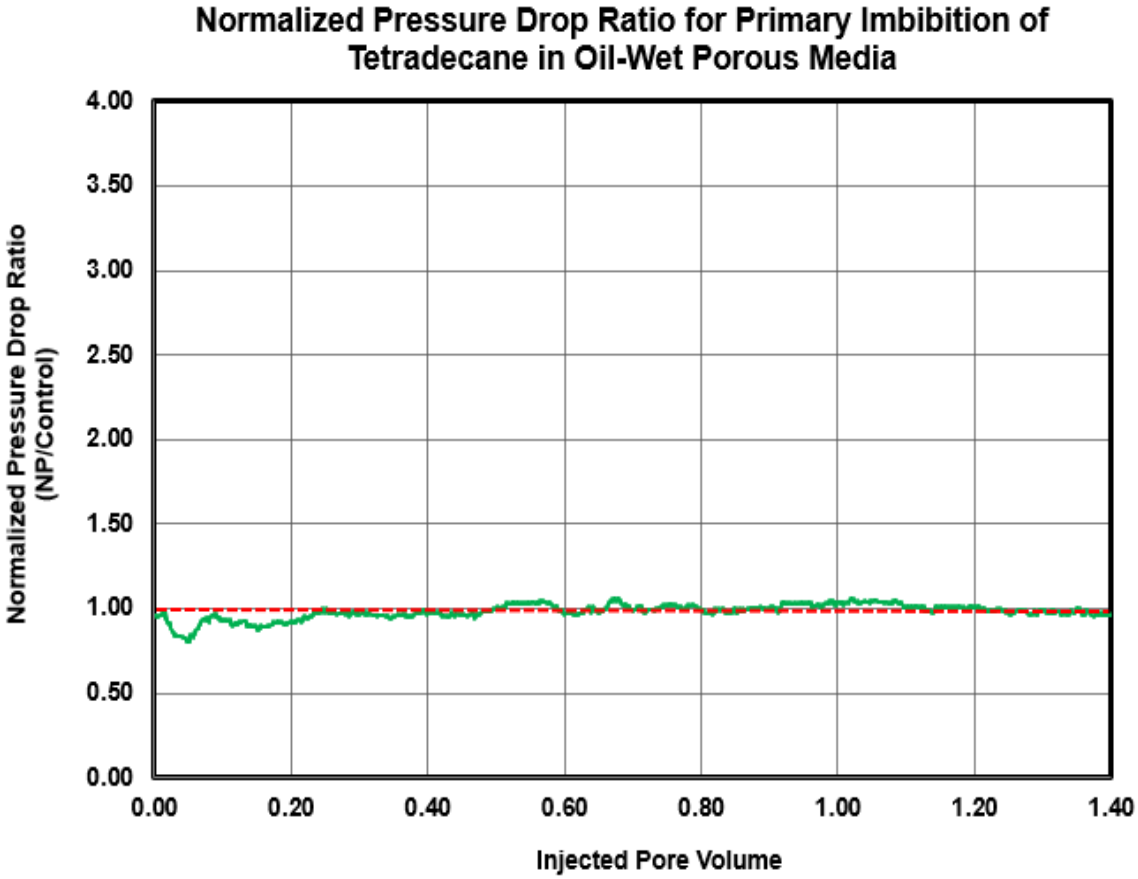


Figure 5.45: Pressure drop ratio calculated by dividing pressure drop measured at each point in time during nanoparticle case over that of the control case measured at the same moment. Ratio is expressed as a function of time for primary imbibition displacement in oil-wet core-F using tetradecane. Red dashed line represents the value of the normalized viscosity ratio between the aqueous nanoparticle dispersion and brine solution.

The endpoint relative permeability for the aqueous phase ($k_{rw}^{o}$) is given by:

$$k_{rw}^{o} = \frac{\Delta P_o \, \mu_w}{\Delta P_w \, \mu_o}$$

In the equation above, $\mu$ is the viscosity of the fluid represented by either *w* for the aqueous phase or *o* for the hydrocarbon phase. $\Delta P_o$ represents the normalized

pressure drop for single phase tetradecane flowing at steady state while $\Delta P_w$ is the value of steady state pressure drop of the aqueous phase flowing at residual hydrocarbon saturation. In all cases, the flow rate was kept the same at 1 ml/min. The calculated endpoint relative permeability was 0.30 for the control case and 0.33 for the nanoparticle indicating an increase of 10 % for the nanoparticle case.

The observations discussed before for this displacement case show that nanoparticle had no significant impact on the displacement dynamics with respect to emulsion generation process. The pressure drop behavior was generally comparable and almost similar for both control and nanoparticle case. The pressure drop ratio ranged from 1.00 to 1.20 which is close to the 1.18 viscosity ratio between nanoparticle-brine solution and brine solution. This increase in the aqueous phase viscosity may have caused a 0.07 delay in the breakthrough time as well as the nearly similar endpoint relative permeability values for both control and nanoparticle case with a difference of 0.03.

One important observation to address is the additional recovery of 5 saturation units of hydrocarbon phase measured at the end of this imbibition displacement. Similar to other imbibition experiments conducted so far, it seems that the presence of ethylene glycol and/or the chemicals used for coating those particles to create a stable aqueous nanoparticle dispersion may have been the reason to explain reduction in residual tetradecane as there was some degree of miscibility which may have resulted in reducing interfacial tension and increasing the capillary number, hence, the decrease in the residual tetradecane saturation.

The observations found here does not indicate the generation of viscous phase inside porous media as no symptoms of such thing were observed. Despite the viscous instability found here as well as the favorable wettability conditions that promote for Haines jump and Roof snap-off to occur in a manner similar to that found during

nanoparticle-brine displacement by n-octane in water-wet system, two arguments can be raised to explain why nanoparticle-stabilized emulsion may not have been generated and its symptoms were not observed. If we assume that both Haines jump and Roof Snap-off occurred during this displacement, one argument is that there may be other controlling elements besides these processes needed for nanoparticle-stabilized emulsion to be generated. One factor could be whether nanoparticles should be placed in the displaced fluid inside the core instead of the injected phase. Another important factor is the wettability of the nanoparticles. The hydrophilic wettability of the nanoparticles hinder the process of generating water-in-oil emulsion as those particles will tend to destabilize these droplets and/or destroy them. In addition to the rock wettability and the aspect ratio of pore body over pore throat, the second argument is that there might be some fluid properties such as density and viscosity that may play a vital role into the physics governing these processes. Differences between the density and the viscosity of the injected fluid and the displaced fluid may control the jumping events as well as whether snap-off at pore inlet will actually happen. The case might be that n-octane jump velocity inside the pore filled with nanoparticle-brine solution is faster than that of nanoparticle-brine solution jumping inside tetradecane filled pores. Despite similarities in term of wettability conditions and viscous instability ratio which was slightly more than 2 for both cases, yet the density of the phase performing the jump action were different. In this argument we hypothesized that jumping speed controls the velocity of the resident phase to invade the pore inlet to occupy the space left by the injected fluid during Haines jump. That velocity will eventually control the force applied at the inlet of the pore to choke off the injected phase and snap it off once snap off criteria is met. Another claim would be that the jumping velocity which depends on the density of the injected fluid may also determine if that speed is enough to the kinetic energy resulted from the jump into

adsorption energy that are needed to brine the nanoparticle to the interface. The previously discussed claims may explain why emulsion generation symptoms were not observed during this displacement as no viscous phase was generated and that nanoparticle had no impact on the displacement performance beside their higher viscosity compared to brine solution. The next section focuses on the performance of secondary drainage as tetradecane is injected back to the core that has some residual tetradecane saturation. It is interesting to see the differences between the displacement performances for the secondary drainage process as wettability is varied from water-wet to oil-wet.

***Secondary Drainage (Core-F)***

A post flush stage followed the primary imbibition displacement with tetradecane invading back to the core. Core-F is now saturated with either brine at 39% residual tetradecane saturation for the control case or nanoparticle-brine dispersion at 34% residual saturation. This displacement stage is known as a secondary drainage as the core is not saturated completely with aqueous phase. The displacement flow rate was kept at 1 ml/min and data were recorded and effluent samples were collected

Figure 5.46 shows the pressure drop trend as a function of pore volume injected. The blue curve represents the pressure drop for the control experiment while the red curve shows the pressure drawdown behavior for the nanoparticles case. The dashed lines show the breakthrough time for both displacements. As shown in the plot, both displacement cases showed a similar pattern of pressure build up behavior where drawdown was increasing almost in linear fashion with more pore volume injected until a peak pressure drop value is reached followed by a plateau for the control case and a general decline

trend for the nanoparticle case reaching a certain leveling off values by the displacement end.

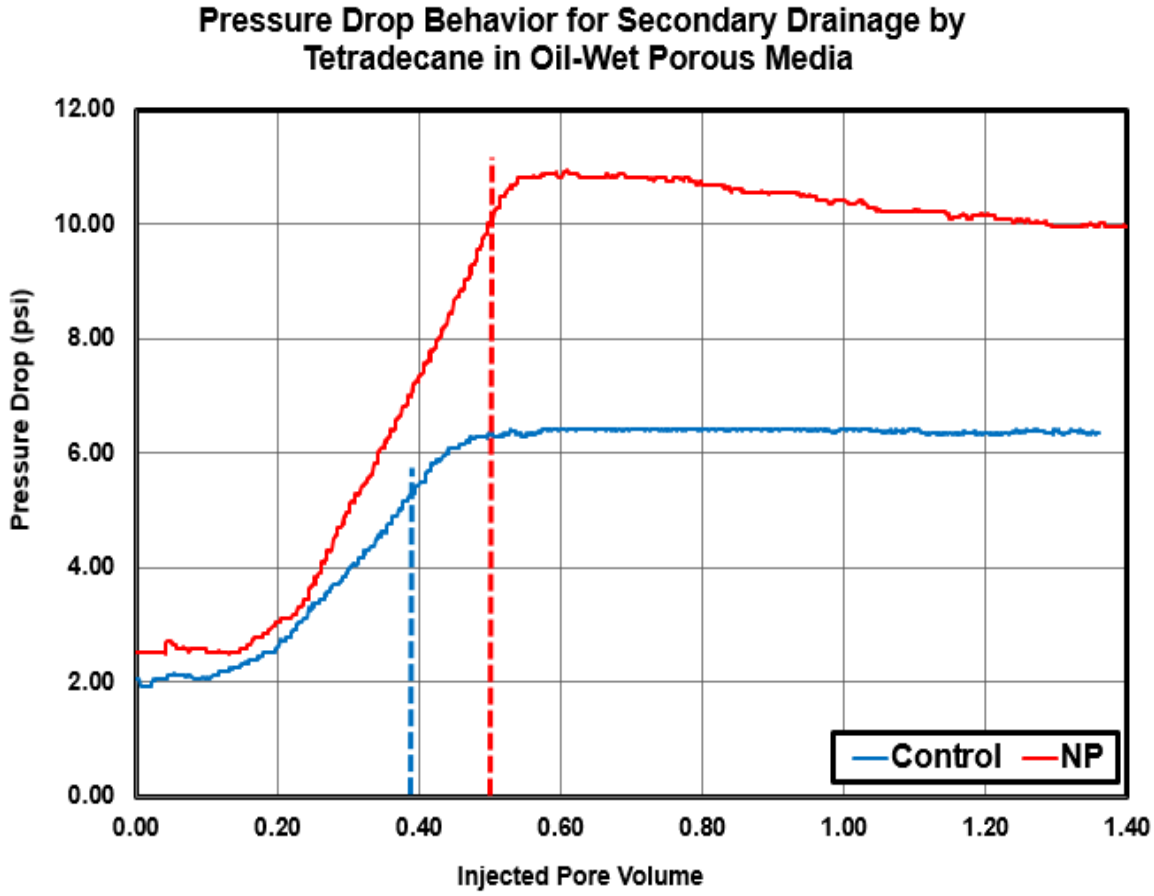


Figure 5.46: Measured pressure drop as a function of pore volume injected for control (blue) and nanoparticle case (red) into Boise sandstone for secondary drainage in oil-wet core-F using tetradecane. The dashed lines indicate breakthrough time.

Pressure normalization was carried in response to correcting for reduction in pore volume and permeability post IPA treatment. This was detailed before when primary imbibition case was presented. Normalized pressure drop curves for both control and nanoparticle case are shown in Figure 5.47.

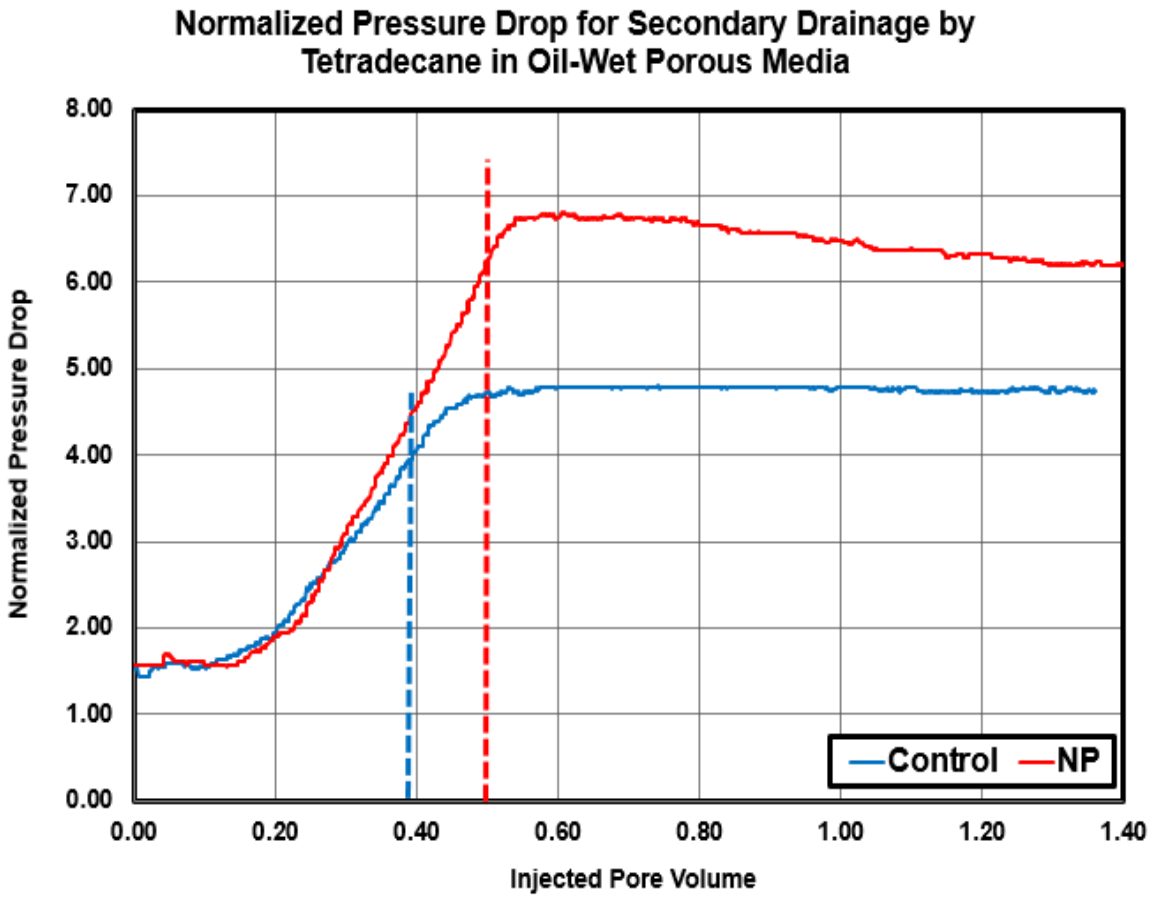


Figure 5.47: Normalized pressure drop as a function of pore volume injected for control (blue) and nanoparticle case (red) into Boise sandstone for secondary drainage in oil-wet core-F using tetradecane. The dashed lines indicate breakthrough time.

For the control experiment as shown in Figure 5.47 by the blue curve, the normalized pressure drop was increasing and reached a value of 4 at breakthrough of 0.39 PV. After that, the pressure drop started to plateau and reached an asymptote value of about 4.75 at 1.38 PV. As for the nanoparticle case as illustrated in Figure 5.47 by the red curve, the normalized pressure drop showed comparable performance to that of the control case as pressure drop increased in a linear fashion and reached a value of 6.25 at breakthrough time of 0.50 PV. After that, the pressure drop started to slowly increase and

reached a peak value of 6.75 before it starts slowly to decrease and reached an asymptote value of about 6.20 at 1.38 PV. It can be seen from Figure 5.47 that the nanoparticle case had a later breakthrough time that is 0.11 PV more compared to the control case (0.50 PV compared to 0.39 PV). In addition, nanoparticle experiment ended up with a slightly higher pressure drop that was 1.45 larger than that of the control case (6.20 compared to 4.75).

Figure 5.48 shows the water cut data which was collected during this displacement process. The blue curve shows the water cut values measured as a function of pore volume injected for the control experiment while the red curve shows the water cut for the nanoparticle case. For the control case, the water cut value maintained a value of 1 until the breakthrough time of 0.39 PV at which the water cut started to decrease until it reached 0 as tetradecane was only flowing at residual aqueous phase saturation. As for the nanoparticle case, the water cut value maintained a value of 1 until the breakthrough time of 0.50 PV after which the water cut started to decrease until it reached 0 as tetradecane was only flowing at residual aqueous phase saturation. Comparing both control and nanoparticle experiments, we see that the water cut reduction for the nanoparticle run occurred at later pore volume injected time that was 0.11 PV more compared to the control.

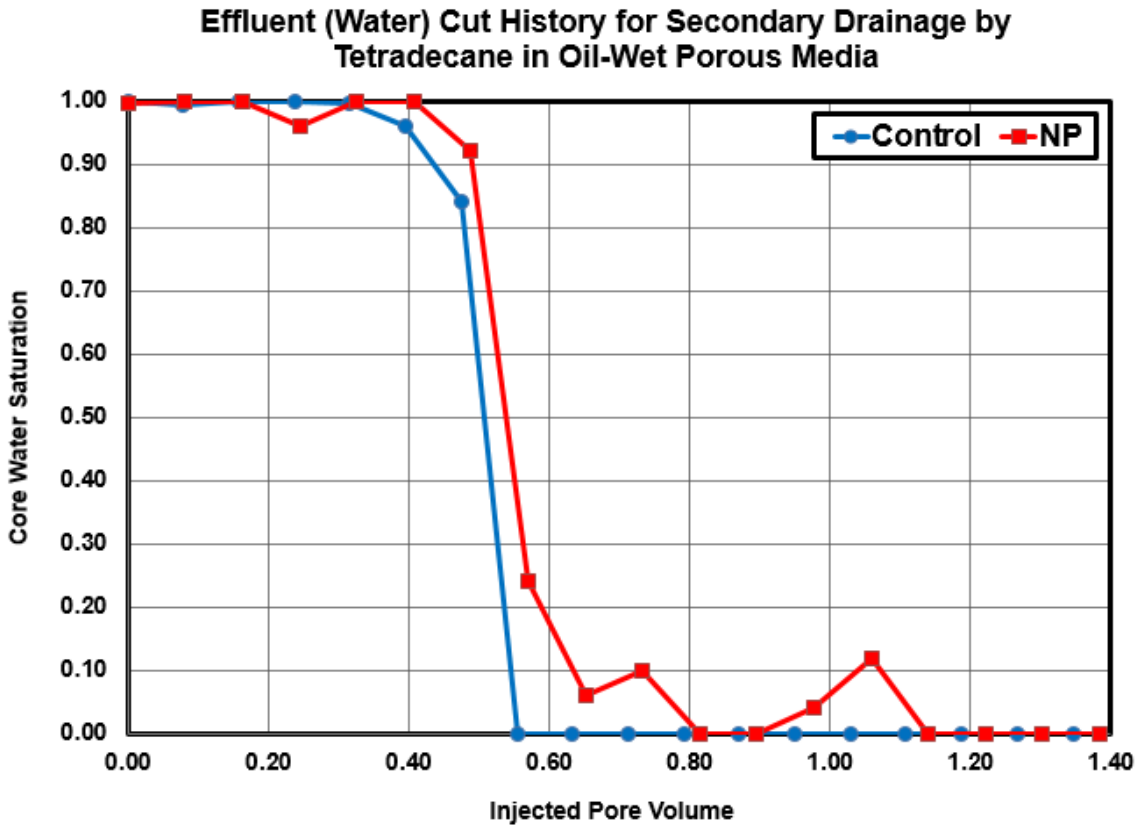


Figure 5.48: Effluent (water) cut as a function of pore volume injected for secondary drainage in oil-wet core-F using tetradecane for both control (blue) and nanoparticle case (red).

The residual saturation of brine or brine containing nanoparticles was calculated based on the water cut measured in the effluent samples collected during the displacement. The core water saturation histories are shown in blue for the control case and in red for the nanoparticle case as clearly illustrated in Figure 5.49. The water saturation was calculated by comparing the total volume of water recovered and the pore volume of the core. The residual aqueous phase saturation for the control case was 16%. As for the nanoparticles run, the residual saturation was 13.5% indicating an average reduction of 2.5%. For the control run, the initial water saturation calculated at the beginning of this displacement stage is 61 % and it decreased until it reached a residual

aqueous phase saturation of 16 %. As for the nanoparticles run, initial water saturation calculated at the beginning of this displacement stage is 66 % and it decreased until it reached a residual aqueous phase saturation of 13.5 % as well. This suggest displacing an additional 7.5 saturation units of the aqueous phase for the nanoparticle case.

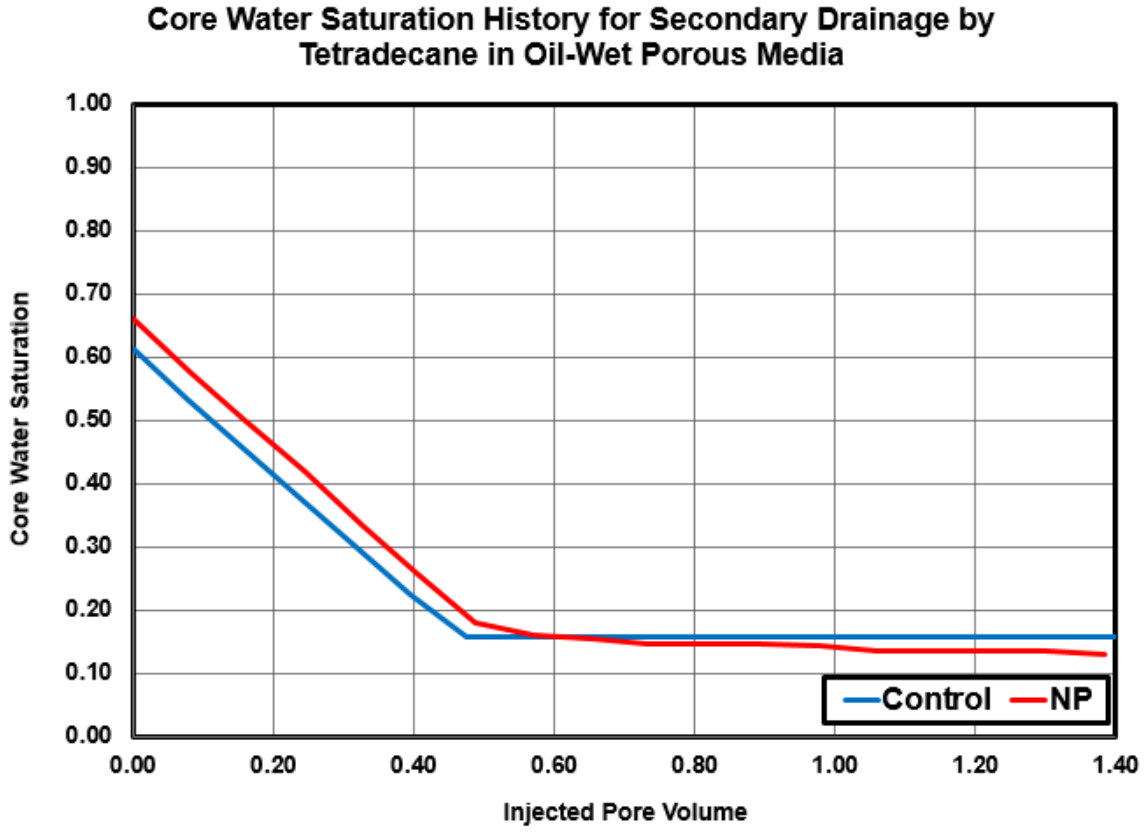


Figure 5.49: Average core water saturation history as a function of pore volume injected for secondary drainage in oil-wet core-F using tetradecane for both control (blue) and nanoparticle case (red).

Figure 5.50 shows the pressure drop ratio of nanoparticles case compared to the control case. The ratio was calculated by dividing the normalized pressure drop of nanoparticles case measured at each point in time by the normalized pressure drop for the control case measured at the same moment. As normalization was conducted in this case,

a ratio of 1 corresponds to 1.18 which is the viscosity ratio between nanoparticle-brine dispersion and brine solution. As shown in the figure, the ratio was fluctuating around 1 increasing from as low as 0.97 to as high as 1.13 throughout the first 0.18 PV injection segment. After that, it started to increase from 1.15 to a maximum of 1.40 after injecting nearly 0.48 PV. The maximum ratio of 1.40 corresponds to the breakthrough time during the nanoparticle displacement case. The ratio has maintained a slow decline afterward but was still higher than 1 throughout the displacement.

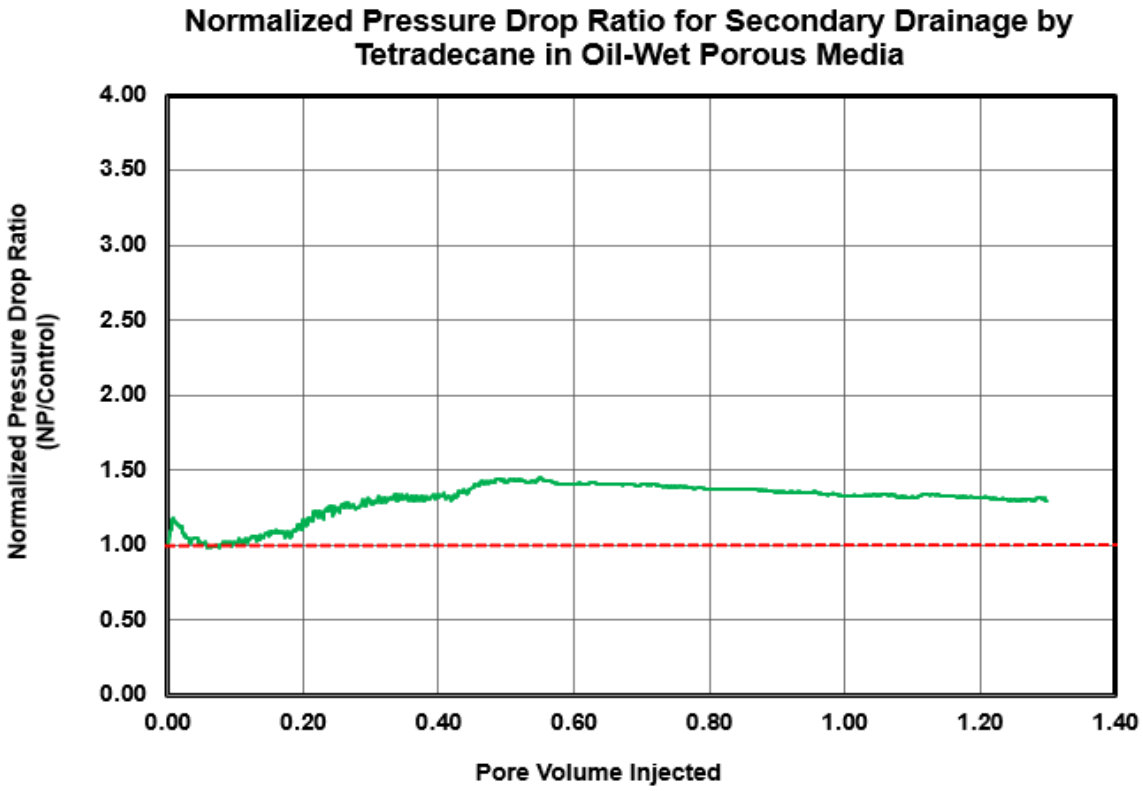


Figure 5.50: Pressure drop ratio calculated by dividing pressure drop measured at each point in time during nanoparticle case over that of the control case measured at the same moment. Ratio is expressed as a function of time for secondary drainage displacement in oil-wet core-F using tetradecane. Red dashed line represents the value of the normalized viscosity ratio between the aqueous nanoparticle dispersion and brine solution.

The calculated endpoint relative permeability for the hydrocarbon phase ($k_{ro}^{o}$) is given by:

$$k_{ro}^{o} = \frac{\Delta P_{o1}}{\Delta P_{o2}}$$

In the equation above, $\Delta P_{o1}$ represents the pressure drop for single phase tetradecane flowing at steady state while $\Delta P_{o2}$ is the value of steady state pressure drop of tetradecane phase flowing at residual aqueous phase saturation by the end of secondary drainage. In all cases, the flow rate was kept the same at 1 ml/min. The calculated end point relative permeability was 0.21 for the control case and 0.16 for the nanoparticle indicating a reduction of 24 % for the nanoparticle case.

The observations found during this experimental protocol had shown that nanoparticles had caused the pressure drop to increase sharply compared to the control case with pressure drop ratio ranging from 1.38 to 1.68 times greater than that of the control case and by far greater than the viscosity ratio of nanoparticle-brine solution and brine solution which is 1.18. This indicate a development of a more viscous phase that resulted in lower invading phase (tetradecane) mobility. This reduction in phase mobility was also confirmed by the 24 % reduction in the endpoint relative permeability for the nanoparticle case as shown before. The reduction in invading phase mobility is mainly due to the fact that tetradecane is forced out of its preferred flow paths it used to have during the control case when nanoparticles were not present. Also, it was shown nanoparticles had caused the residual aqueous phase saturation to decrease with an average reduction of 8 saturation units. In addition, the observed behavior of the displacement showed that nanoparticle case had a later breakthrough of 0.10 PV

All in all, all of the previously discussed observations and measured data indicate the generations of viscous phase inside porous media as many symptoms were observed. The Pressure drop behavior, breakthrough time, and residual tetradecane saturation profile all correlate well with each other. Compared to the same displacement scenario in water-wet system, the hypothesized generated emulsion occurred prior to the breakthrough of tetradecane. With rock being oil-wet, it seems it is easier for tetradecane to become connected and reach the necessary saturation for emulsion generating processes. As a result, the hydrophobicity of the rock may have resulted in aiding the emulsion generation processes as tetradecane was mainly covering the grains and occupying small pores spaces. Despite the isolated and more disconnected blobs of tetradecane found after the primary imbibition in water-wet condition, the displacement showed what believed to be some symptoms of emulsion generation inside porous media as discussed before. Yet, it seems that the hydrophobicity of the core had enable emulsion generation and made it easy to observe the symptoms.

It is interesting that emulsion generation symptoms were observed under both oil-wet and water-wet. In fact, the behavior was similar to that of secondary drainage process using n-octane as a hydrocarbon phase. This observation may be explained by the same two arguments we presented before of the n-octane case. Given that no Haines jump and Roof snap-off may not occur in the aqueous phase displacement by oil phase under oil-wet conditions, it seems that nanoparticle-stabilized emulsion will form regardless of the existence of those pore scale events. In this case and under oil-wet conditions, it seems that as long as nanoparticles of suitable wettability are placed in the displaced fluid inside porous media and then was displaced by another displacing fluid, nanoparticle-stabilized emulsion will form. In this case, any pore scale event that may lead to the snap-off of the displacing fluid may cause nanoparticle-stabilized emulsion to form. Because those

emulsion signs were seen in a viscously stable displacement, these processes may require wettability of nanoparticle to be switched from hydrophilic to hydrophobic in order to help generate water-in-oil emulsion. The reason for this claim is that no emulsion generation symptoms were observed during primary imbibition in both oil-wet and water-wet displacement involving tetradecane as a hydrocarbon phase.

The second argument regarding the emulsion generation symptoms observed during the secondary drainage in oil-wet core is that the core started to act like a water-wet core. In this claim, it is hypothesized that nanoparticles have been brought to the interface between tetradecane and the aqueous phase at the some sites inside the rock. As those particles generally stabilize the interface, this would suggest, if this happen, that nanoparticle dispersion is now covering the hydrocarbon layer attached to the rock through chemical means and form a hydrophilic coating attached to the oil layers covering the grains. In other words, the injected n-octane would now see the rock as if it were water-wet at least in some sites. As a result, the hypothesis of Haines jump and Roof snap-off being responsible for generating emulsion in porous media may still hold true in this case. To further test this claim, a capillary pressure vs. saturation curve has to be established to quantify the wettability behavior of the rock. The value of residual tetradecane saturation may play a role in the hypothesized emulsion generation process. In this experiment, the morphology of how tetradecane was distributed inside the rock after the primary imbibition as well as the higher tetradecane saturation may have simplified the processes to generating nanoparticle-stabilized emulsion which was observed through the symptoms previously mentioned.

## 5.4 HYDROPHOBIC NANOPARTICLES DISPLACEMENT ATTEMPT

An experimental attempt was to conduct a primary imbibition and secondary drainage experiment similar to that conducted on core-F. The attempt was planned on core-H using a lower viscosity toluene as a hydrocarbon phase. Similar to all experiments conducted using hydrophilic nanoparticle, the concentration of the hydrophobic was maintained to be 5 wt. % of the entire hydrocarbon dispersion and was planned to be placed inside porous media to be displaced by invading brine. The displacement test was conducted and all measurements were recorded for the control case. However, when the nanoparticle run was started, the hydrophobic nanoparticle solution exhibit instability causing the dispersion to start gelling as it became in contact with brine inside the accumulator as brine was attempting to displace it inside the core. Pressure drop data showed an excessive and rapid increase in pressure drop suggesting that the core is plugging. Despite being normally a stable dispersion, the dispersion of the hydrophobic nanoparticles (TOL-ST) was apparently affected by the dilution process that reduced the nanoparticle concentration from 40 % to 5 %. The inability to complete the nanoparticle run because of core plugging suggest that further work and research must be done in order to design a stable hydrophobic nanoparticle dispersion that maintain stability under different concentration as well as whenever pumped inside porous media.

## 5.5 OBSERVATIONS AND FINDINGS SUMMARY

This section summarize the important findings of all core flooding tests evaluated previously. The objective was to examine the impact of nanoparticle presence in different displacement types including primary drainage, primary imbibition, secondary drainage, and secondary imbibition. The hypothesis being tested in this research states that nanoparticles can help in stabilizing emulsion in porous media utilizing pore scale

mechanisms of Haines jump and Roof snap-off. This study provided additional tests to verify this hypothesis as well as study the effect of rock wettability, viscous stability, and potentially the nanoparticle wettability as well on the emulsion generation processes. As stated before, because no emulsion was observed inside porous media, only its symptoms and indications were observed and analyzed. These symptoms include the rapid increase in pressure drop which exceeds the viscosity ratio between brine and nanoparticle-brine dispersion of 1.18. Also, it include having a later breakthrough of the main displacement front which ranged to be between 0.1 to 0.2 PV in some cases. This was even supported by reduction in end point relative permeability of the invading phase. In addition, the increase in entrapment of the invading phase and the additional sweep of the resident phase has also been observed as another sign of the development of viscous phase inside porous media. Table 5.1 presents the experimental findings based on measured and calculated properties for all displacement scenarios under water-wet conditions for nanoparticle run compared to the control case. As defined before, imbibition (I) is defined as water is the displacing phase while drainage (D) is when water is displaced out of the core. The note “primary” or “P” indicate that the core is at 100% saturation of the whatever initial resident fluid while “secondary” or “S” indicate the core is partially saturated with one phase at the residual saturation of the other phase. Table 5.2, on the other hand, presents the experimental findings based on measured and calculated properties for all displacement scenarios under oil-wet conditions for nanoparticle run compared to the control case

| (a) **Displacement With n-Octane as a Hydrocarbon Phase ($\mu_o < \mu_w$)** | | | | | |
|---|---|---|---|---|---|
| Flow Scenario | Pressure Drop Ratio | Breakthrough Time | End of Displacement Aqueous phase Saturation (SU)* | End Pt. ($k_{ri}^o$) | Emulsion Signs (Y/N) |
| PD | 2.00 – 2.70 | Delay of 0.2 PV | $S_{wr}$ down by 11 | $k_{ro}^o$ down by 54% | Y |
| SI | | | | | |
| PI | 1.00 – 1.20 | Delay of 0.09 PV | $S_{wr}$ Up by 7 | $k_{rw}^o$ Up by 4% | N |
| SD | 1.20 – 2.70 | Delay of 0.2 PV | $S_{wr}$down by 13 | $k_{ro}^o$ down by 64% | Y |
| (b) **Displacement With Tetradecane as a Hydrocarbon Phase ($\mu_o > \mu_w$)** | | | | | |
| PD | 1.20 – 2.25 | Delay of 0.18 PV | $S_{wr}$ down by 11 | $k_{ro}^o$ down by 14% | Y |
| SI | 1.10 – 1.22 | Delay of 0.1 PV | $S_{wr}$ up by 5 | $k_{rw}^o$ down by 5% | N |
| PI | 1.00 – 1.20 | Delay of 0.05 PV | $S_{wr}$ Up by 8 | $k_{rw}^o$ down by 5% | N |
| SD | 1.30 – 1.62 | Same as Control | $S_{wr}$ down by 8 | $k_{ro}^o$ down by 18% | Y |

Table 5.1: Summary of the findings and observations for core evaluation tests conducted under water-wet conditions showing the effect of nanoparticle presence. These results are also presented under different viscous stability with (a) n-octane as a lower viscosity hydrocarbon phase and (b) tetradecane as more viscous hydrocarbon phase. * (SU) represents saturation unit(s).

| (a) **Displacement With n-Octane as a Hydrocarbon Phase ($\mu_o < \mu_w$)** | | | | | |
|---|---|---|---|---|---|
| Flow Scenario | . Pressure Drop Ratio | Breakthrough Time | End of Displacement Aqueous Phase Saturation (SU) | End Pt. ($k_{ri}^o$) | Emulsion Signs (Y/N) |
| PD | | | | | |
| SI | | | | | |
| PI | 1.20 – 1.30 | Same as Control | $S_{wr}$ Up by 5 | $k_{rw}^o$ down by 7% | N |
| SD | 1.20 – 2.70 | Delay of 0.09 PV | $S_{wr}$ down by 1 | $k_{ro}^o$ down by 63% | Y |
| (b) **Displacement With Tetradecane as a Hydrocarbon Phase ($\mu_o > \mu_w$)** | | | | | |
| PD | | | | | |
| SI | | | | | |
| PI | 1.00 – 1.20 | Delay of 0.07 PV | $S_{wr}$ up by 5 | $k_{rw}^o$ up by 10% | N |
| SD | 1.38 – 1.68 | Delay of 0.10 PV | $S_{wr}$ down by 7.5 | $k_{ro}^o$ down by 24% | Y |

Table 5.2: Summary of the findings and observations for core evaluation tests conducted under oil-wet conditions showing the effect of nanoparticle presence. These results are also presented under different viscous stability with (a) n-octane as a lower viscosity hydrocarbon phase and (b) tetradecane as more viscous hydrocarbon phase. (SU) represents saturation unit(s)

# Chapter 6: Conclusions and Future Work

## 6.1 CONCLUDING REMARKS

The findings of all experimental core displacement tests showed that the presence of nanoparticle has different kinds of impact on the flow performance of all displacement cases. Yet, those effects are different depending on the type of the displacement which govern the physics responsible for different types of pore scale events. The test for the main hypothesis was inconclusive due to the difficulty of generating a stable dispersion as more work is needed in this front. Yet, the research have addressed several findings which were observed during the displacement as well as discusses effect of several factors such as rock wettability, displacement type, initial core conditions , and viscous stability. Understanding these fundamental facts regarding the necessary conditions that govern nanoparticle-stabilized emulsion inside porous media have raised a great potential of success for the proposed hypothesis

Two main important effects have been observed during all the core flooding operation conducted. The first one is that nanoparticles have impacted the all of the drainage type displacement under both oil-wet and water conditions as well as under different viscous stability conditions. The impact was generally seen as an indirect symptoms of nanoparticle-stabilized emulsion generation inside porous media observed through an excessive pressure drop build up across the core which exceed by far the 1.18 viscosity ratio between brine and nanoparticle-brine solution, later front breakthrough, reduction in the displaced fluid residual saturation as well as reduction in invading phase mobility. All of these sings were observed as an indication of improved sweep action inside the core. In these experiments, pressure drop increase shows an indirect evidence of what seems to be the development of a more viscous phase with higher apparent viscosity. The development of such phase had hypothetical forced out the invading

hydrocarbon phase out of its preferred paths causing more restriction on the flow, hence, increase in pressure, change in fluid saturation, and of course reduction in endpoint relative permeability of the invading phase. Because the displacing phase is forced out of its preferred paths, it now accesses other paths inside porous media yielding into improving sweep action and therefore reduction in the displaced fluid residual saturation was observed.

The magnitude and the strength of these emulsion generation signs were different and were influenced by factors such rock wettability, displacement viscous stability, and initial core trapping of some of the hydrocarbon phase filling out pore bodies. The distribution of hydrocarbon phase inside porous media after the primary imbibition stage plays a role in how quickly the phase becomes connected and that the core reaches a certain saturation after which emulsion generation processes started to occur. Another important observation was the trend of pressure drop increase observed during primary drainage and secondary drainage under the same wettability conditions. We found that the maximum pressure drop increase was 500 % more compared to the initial value during n-octane displacement under water-wet condition while it was only 60 % more compared to the initial pressure drop during the secondary drainage experiment under the same wettability condition. This is because that some of the pore bodies are not fully saturated with displaced fluid containing nanoparticles and that the residual displacing phase is occupying some of these pores hindering the likelihood as well as interrupt the frequency of the events that might be responsible for emulsion generation unlike primary drainage type displacement where those pore bodies are fully saturated with displaced fluid containing nanoparticles. Another important finding related to this point is that the increase in the viscosity of the displacing fluid was found to show strong signs for emulsion generation. In other words, comparing the pressure drop increase trend

measured during primary drainage using either n-octane or tetradecane, we see that maximum pressure drop was 500 % more compared to the initial value while for tetradecane, the increase in pressure drop trend was nearly 700 % for the same displacement scenario. The observed symptoms during both primary drainage and secondary drainage displacement under wet-wet conditions supports that Haines jump followed by Roof snap-off will provide the necessary physical work to bring the hydrophilic nanoparticle to the interface between the wetting phase and the non-wetting phase to armor the non-wetting phase droplets and stabilize them and prevent them from coalescing. As for oil-wet condition, the observed emulsion generation symptoms suggest two possible arguments. The first argument is that there are other processes, beside Haines jump and Roof snap-off to stabilize nanoparticle emulsion, that are dependent on fluid type and properties such as viscosity and density. This argument suggest that regardless of rock wettability, nanoparticle-stabilized emulsion may likely be generated as long as nanoparticles of suitable wettability are placed inside the displaced phase which in turns is displaced by another displacing immiscible fluid. The second argument is that it might be possible that the hydrophilic nanoparticles caused the rock to behave like water-wet at the particle coat the external layer of the hydrocarbon film covering the grains. In this case, Haines jump and Roof snap-off is still the main mechanism responsible for generating nanoparticle-stabilized emulsion inside porous media.

The Haines jump and Roof snap-off hypothesis , which occurs mainly during the displacement of wetting phase by non-wetting phase, was also put in test under imbibition displacement scenario. Experimental runs show that Roof snap-off is not likely to occur under water-wet condition as the wetting phase is advancing. As for oil-wet case, Haines jump and Roof snap-off are high likely to occur as the wetting hydrocarbon phase is being displaced by the non-wetting aqueous phase. However, no

emulsion generation signs were observed which might due to the fact that nanoparticles are placed in the displacing phase instead of displaced phase. In addition, the hydrophilic wettability of the particles may hinder the stability of the armored droplets and cause them to either coalesce or be destroyed. Therefore, the presence of nanoparticle did not show evidence of altering the dynamics of the imbibition displacement under both water-wet and oil-wet conditions from at least from the emulsion generation perspective. This was confirmed by pressure drop ratio data as well as the slight, if not negligible, change in the endpoint relative permeability of the invading phase. However, it was shown that the presence of ethylene glycol and/or other coating chemicals used to maintain stability of nanoparticle aqueous dispersion may have caused the reduction of hydrocarbon phase residual saturation during all imbibition type displacement.

This research shows that further evaluation is still needed to test if hydrophilic nanoparticles can somehow change the oil-wet rock to behave like water-wet one by measuring core wettability. If so, then this research confirms that Haines jump and Roof snap-off are the main processes to stabilized nanoparticle emulsion in porous media. Otherwise, emulsion generation inside porous media is then dependent on nanoparticle wettability and the fact that they should be placed in the displaced phase regardless of the wettability of the rock. The potential benefits of understanding the fundamental processes and conditions governing the emulsion generation processes may lead into developing possible solution to chemically shut off high permeability thief zones in water injection wells or oil producing wells. This shut-off would lead to improve fluid distribution more evenly during the injection process as well as help maintain a better uniform pressure drawdown. In addition, this may lead into developing a possible chemical solutions that utilize both nanoparticles as well as polymers to enable smarter and efficient enhanced oil recovery.

## 6.2 FUTURE WORKS

### Displacement Experiments Using Hydrophobic Nanoparticles

One possible argument that explains why no signs of nanoparticle-stabilized emulsion were observed during the imbibition process under oil-wet condition is that the hydrophilic nanoparticles have destabilized and/or destroyed the water droplets inside the oil-filled pore preventing it from forming water-in-oil emulsion. However, the use of stable and carefully designed hydrophobic nanoparticles, as was attempted in this research, may lead into stabilizing these droplets and cause the water-in-oil emulsion to form and the symptoms to be observed.

### Evaluating Core Wettability Using Capillary Pressure – Saturation Tests

One possible argument that explains why signs of nanoparticle-stabilized emulsion were observed during the secondary drainage under oil-wet condition, despite that these condition does not support Haines jump and Roof snap-off to occur, is that the hydrophilic nanoparticles were able to change the rock to behave like water-wet which enable Haines jump and Roof snap-off processes to occur. Capillary pressure and core saturation measurement experiments can be conducted to generate drainage and imbibition curves in order to quantify the wettability behavior of the rock.

# Appendices

## A1 EPOXY CORE PREPARATION

Epoxy core is an alternative and cheap way to prepare the cores for flooding experiments under room temperature and low pressure application. This section provides the operational details intended to epoxy the cores. In addition to the epoxy materials, tubes with end caps made of polycarbonate (PC) materials were used mainly for experiments conducted under water-wet conditions. On the other hand, cores intended for oil-wet core flood evaluation had to go through a wettability alteration process to change their wettability from water-wet to oil-wet. Such process involves using some corrosive chemicals such as hexane, acetone, and organosilane solutions that are not compatible with PC. Therefore, a much more resistant ULTEM tubes and end caps were used for core preparation prior to oil-wet experiments. The following preparation steps are applicable for 1-inch diameter and 1-foot long cores and include the following:

1. Arrange for all the necessary epoxying materials to be available which should include one core with previously mentioned dimensions as shown in Figure A1.1, one tube with a diameter of 1.5” and 15” in length which can be made of polycarbonate (PC) for water-wet experiments as showing in Figure A1.2 (a) or Polyetherimide (ULTEM), shown in Figure A1.2 (b) for oil-wet experimental tests. The material should also include 2 NPT end caps made from the same material that the tube is made of. In addition, 5-mintue epoxy (Devcon), epoxy resin (Miller-Stephenson EPON Resin 828), hardener (Miller-Stephenson Versamid 125), rubber stopper, wax paper, tape, and a scissor. The technical drawing for the tube design and end caps is shown in Figure A1.3.

Figure A1.1: Boise sandstone core (Chung, 2013).

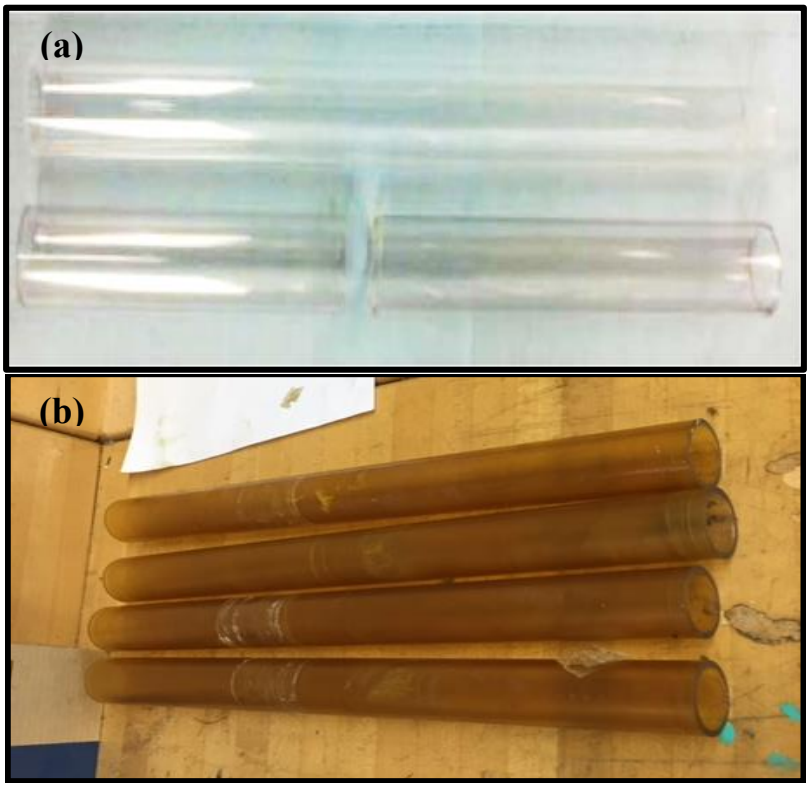


Figure A1.2: Different tubes with different lengths shown here to be made of either (a) polycarbonate (PC) (Roberts, 2011) or (b) polyetherimide (ULTEM).

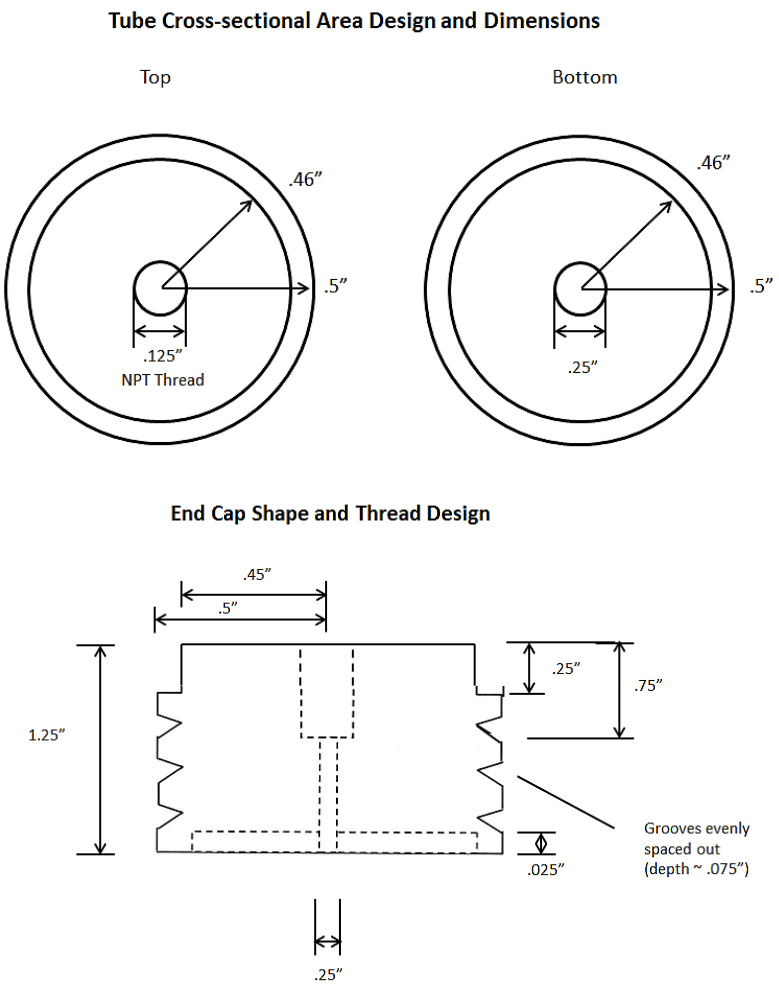


Figure A1.3: Technical drawing showing the design and dimensions used for making end caps (Chung, 2013).

2. First, after positioning the core vertically, carefully place the end cap on the top of the core covering the circular face of the sand. As shown in Figure A1.4, start sealing the edge between the end caps and rock using the 5-mintue epoxy and wait for at least 5 minute to set.

Figure A1.4: Sealing and joining the edge of the end cap made from PC (left) and ULTEM (right) to the upper face of the core using 5-mintue epoxy

3. Cover the face of the end cap with a tape as illustrated in Figure A1.5. This is done in order to block the hole and prevent any epoxy from flowing inside the threaded part. Repeat step 2 and 3 for the other face of the core.

Figure A1.5: Covering the top of the end cap to block the threaded hole (Chung, 2013).

4. Take the tube, which is intended to contain the core-epoxy system, and placed on the top the rubber stopper. Be sure that the rubber stopper is covered with wax paper before and that it is inserted only from one end of the tube. Figure A1.6 illustrate the process.

Figure A1.6: Rubber stopper inserted at the end of the tube being used for epoxying process after it was covered by a wax paper (Chung, 2013).

5. Mount the tube into a stand using a clamp. The carefully placed the core with end caps inside the tube and centralized as much as possible.
6. Start mixing the epoxy fluid and the hardener agent until the mixture changes color to nearly white and become homogeneous as shown in Figure A1.7.

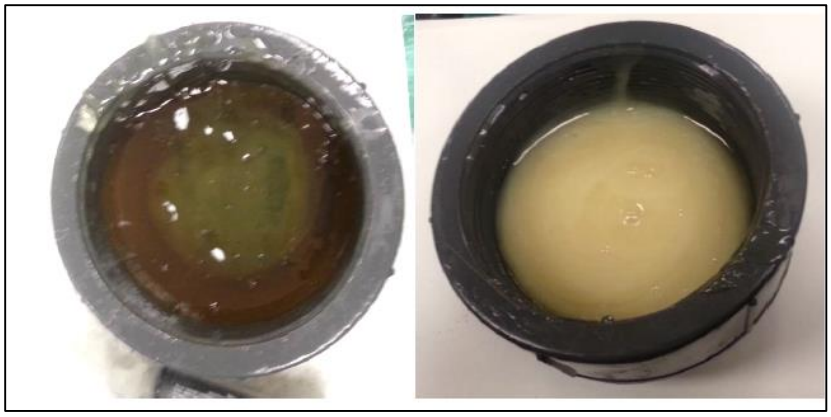

Figure A1.7: Epoxy and hardener mixture before mixing (left) and after mixing (right) (Chung, 2013).

7. Start by slowly pouring the epoxy mixture from the top and fill up the entire tube without covering the face of the top end cap. Once filled, let the epoxy set for at least 24 hours. Figure A1.8 shows the core epoxy system after it sets.

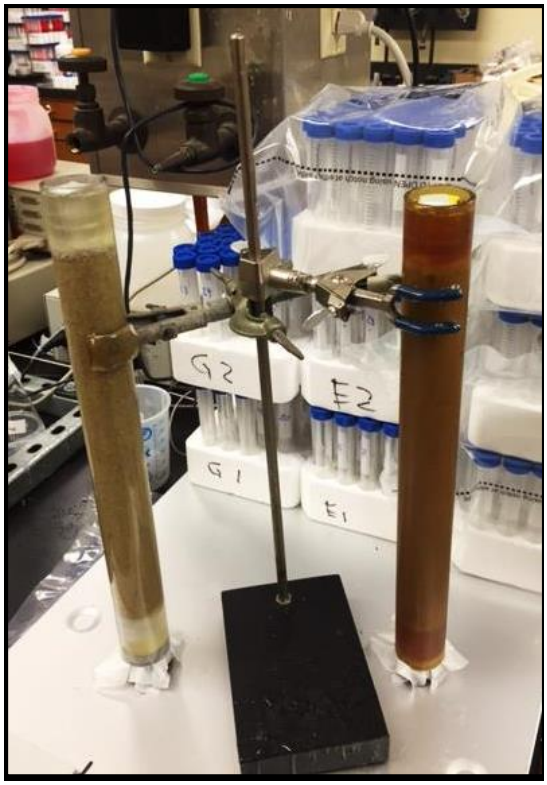


Figure A1.8: Epoxy mixture was filled in for both cores shown here with PC tubing (left) and ULTEM tubing (right) and hardened after 24 hours.

8. Remove the taped covering the end caps and start inserting the NPT fittings and connect them to Swagelok valves. Ensure that the fittings are covered with Teflon tape to ensure a better seal. This step is shown in Figure A1.9.

Figure A1.9: NPT fittings are inserted inside the threaded end caps (left) and connected to three-way Swagelok valve (right) (Chung, 2013).

## A2 CORE PORE VOLUME CORRECTION STEPS

The Winland correlation that describes the relationship between porosity and permeability is used to translate any changes in core permeability to pore volume adjustment. This was done mainly for those cores where the core was not restored to its original state post IPA treatment. Winland correlation relates the pore throat radius that corresponds to 35 % mercury saturation (R35) in capillary pressure measurement to both core permeability and porosity. In other words, a relationship between porosity and permeability can be established once the value of R35 is known. The general Winland equation is given by:

$$\log(R_{35}) = 0.732 + 0.588\log(k) - 0.864\log(\emptyset)$$

In the equation above, k is the permeability of the rock and ∅ is porosity. Using the $R_{35}$ value of 47 (obtained from capillary pressure data measurement), the permeability and porosity relationship used to relate both properties and used to perform any necessary correction is simplified to the following expression given below:

$$\emptyset = \left(\frac{k}{40.523}\right)^{0.68}$$

# References


1. Alshehri, A.A., Ellis, E.S., Servin, J.M.S., Kosynkin, D.V., Kanj, M.Y., and Schmidt, H.K. Illuminating the Reservoir: Magnetic Nano Mappers. Presented at SPE Middle East Oil and Gas Show and Exhibition, Manama, Bahrain. SPE 164461 (2013).
2. Aminzadeh, B. Experimental Measurement of Sweep Efficiency during Multi-Phase Displacement in the Presence of Nanoparticles, Ph.D. Dissertation, The University of Texas at Austin (2013).
3. Belgrave, J. D. M., and Win, T. Vertical Sweep Efficiency and Oil Recovery from Gas Injection in Heterogeneous Horizontal Reservoirs. Paper was presented at SPE Western Regional Meeting held in Anchorage, Alaska, U.S.A., SPE 26085 (1993).
4. Binks, B.P. and Horozov, T.S., Colloidal Particles at fluid interfaces: An introduction in Colloidal Particle at Liquid Interfaces. Cambridge University Press, Cambridge, UK, 2006.
5. Bragg, J.R. Solids-Stabilized Emulsion, *U.S. Patent*, 5910467 (1999).
6. Braggs, J.R., and R. Varadaraj. Solids-Stabilized Oil-in-Water Emulsion and a Method for Preparing the Same, *World Intellectual Property Organization*, WO 03/057793, (2003).
7. Chung, D.H., Transport of Nanoparticles during Drainage and Imbibition Displacement in Porous Media. Master Thesis, The University of Texas at Austin, August 2013.
8. Das, S., Electro-Magnetic Heating in Viscous Oil Reservoir. Presented at the SPE International Thermal Operations and Heavy Oil Symposium, Calgary, Alberta, Canada. SPE 117693 (2008).

9. Davidson, A., Huh, C., and Bryant, S.L., Focused Magnetic Heating Utilizing Superparamagnetic Nanoparticles for Improved Oil Production Applications. Presented at the SPE International Oilfield Nanotechnology Conference, Noordwijk, The Netherlands. SPE 157046 (2012)
10. DiCarlo, D.A., B. Aminzadeh, M. Roberts, D.H. Chung, S.L. Bryant, and C. Huh. Mobility Control Through Spontaneous Formation of Nanoparticle Stabilized Emulsions, *Geophysical Research Letters*, Vol. 38, L24404 (2011)
11. Dickson, J.L., B.P. Binks, K.P. Johnston. Stabilization of Carbon Dioxide-in-Water Emulsions with Silica Nanoparticles, *Langmuir*, 20, 7976-7983 (2004).
12. Enick, R.M. and Klara, S.M., CO2 Solubility in Water and Brine Under Reservoir Conditions. Chem. Eng. Commun., 90(1):23-33, 1990.
13. Enick, R.M. and Olsen, D.K., Mobility and Conformance Control for Caron Dioxide Enhanced Oil Recovery ($CO_2$-EOR) via Thickeners, Foams, and Gels a detailed literature review of 40 years of research. Technical report, DOE/NETL 2012/1550; Activity 4003.200.01, December 2011.
14. Espinosa, D. Nanoparticle Stabilized Supercritical $CO_2$ Foams for Potential Mobility Control Applications, M.S.E. Thesis, The University of Texas at Austin (2011).
15. Espinosa, D., Caldelas, F., Johnston, K.P., Bryant, S.L., and Huh, C., Nanoparticles Stabilized Supercritical $CO_2$ foams for Potential Mobility Control Applications. Presented at the SPE Improved Oil Recovery Symposium, Tulsa, Oklahoma, U.S.A., SPE 129925 (2010).
16. Gladkikh, M.N., A priori prediction of macroscopic properties of sedimentary rocks containing two immiscible fluids. PhD. Thesis, The University of Texas at Austin (2005).

17. Haines, W.B. Studies in the Physical Properties of Soil. IV. A Further Investigation to the Theory of Capillary Phenomena in Soils, *Jour. Agri. Sci.*, 17, 264 (1927).
18. Hariz, T.R., Nanoparticle-Stabilized $CO_2$ Foams for Potential Mobility Control Applications. Master Thesis, The University of Texas at Austin, December 2012.
19. Ju B., T. Fan, Z. Li. Improving Water Injectivity and Enhancing Oil Recovery by Wettability Control Using Nanopowders" Journal of Petroleum Science and Engineering, Volumes 86–87, May 2012, Pages 206–216 (SCI)
20. Ko, S., Prigiobbe, V., Huh, C., and Bryant, S.L., Accelerated Oil Droplet Separation from Produced Water Using Magnetic Nanoparticles. Presented at the SPE Annual Technical Conference and Exhibition, Amsterdam, The Netherlands. SPE-170828-MS (2014)
21. Kovscek, A.R., G.-Q. Tang and C.J. Radke. Verification of Roof snap off as a foam-generation mechanism in porous media at steady state, *Colloids and Surfaces A: Physicochem. Eng. Aspects*, 302, 251 - 260 (2007).
22. Lake, L.W. Enhanced Oil Recovery. Englewood Cliffs, NJ: Prentice Hall (1989).
23. Melrose, J.C. Wettability as Related to Capillary Action in Porous Media, Presented at the SPE-AIChE Joint Symposium on Wetting and Capillary in Fluid Displacement Processes, Kansas City, MO, SPE 1085 (1965).
24. Onyekonwu, M.O. and Ogolo, N.A., Investigating the Use of Nanoparticles in Enhancing Oil Recovery. Prepared for presentation at the 34$^{th}$ Annual SPE International Conference and Exhibition, Tinapa-Calabar, Nigeria. SPE 140744 (2010)
25. Permadi, A.K., Yuwono, I. P., and Simanjuntak, A. J. S. Effects of Vertical Heterogeneity on Waterflood Performance in Stratified Reservoirs: A Case Study in

Bangko Field, Indonesia. Presented at SPE Asia Pacific Conference, Kuala Lumpur, Malaysia, SPE 87016 (2004)

26. Peters, E. J. Advanced Petrophysics: Volume 1, Greenleaf Book Group (2012).
27. Rahmani, A.R., Athey, A.E., Ahmadian, M., Wilt, M.J., Chen, J., Bryant, S.L., and Huh, C. Crosswell Magnetic Sensing of Superparamagnetic Nanoparticles for Subsurface Applications. Presented at SPE Annual Technical Conference and Exhibition, New Orleans, Louisiana, U.S.A., SPE 166140 (2013).
28. Rahmani, A.R., Bryant, S.L., Huh, C., and Ahmadian, M., Characterizing Reservoir Heterogeneities Using Magnetic Nanoparticles. Presented at SPE Reservoir Simulation Symposium, Houston, Texas, U.S.A., SPE 173195 (2015).
29. Roberts, M.R. Shear-Induced Emulsions Stabilized with Surface-Modified Silica Nanoparticles, M.S.E. Thesis, The University of Texas at Austin (2011).
30. Roof, J.G. Snap-Off of Oil Droplets in Water-Wet Pores, *SPE J.*, 10, 85-90 (1970).
31. Rosenweig, R.E., Heating Magnetic Fluid with Alternating Magnetic Field. Journal of Magnetism and Magnetic Materials, 252, 370-374 (2002).
32. Roth, R.F., Direct Electrical Heating of Flowlines-Guide to Uses and Benefits. Presented at Offshore Technology Conference, Rio De Janiro, Brazil. OTC 22631 (2011).
33. Sharma, M.M., Zhang, R., Chenevert, M.E., Ji, Q., Guo, J., and Friedheim, M-I. A New Family of Nanoparticle Based Drilling Fluids. SPE 160045 (2012)
34. Tadros, T.F., Emulsion Science and Technology. WILEY-VCH, Weinheim (2009)
35. Urdahl, O., Børnes, A.H., Kinnari, K.J., and Holme, R., Operational Experience by Applying Direct Electrical Heating for Hydrate Prevention. Presented at Offshore Technology Conference, Houston, Texas, U.S.A. OTC 15189 (2003).

36. Yu, H., Kotsmar, C., Yoon, K.Y., Ingram, D.R., Johnston, K.P., Bryant, S.L., and Huh, C. Transport and Retention of Aqueous Dispersions of Paramagnetic Nanoparticles in Reservoir Rocks. Presented at SPE Improved Oil Recovery Symposium, Tulsa, OK, U.S.A., SPE 129887 (2010).
37. Zakaria, M.F., Husein, M., and Hareland, G., Novel Nanoparticle-Based Drilling Fluid with Improved Characteristics. SPE 156992 (2012).
38. Zhang, T., Espinosa, D.A., Yoon, K.Y., Rahmani, A.R., Yu, H., Caldelas, F.M., Ryoo, S., Roberts, M.R., Prodanovic, M., Johnson, K.P., Milner, T.E., Bryant, S.L., and Huh, C. Engineered Nanoparticles as Harsh-Condition Emulsion and Foam Stabilizers and as Novel Sensors, Prepared for presentation at the Offshore Technology Conference, Houston, TX, OTC 21212 (2011)
39. Zhang, T., Roberts, M.R., Bryant, S.L., and Huh, C. Foams and Emulsions Stabilized with Nanoparticles for Potential Conformance Control Applications, Presented at the SPE International Symposium on Oilfield Chemistry, Woodlands, TX, SPE 121744 (2009).